Afdelingen for Bærende Konstruktioner
Department of Structural Engineering
Danmarks Tekniske Højskole · Technical University of Denmark

THE STRENGTH OF OVERLAPPED DEFORMED TENSILE REINFORCEMENT SPLICES IN HIGH STRENGTH CONCRETE

NICHOLAUS HOLKMANN OLSEN

Serie R No 234 1990

THE STRENGTH OF OVERLAPPED DEFORMED TENSILE REINFORCEMENT SPLICES IN HIGH STRENGTH CONCRETE

NICHOLAUS HOLKMANN OLSEN

The Strength of Overlapped Deformed Tensile Reinforcement Splices in High Strength Concrete

Tryk:
Afdelingen for Bærende Konstruktioner
Danmarks Tekniske Højskole
Lyngby
ISBN 87-7740-054-2

PREFACE

This report has been prepared as one part of the thesis required to obtain the degree of "teknisk licentiat", equivalent to the Ph.D. degree.

The thesis consists of this report and the following three reports:

- Heat-Induced Explosion in High Strength Concrete
- Uniaxial Stress-Strain Curves of High Strength Concrete
- Design Proposal for High Strength Concrete Sections Subjected to Flexural and Axial Loads.

This thesis has been carried out at the Department of Structural Engineering, Technical University of Denmark under the supervision of Lecturer M.Sc. Erik Skettrup, Lecturer, Dr. Herbert Krenchel and Professor Emeritus, Dr. Troels Brøndum-Nielsen.

I would like to express my gratitude to the staff of the Department, who have contributed to the completion of the Ph.D. study and this report.

Finally, I wish to acknowledge the support and financial backing of the Danish Technical Research Council through Contract No.: FTU 5.17.3.6.11, without which it had not been possible to carry out this research.

ABSTRACT

The thesis deals with the following four investigations:

- Heat-Induced Explosion in High Strength Concrete.
- Uniaxial Stress-Strain Curves of High Strength Concrete.
- Design Proposal for High Strength Concrete Sections Subjected to Flexural and Axial Loads.
- The Strength of Overlapped Deformed Tensile Reinforcement Splices in High Strength Concrete.

The thesis consist of four seperate reports. A short summary of these is given below.

Heat-Induced Explosions in High Strength Concrete.

This report contains the result and description of a series of tests which have been carried out in order to evaluate the explosion risk of heat induced high strength concrete as compared to normal strength concrete.

The tests were carried out with concrete test specimens shaped as ø100 x 200 mm cylinders with a compressive strength in the range from 30 MPa to 90 MPa. The cylinders were cured in two different ways:

a: 7 days in water followed by 21 days in laboratory atmosphere (20^{o} C and 60 % RH).

b: 7 days in water followed by 21 days sealed with plastic aluminum foil.

A total of 36 concrete cylinders were heated in an electrical oven at a heating rate of 2.5° C per min. until reaching a temperature of 600° C. After 2 hours at this temperature the cylinders were cooled at a rate of up to 1° C per min.

The tests show that the explosion risk depends on the curing conditions and that the explosion risk in the case of high strength concrete is not higher than for normal strength concrete especially for concrete cured under condition a.

Uniaxial Stress-Strain Curves of High Strength Concrete.

This report describes a special test-rig developed in order to obtain the ascending as well as the descending part of uniaxial stress-strain curves. Test results is reported from test series where the complete stress-strain curve is determined for concrete with compressive strength in the range from 40 MPa to 92 MPa.

The test results show that the ascending part of the uniaxial stress-strain curves are more linear and steeper for high strength concrete when compared to normal strength concrete and that the descending branch becomes steeper the higher the strength level.

The inclination of the ascending part of the obtained uniaxial stress-strain curves for high strength concrete is steeper and the strain at peak stress is less when compared to results from USA and Norway. The declination of the descending part seems less when compared to the results from Norway and only slightly steeper when compared to results from USA.

Design Proposal for High Strength Concrete Sections Subjected to Flexural and Axial Loads.

In this report an investigation is carried out of the consequences when predicting the ultimate capacity of reinforced high strength concrete sections subjected to pure bending or combined bending and axial load by extrapolating DS 411 to the compressive strength level of 90 MPa. The investigation is based on calculated results using obtained knowledge of the complete uniaxial stress-strain curves for concrete and applying nonlinear computerized methods.

The investigation show that extrapolation of DS 411 overestimates the ultimate capacity of reinforced high strength concrete sections when subjected to pure bending with as much as 33 %, while DS 411 in the case of sections subjected to combined bending and axial load overestimates the ultimate capasity with as much as 39 %.

A design proposal is suggested for calculating the ultimate capacity of high strength concrete sections subjected to pure bending or combined bending and axial load. The design proposal is based on the same principles as DS 411 and the results from the nonlinear calculations using the knowledge of the complete uniaxial stress-strain curves as mentioned above.

The curvature ductility of single reinforced high strength concrete sections compared to normal strength concrete sections is also investigated on the basis of results from the nonlinear calculations. The investigation show that the ductility of high strength concrete sections is less than the ductility of normal strength concrete sections regardless of the reinforcement degree and that it can be reduced to as much as 78 %.

The Strength of Overlapped Deformed Tensile Reinforcement Splices in High Strength Concrete.

This report decribes a test series carried out in order to evaluate the strength of overlapped tensile splices in high strength concrete and the anchorage strength of deformed bars in pull-out test specimens similar to that of DS 2082.

The influence of concrete compressive strength, splitting strength and fracture energy, G_F, on the strength of overlapped tensile splices is evaluated on the basis of 22 tests. The test indicate that the fracture energy of concrete appears to be a more governing property to the strength of splices than the compressive strength and splitting strength.

The results from the tests with overlapped splices is compared to the Danish Code of Practice for the use of Concrete, DS 411. The comparison show that extrapolating DS 411 for the design of overlapped splices in high strength concrete will yield more conservative results than in the case of normal strength concrete.

The results from the tests with overlapped splices have also been compared to estimated values from a theoretical model developed at the Department of Structural Engineering by B. S. Andreasen. The model is based on the theory of plasticity and tests with concrete in the normal strength range. The comparison show that the model developed by Andreasen overestimates the strength of overlapped splices for high strength concrete. A modification to the ν-expression used in the model is suggested, yielding more acceptable deviations from the test results.

Estimated values from an empirical formula developed by Orangun et al. is compared to the results from the tests with overlapped splices. The comparison show that the empirical formula overestimates the strength of overlapped splices in high strength concrete.

The influence of concrete compressive strength, splitting strength and fracture energy, G_F, on the anchorage strength of deformed bars in pull-out test specimens is evaluated on the basis of 84 tests. No clear conclusion could be made from the tests regarding which proporty were the most governing on the anchorage strength.

A model is suggested for calculating the anchorage strength of deformed bars in pull-out test specimens similar to that of DS 2082. The model is based on the theory of plasticity as well as the experimental results and the principles used by Andreasen in his model for estimating the strength of overlapped splices.

The results from the tests with overlapped splices and pull-out tests are compared. The comparison indicates that the anchorage strength from the pull-out tests are considerably larger than the strength from overlapped splices regardless of the concrete compressive strength level. The reason for this is partly the surrounding spiral reinforcement in the pull-out test specimen which confine the concrete around the anchored bar and that the failure mechanism is completely different from that of overlapped splices.

RESUME

Afhandlingen omhandler følgende undersøgelser af højstyrkebeton:

- Heat-Induced Explosion in High Strength Concrete.

- Uniaxial Stress-Strain Curves of High Strength Concrete.

- Design Proposal for High Strength Concrete Sections Subjected to Flexural and Axial Loads.

- The Strength of Overlapped Deformed Tensile Reinforcement Splices in High Strength Concrete.

Afhandlingen foreligger som fire seperate rapporter over undersøgelserne og er kort resumeret nedenfor.

Heat-Induced Explosion in High Strength Concrete.

Denne rapport indeholder resultater og beskrivelse af en forsøgsrække udført med det formål, at undersøge explosionsrisikoen af varmepåvirket højstyrkebeton i forhold til normalstyrkebeton.

Undersøgelsen omfatter betonprøvelegemer formet som ø100 x 200 mm cylindre med en trykstyrke i intervallet 30 - 90 MPa, som er hærdnet på to forskellige måder :

a: 7 dage i vand efterfulgt af 21 dage i laboratoriet ved 20^{o} C og 60 % RH.

b: 7 dage i vand efterfulgt af 21 dage forseglet med plastik og aluminiums folie.

Ialt 36 betoncylindre blev opvarmet i en elektrisk ovn med en opvarmningshastighed på 2.5° C pr. min. op til 600° C. Efter 2 timer ved 600° C blev cylindrene nedkølet med en hastighed på maksimalt 1° C pr. min.

Forsøgene viste, at explosionsrisikoen afhænger af hærdningsforholdene, samt at risikoen for højstyrkebeton ikke er væsentligt højere end for normalstyrkebeton, specielt når disse hærdes som under a.

Uniaxial Stress-Strain Curves of High Strength Concrete.

Rapporten beskriver en specielt udviklet forsøgsopstilling, som muliggør bestemmelse af den stigende og faldende del af enaksede betonarbejdskurver.

Rapporten indeholder derudover resultater fra forsøgsrækker, hvor hele den enaksede arbejdskurve er bestemt for beton med trykstyrker i intervallet 40 - 92 MPa. De bestemte enaksede arbejdskurver af højstyrkebeton udviser i forhold til normalstyrkebeton et mere lineært og stejlere forløb af den nedadgående del.

De opnåede arbejdskurver for højstyrkebeton udviser sammenlignet med tilsvarende arbejdskurver fra USA og Norge et stejlere forløb af den stigende del af arbejdskurven, og en mindre tøjning ved maksimal spænding, mens den nedadgående del er mindre stejl sammenlingnet med de norske resultater og stejlere sammenlignet med de amerikanske resultater.

Design Proposal for High Strength Concrete Sections Subjected to Flexural and Axial Loads.

I denne rapport vurderes om beregningsmetoden i DS 411 til bestemmelse af betontværsnits bæreevne, påvirket til ren bøjning eller kombineret bøjning og normalkraft, kan ekstrapoleres til betonstyrker i intervallet 50 -90 MPa. Vurderingen er baseret på resultaterne fra en ulineær beregningsmodel, hvor der indgår både den stigende og den faldende del af eksperimentelt bestemte enaksede betonarbejdskurver fra en tidligere undersøgelse.

Bestemmes højstyrkebetontværsnits bæreevne ved ekstrapolering af DS 411 kan bæreevnen af tværsnit med balanceret armeringsgrad påvirket til ren bøjning overvuderes med op til 33 % i forhold til resultaterne fra den ulineære beregning, mens bæreevnen af tværsnit påvirket til kombineret bøjning og normalkraft kan overvuderes med op til 39 %.

Et beregningsforslag er derfor udarbejdet til bestemmelse af højstyrkebetontværsnits bæreevne påvirket til ren bøjning eller kombineret bøjning med normalkraft. Forslaget er baseret på de samme principper som DS 411 og resultater fra den ulineære beregningsmodel.

Endvidere er duktiliteten af højstyrkebetontværsnit vurderet i forhold til normalstyrkebetontværsnit på baggrund af resultaterne fra den ulineære beregningsmodel.

Resultaterne indikerer, at duktiliteten af højstyrkebetontværsnit er mindre uanset armeringsgraden af tværsnittet og kan forminskes ned til 78 % af tilsvarende normalbetontværsnit.

The Strength of Overlapped Deformed Tensile Reinforcement Splices in High Strength Concrete.

I denne rapport beskrives for både højstyrkebeton og normalstyrkebeton en eksperimentel behandling af overlapningsstøds bæreevne samt bæreevnen af forkammet armering forankret i prøvelegemer meget lig prøvelegemet efter Dansk Standard DS 2082.

Inflydelsen af betons trykstyrke, spaltetrækstyrke og brudenergi, G_F, på bæreevnen of overlapningsstød er undersøgt på basis af 22 forsøg. Undersøgelsen viser, at betons brudenergi G_F har større inflydelse på bæreevnen af overlapningsstød end betons trykstyrke og spaltetrækstyrke.

Der er foretaget en undersøgelse af muligheden for, at ekstrapolere beregningsmodellen i DS 411 til beregning af nødvendig overlapningslængde af stød til betonstyrker i intervallet 50 - 90 MPa. Denne undersøgelse viser, at DS 411 ved ekstrapolering giver mere konservative resultater af nødvendig overlapningslængde for højstyrkebeton end for normalstyrkebeton.

Resultaterne af forsøgene med overlapningsstød er sammenlignet med resultater fra en beregningsmodel udviklet på Afdelingen for Bærende Konstruktioner af B. S. Andreasen. Modellen der baseres på plasticitetsteorien og forsøg primært med betontrykstyrker i intervallet 6 - 50 MPa, overvurderer bæreevnen af overlapningsstød i højstyrkebeton. Et forslag til et andet ν-udtryk til beregningsmodellen er derfor udarbejdet.

Derudover er forssøgsresultaterne med overlapningsstød sammenlignet med resultater fra en empirisk formel udviklet af Orangun et al, der viser at den empiriske formel overvurderer bæreevnen af overlapningsstød i højstyrkebeton.

Inflydelsen af betons trykstyrke, spaltetrækstyrke og brudenergi G_F på bæreevnen af forankret armering i prøvelegemer meget lig prøvelegemer efter DS 2082 er undersøgt på basis af 84 forsøg. Det har ikke på baggrund af disse forsøg været muligt at fastslå hvilken af ovennævnte parametre, der har størst inflydelse på bæreevnen.

Et forslag til en beregningsmodel er udviklet til beregning af forkammet armerings bæreevne i prøvelegemer meget lig prøvelegemet i DS 2082. Beregningsmodellen er baseret på plasticitsteorien og de gennemførte forsøg samt principperne anvendt af Andreasen i beregningsmodellen for bæreevnen af overlapningsstød.

En sammenligning mellem de eksperimentelt fundne bæreevner af overlapningsstød og forankring af forkammet armering viser, at sidstnævnte generelt har højere bæreevne. Dette kan skyldes, at spiralarmeringen omslutter betonen hvori armeringsjernet er forankret samt, at brudmekanismen er forskellig fra brudmekanismen i overlapningsstød.

CONTENTS PAGE

LIST OF TABLES PAGE

LIST OF FIGURES PAGE

LIST OF PHOTOS PAGE

NOTATIONS

The most commonly used symbols are listed below. Exceptions from the list may appear, but this will be mentioned in the text in connection with the actual symbol.

a	Distance between ribs.
b	Width of beam section.
d	Diameter of anchored or spliced bar.
d_s	Diameter of transverse/surrounding reinforcement. (Stirrups or spirals).
f_c	Uniaxial cylindrical compressive strength of concrete.
f_{cube}	Compressive strength of concrete measured on cubes.
f_{cp}	Plastic uniaxial compressive strength of concrete.
f_{sp}	Splitting tensile strength of concrete.
f_{tp}	Plastic uniaxial tensile strength of concrete.
f_{ys}	Yield strength of reinforcement.
g	Acceleration due to gravity.
k, k_1, k_2	Constants.
h_d	Depth of ribs on the reinforcement.
l_{sp}	Splice length.
l_a	Anchorage length.
m_t	Weight of G_F-specimen.
n_s	Number of stirrups or spirals over the splice/-anchorage length.
n_{ss}	Number of stirrups or spirals crossed by the horizontal yield line.
n_{sp}	Number of lap splices in a section.
s	Vertical distance from the bottom of the beam to the center of the reinforcement.

V	Increment in displacement (velocity).
A_{lign}	Area of alignment.
A_{ss}	Cross sectional area of surrounding reinforcement.
C	Dimensionless internal work from the surroundings.
D	Dimensionless rib parameter.
E	Modulus of elasticity.
F	Dimensionless rib parameter.
G_F	Fracture energy of concrete.
P_a	Average failure load applied to bars in pull-out tests.
P_{ao}	Average failure load applied to four spliced bars in tests with overlapped splices.
T_y	Yield load of reinforcement.
T_u	Ultimate load of reinforcement.
$T_{0.2}$	0.2 per cent proofstress of the reinforcement.
W_i	Internal work.
W_o	Area below recorded load-deflection curve from G_F-tests.
ϵ_e	Permanent elongation in per cent.
δ_o	Central deflection of G_F-specimen when the load has descended to zero and final rapture occurs.
ζ	Anchorage factor used in DS 411.
ν	Effectiveness factor for compression.
ρ	Effectiveness factor for tension.
ψ	Stirrup/spiral reinforcement degree.
τ_u	Average shear stress at failure.

1. INTRODUCTION

1.1 General

In recent years efforts directed towards improving the compressive strength of concrete have been very successful and utilization of high strength concrete in the range between 50-100 MPa is becoming increasingly common [1].

Although knowledge of the properties of high strength concrete and the structural behaviour when using high strength concrete has been obtained [1], [2], [3], there is still more research needed and among this the strength of overlapped tensile reinforcement splices and anchorage lengths in high strength concrete, which is the subject of this report.

The design of lap splices and anchorage lengths of deformed tensile reinforcement in reinforced concrete is of permanent interest to the structural engineer because of the impact of splice lengths and anchorage lengths on detailing and on structural performance. Present design methods for the strength of overlapped splices and anchorage lengths are based on tests, generally using concrete with compressive strengths from 10 MPa to 40 MPa [30]. Although some information has recently become available concerning high strength concrete [4], not enough data has been obtained to permit recom- mendations.

It is well known, that the strength of overlapped splices and anchorage lengths in normal strength concrete is strongly affected by many parameters. The following section gives a short literature review of some of the more important parameters.

1.2 Literature Review

One of the most important parameters to have an effect on the strength of overlapped splices and anchorage lengths is the concrete strength.

Efsen [5] concluded from pull-out tests of tensile reinforcement in spiral sockets that $\Delta\tau_u/\Delta f_{cube} = 0.25$, for f_{cube} in the range from 20 MPa to 50 MPa. f_{cube} is the concrete compressive strength determined by testing concrete cubes and τ_u is the average shear stress along the anchorage length at failure, assuming an even distribution of shear stress.

From tests on anchorage strength in beams conducted by Ferguson and Thompson [6], [7] and Østlund [8] it was concluded, that τ_u is proportional to $\sqrt{f_c}$, where f_c is the concrete compressive strength.

From beam tests with overlapped splices without surrounding reinforcement conducted by Chin et al. [9], Ferguson and Breen [10], Chamberlin [11] and Ferguson and Krishnaswamy [12], it was concluded that also in this case τ_u was proportional to $\sqrt{f_c}$. Also Tepfers [13] concluded from beam tests with overlapped splices without surrounding reinforcement that τ_u is proportional to $\sqrt{f_{cube}}$ up to $f_{cube} \approx 70$ MPa. The favourable influence of the concrete strength was then observed to be lost and even to become negative. Tepfers [13] explained this as being due to shrinkage of the concrete because a large quantity of cement was used (up to 1693 kg/m^3) in order to produce concrete with compressive strengths above the 70 MPa level. Shrinkage creates tensile stresses in the concrete around the reinforcing bars and these are superimposed on the stresses due to bond and, consequently, reduces the value of τ_u. The stress component due to shrinkage might become dominant for high strength concrete where larger quantity of cement usually is used, leaving an increasingly small

portion of the ultimate stress available for bond as the concrete strength increases.

Only the influence of the concrete compressive strength on the strength of overlapped splices and anchorage length is mentioned above, but the concrete tensile strength has most likely an equally strong influence. The fact that the influence of concrete compressive strength can be difficult to observe may be caused by variations in the concrete tensile strength. Often it is the fact that τ_u is proportional to $\sqrt{f_c'}$, taken as an argument that τ_u is in reality proportional to the concrete tensile strength because many empirical formulas state that the tensile strength is proportional to $\sqrt{f_c'}$. The test results on which the empirical formulas are based have, however, considerable scatter and the compressive strength may therefore not be a good indicator of the tensile strength. Unfortunately, the concrete tensile strength is seldom reported in most test series, leaving it difficult to judge the influence of concrete strength on the strength of overlapped splices and anchorage lengths.

Another parameter besides the concrete strength having a strong influence is the overlap length and the length of the anchorage.

From anchorage tests conducted by Mains [14], Matley and Watstein [15] it could be concluded that τ_u decreases as the anchorage length increases. From investigations carried out by Mains [14] and Perry [16] this is explained by an unevenly distribution of shear stress along the anchorage length.

This unevenly distribution of stresses is verified by tests carried out by Mains [14] and Perry [16]. These tests showed that the tensile stresses in the bars at failure along the anchored bar were not distributed in a linear way but were nearly constant at the first part of the anchored bar at the loaded end, rapidly reduced at the center part and nearly zero at the end of the bar.

This stress variation along an anchored bar at failure is by Jensen [17] explained by the deformations of the bar when loaded. When the load applied to an anchored bar increases, the slip and thereby the shear stress along the bar will also increase. If the slip becomes too large, local anchorage failure occur and as a consequence the shear stresses decreases. The above will first occur at the loaded end of the anchored bar and if the slip becomes so large that the shear stress drops to zero, a "zipper" effect may start, since the load in the anchored bar now has to be obtained by the next part of the anchored bar, but here the situation will be the same as at the loaded end bar, the slip becomes too large so that the shear stress drops to zero, etc.

The above hypothesis from Jensen [17] explains why anchorage tests often have a rapid and sudden failure. The "zipper" effect could, according to Jensen [17] also explain why τ_u from anchorage tests is not proportional to the concrete compressive strength of higher strength concrete, since this concrete is less ductile and a local anchorage failure will result in a more rapid decrease of shear stress.

Also from beam tests with overlapped splices without surrounding reinforcement conducted by Tepfers [13] and Ferguson and Breen [10] it was concluded that τ_u decreases as the overlap length increases.

Surrounding reinforcement along an overlapped splice or along an anchorage length is known to have a strong influence on the strength of overlapped splices and anchorage lengths. Efsen [5] concluded from pull-out tests of tensile reinforcement in spiral sockets that certain amount of transverse reinforcement is necessary in order to have an effect on τ_u. An increase over and above that amount of transverse reinforcement will increase the value of τ_u.

Rathkjen [18] concluded from beam tests that the anchorage strength increases with increasing amount of transverse reinforcement along the anchorage length. Beam tests with overlapped splices containing transverse reinforcement conducted by Tepfers [13] concluded that the strength contribution by the transverse steel depends both on the splice length and the amount of surrounding reinforcement. Test results from Thompson et al. [19] indicate, that an upper limit of the amount of transverse reinforcement exists after which further increase has no effect on τ_u.

There is a growing international interest concerning the application of fracture mechanics to concrete structures which has given new ways to understand and model phenomena which earlier only could be treated empirically. The fracture energy parameter, G_F, is suggested by Hillerborg [20], [21] as one way of quantifying the toughness of the concrete and could therefore be a parameter with a strong influence on the strength of overlapped splices and anchorage lengths, which is also indicated in recent studies by Olsson [22] on the strength of anchorage lengths in pull-out tests. No beam test series exist, however, with overlapped splices or anchorage lengths where the fracture energy of the concrete is determined.

1.3 The Purpose of the Investigation

As mentioned in the previous sections only very limited information exists on the strength of overlapped tensile splices in the regions with constant moment for high strength concrete. An experimental program is therefore established for concrete compressive strengths ranging from 40 MPa to 100 MPa. The purposes of the investigation are as follows:

a) To study the effect of increasing concrete strength on the strength of overlapped splices.

b) To study the effect of overlap length of the strength of overlapped splices.

c) To study the effect of the fracture energy parameter, G_F, on the strength of overlapped splices.

d) To investigate experimentally if the parameter effect observed from the tests results of the strength of overlapped splices correspond to pull-out test results.

e) To investigate if the empirical formula of Orangun et al. [23] which estimates the strength of overlapped splices in normal strength concrete also can be used in cases of high strength concrete.

f) To investigate if the strength of overlapped splices can be estimated in the high strength concrete range when using the theory of Andreasen [24] which is based on the theory of plasticity in cases of normal strength concrete.

g) To investigate if the Danish Code DS 411, [25], can be used to estimate the strength of overlapped splices for high strength concrete.

2. EXPERIMENTAL PROGRAM

2.1 Introduction

Three series of tests were carried out.

1: The first, called simulated beam specimen series (S.B.- specimen series), because it simulates a beam subjected to a constant moment. These series were directed towards the study of strengths of overlapped splices of tensile steel.

2: The second, called EF.-specimen series, named after Professor Efsen, was directed towards the study of correlation between pull-out strengths from EF.-specimens, and overlapped splice strengths from S.B.-specimens.

3: The third, called G_F-specimen series, generated data needed to be investigated if the fracture energy G_F has any substantial influence on the strength of overlapped splices.

2.1.1 Batch No., S.B. No. and EF. No

From every single batch of concrete, one S.B.-specimen, 12 ø100 x 200 mm cylinders and 4 or more G_F-specimens were always produced. From most batches, 6 EF.-specimens were produced together with numerous ø150 x 300 mm cylinders, depending on the size of the EF.-specimen.

A batch No. refers to the intended compressive strength of the concrete and the length of the overlapped splice in the produced S.B.-specimen. For instance, Batch No. 30/12.5 means that the concrete was intended to have a compressive strength of 30 MPa and the overlapped splice length was 12.5 times 16 mm which is the diameter of the tensile steel used before cold stretching (see section 2.2.2.3). Therefore the S.B.-specimen number corresponds to the Batch No.

As for S.B.-specimen, EF.-specimen is also characterized by a number, i.e. EF. 30/07.5 which means that the concrete was intended to have a compressive strength of 30 MPa and the anchorage length of 7.5 times 16 mm which is the diameter of the tensile steel before cold stretching (see section 2.2.2.3).

Correlation between EF. No. and Batch No. is shown in Table 2.1 as well as the number of G_F-specimens and ø150 x 300 cylinders produced from each batch.

2.2 Materials

2.2.1 Concrete

Experience in producing high strength concrete has been obtained from a previous investigation where heat induced explosion tests with high strength concrete were carried out.

Material used and mix proportions will be described in the following as well as mixing, casting and curing of cylinders.

Furthermore, compressive test results and splitting tests will be described and discussed.

2.2.1.1 Materials

Cement: Rapid Hardening Portland Cement, ASTM Type III supplied by Ålborg Portland. Specific Gravity was assumed to be $3.3 \cdot 10^3$ kg/m^3.

Fly Ash: Fly ash supplied by Amagerværket, Copenhagen was used in the mix when producing concrete with intended compressive strength at the 50 MPa level. Specific Gravity was assumed to be $2.2 \cdot 10^3$ kg/m^3.

Silica Fume: Silica fume, supplied by Ålborg Portland, Ålborg used in the mixes when producing high strength concrete. Specific gravity was assumed to be $2.2 \cdot 10^3$ kg/m^3.

Fine Aggregate: Sand (0-4 mm) from Danish Marine Deposits, supplied by Carl Nielsen A/S, Copenhagen. Specific gravity was assumed to be $2.62 \cdot 10^3$ kg/m^3.

Coarse Aggregate: Gravel (4-16 mm) from Danish Marine Deposits, supplied by Carl Nielsen A/S, Copenhagen. Specific gravity was assumed to be $2.62 \cdot 10^3$ kg/m^3.

Admixtures: Superplasticizer Mighty 100, supplied under the name of Scan Cem SP 62/SP 63 by Cemton, Norway.

Water: Tap water from the city's network was used.

2.2.1.2 Mix Proportions

Four different mixes were used to produce the four compressive strength levels desired: High strength concrete at the 90 MPa and 70 MPa level and normal strength concrete at the 50 MPa and 30 MPa level. Mix proportions are given in Table 2.2. It should be noted that batch 30/30 was produced with more superplasticizer than given in Table 2.2 which led to some segregation and bleeding. As a consequence, the compressive strength was low.

2.2.1.3 Mixing, Casting and Curing of Cylinders

Mixing A 0.3 m^3 capacity paddle mixer was used in order to produce batches of 0.165 m^3 of concrete for the test specimens and cylinders. Sand and coarse aggregates were mixed dry with cement and silica fume or fly ash. After 1 min. of mixing, the water and superplasticizer were added and thorough mixing was achieved within 6 min.

Casting 12 cylinders, ø100 x 200 mm, from each batch were cast in polyethylene moulds and 4 or more, ø150 x 300 mm, cylinders were cast in steel moulds. A vibrator table was used to compact the concrete.

Concerning casting of the test specimens, see sections 2.3.2.3, 2.4.2.3 and 2.5.2.3.

Curing After approximately 24 hours, the moulds were removed and the cylinders were cured 7 days in water and 28 days at 20^{o} and 60 % RH.

2.2.1.4 Test Apparatus and Procedure for Cylinder Tests

For each batch 6 ø100 x 200 mm cylinders and 4 or more ø150 x 300 mm cylinders were tested in order to determine the compressive strength. Furthermore, 6 ø100 x 200 mm cylinders were tested to determine the splitting strength.

All the cylinders were tested in a 200 MP MFL (Prüff and Mess MFL System) compressing test machine. The machine was servo controlled by a Walter and Bai SRG 5000.

Test specimens for compression tests were prepared for testing by placing wood fiber plates at the top and bottom surfaces and tested at a rate of 0.4 MPa/sec. Splitting strength was determinated with a testing rate of 0.04 MPa/sec.

2.2.1.5 Compressive Results

Table 2.3 shows the compressive strength results measures on ø100 x 200 m and ø150 x 300 mm cylinders.

The average compressive strength of the concrete with intended compressive strength of 90 MPa, was found to be 91.4 MPa measured on ø100 x 200 mm cylinders. As for the concrete with intended compressive strength of 70 MPa, 50 MPa and 30 MPa, the average was 82.2 MPa, 51.9 MPa and 39.6 MPa, respectively.
In Fig. 2.1 the compressive strength of the two different sizes of cylinders is shown. Blanks and McNamara [26] and DS 411 [25] suggests that the ratio between compressive strength determined from ø150 and ø100 mm cylinders is 0.95 up to approximately 50 MPa. The ratio is also shown in Fig. 2.1.

It can be seen from Fig. 2.1 that the ratio $f_c(ø150)/f_c(ø100)$ could be taken as 0.95 also at the level of 80-100 MPa.

2.2.1.6 Splitting Results

Table 2.3 shows the splitting strength results measured on ø100 x 200 mm cylinders.

From [25] and [27] the concrete splitting strength for normal strength concrete can be estimated by the following formula.

$$f_{sp} = \frac{1}{0.6} \cdot \sqrt{\frac{f_c}{10}} \qquad (2.1)$$

The actual test results and the values found according to the formula (2.1) are shown in Fig. 2.2.

It can be seen that the formula (2.1) seems to underestimate the concrete splitting strength for high strength concrete.

2.2.2 Reinforcement

2.2.2.1 Introduction

The following sections describe the reinforcement used in the S.B.-specimens and EF.-specimens.

Swedish Kam Steel Ks 600 S ø8 mm was used as stirrups and compression steel in the S.B.-specimens. Stirrups along the splice length in the S.B.-specimens were made from Danish Kam Steel Ks 410 S ø6 mm or from Danish Profiled Steel W.4301 ø5 mm.

The steel types mentioned are described in detail in section 2.2.2.2, see also Fig. 2.8 and 2.9.

The tensile reinforcement used in the S.B.-specimen and EF.- specimen was Swedish Kam Steel Ks 600 S ø16 mm. In order to obtain the longest possible splice lengths and anchorage lengths, all tensile reinforcements as well as Swedish Kam Steel ø8 mm used in the EF.-specimen were cold stretched.

The cold stretched reinforcements are described in section 2.2.2.3, together with the procedure used for stretching.

2.2.2.2 Stirrups and Compression Steel in the S.B.-specimen

The tension tests conducted on the reinforcement used as stirrups and compression steel in the S.B.-specimen were carried out with the use of a 60 Mp Mohr und Federhaff AG universal test machine. An Amsler Extensiometer, type EDL 113/22 with a measurement amplifier type Amsler MDL 1147 was used when obtaining load- deformation curves.

The typical relation between load and deformation for Swedish Kam Steel Ks 600 S ø8 mm used as stirrups and compression steel is shown in Fig. 2.3. The typical relation for Danish Kam Steel Ks 410 S ø6 mm and Danish Profiled Steel W 4301 ø5 mm used as stirrups is shown in Fig. 2.4 and 2.5, respectively.

Table 2.4 gives the modulus of elasticity E, yield load T_y, and ultimate load T_u, of the Swedish Kam Steel Ks 600 S ø8 mm.

In Tables 2.5 and 2.6 E and T_u are given for the Danish Kam Steel Ks 410 S and Danish Profiled Steel W 4301 respectively, together with $T_{0.2}$ which is defined as the load where the permanent steel elongation is 0.2 %.

2.2.2.3 Cold Stretching of Tensile Reinforcement

Swedish Kam Steel Ks 600 S ø16 mm, used as tensile reinforcement, was cold stretched in order to obtain the longest possible splice lengths in the S.B.-specimens as well as the longest possible anchorage lengths in the EF.-specimens.

Cold stretching of the reinforcement was carried out in a 200 Mp Mohr und Federhaff AG universal test machine. All bars were cold stretched to a load of 156 KN and the bars were then stored in an electrical oven for 24 hours at a temperature of 110°C in order to age the reinforcement. After ageing the bars, the permanent elongation was measured. A typical load and deformation curve for the cold stretching is shown in Fig. 2.6.

The nominal diameter of the cold stretched Swedish Kam Steel ø16 mm is calculated by the formula

$$d = 16 \cdot \sqrt{1 + \epsilon_e/100} \qquad (2.2)$$

where

d : Diameter in mm of the cold stretched Swedish Kam Steel Ks 600 S ø16.

ϵ_e : Permanent elongation in per cent.

Table 2.7 gives the modulus of elasticity, E, yield load, T_y, of the Swedish Kam Steel Ks 600 S ø16 mm as well as the calculated nominal diameter, d, and the ultimate load of the cold stretched steel.

Swedish Kam Steel Ks 600 S ø8 mm, used in EF.-specimen, was also cold stretched using a 60 Hp Mohr und Federhaff AG universal test machine. All bars were stretched to a load of 39 kN and aged at 110°C for 24 hours after which period the permanent elongation was measured. A typical load and deformation curve for cold stretching Swedish Kam Steel Ks 600 S ø8 mm is shown in Fig. 2.7.

Table 2.8 gives the modulus of elasticity, E, yield load, T_y, of the Swedish Kam Steel Ks 600 S ø8 mm together the ultimate load, T_u, of the cold stretched steel.

2.3 S.B.-tests

2.3.1 General

These series were designed primarily to study the strength of overlapping tensile splices in high strength concrete and the shear stress distribution along the splice in regions of constant moment.

The S.B.-specimen and test rig arrangement (see sections 2.3.2.2 and 2.3.3.1) were chosen instead of testing ordinary beams for the following reasons:

1) It would be possible to produce one S.B.-specimen, 6 EF.-specimens, 12 ø100 m x 200 mm and 4 or more ø150 mm x 300 mm cylinders, and 4 or more G_F specimens from one single batch.

This made it possible to compare the ultimate average shear stress along the splice in the S.B.-specimen at failure with the ultimate average shear stress along the anchorage length in the EF.-specimen. The G_F-specimens made it possible to study if the fracture energy is a more covering material property to the strength of overlapped splices than the compressive and splitting strength.

2) The shape and size of the S.B.-specimen made it possible to measure the strain of each of the four overlapped bars outside the concrete simultaneously and relatively close to the splice, thus avoiding problems associated with the presence of tensile stresses and cracking of the concrete.

3) The S.B.-specimen and test rig arrangement made it possible to adjust the load on each of the four reinforcing bars to the same load before the test commenced.

A total of 21 S.B.-specimens were cast and all were tested until splice failure occurred. Problems associated with strain hardening of the tensile steel occurred when testing S.B. 70/20, but the test is nevertheless still reported.

2.3.2 S.B.-specimens

2.3.2.1 Controlled Variables

Concrete compressive strength, f_c, at the time of testing and the overlapping splice length of the tensile steel were the only experimental variables.

Four types of concrete were tested with varying splice lengths:

1) High strength concrete with an intended compressive strength of 90 MPa and splice lengths varying from 240 mm to 80 mm.

2) High strength concrete with an intended compressive strength of 70 MPa and splice lengths varying from 320 mm to 80 mm.

3) Medium strength concrete with an intended compressive strength of 50 MPa and splice lengths varying from 320 mm to 120 mm.

4) Normal strength concrete with an intended compressive strength of 30 MPa and splice lengths varying from 480 mm to 120 mm.

Table 2.3 summarizes the individual values for each test.

2.3.2.2 Specimen Dimensions and Reinforcing Details

As mentioned in section 2.2.2.3 the longitudinal tensile reinforcement of the S.B.-specimens were cold stretched prior to placing it in the form, and grooves were cut in all bars, so that strain gauges could be mounted into the grooves. A detailed description can be found in section 2.3.2.4. Furthermore, the bars were threaded in one end for the use of a special anchorage detail, described in section 2.3.3.1.
The dimensions of the specimens and reinforcing details are shown in Fig. 2.8 and 2.9.

In Fig. 2.8 three different types of reinforcement arrangements are shown which were used for the following splice lengths:

Type I: Reinforcement arrangement used for the splice lengths 480 mm, 240 mm, 200 mm and 160 mm.

Type II: Reinforcement arrangement used only for splice lengths 320 mm.

Type III: Reinforcement arrangement used for the splice lengths 120 mm and 80 mm.

Fig. 2.9 shows the details of the transverse reinforcement together with the details of the threaded end. All stirrups were tied to the longitudinal tensile and compression bars with standard tie wire. Photo 2.1 shows an example of the reinforcement arrangement type I.

2.3.2.3 Casting and Curing

Sections 2.2.1.2 and 2.2.1.3 describe the mix proportions and mixing procedure. In the following only the casting and curing of the S.B.-specimens will be described.

Casting: S.B.-specimens were cast in a horizontal position and with the tensile longitudinal bars placed in the bottom of the form. The forms were made of 12 mm thick plywood. Flexible soft vibrators were used during the placing and care was taken to avoid direct application of the vibrator near the center of the specimens where the strain gauges were located. Once the placing was completed, the exposed top faces were trowelled smooth.

Curing: When sufficient hardening of the concrete was obtained, after approximately 48 hours, the forms were removed and the specimens were cured 7 days in water and 27 days at 20^{o}C and 60 % RH.

2.3.2.4 Instrumentation

As mentioned in section 2.3.2.2 grooves were cut in all longitudinal tensile reinforcements in order to place strain gauges. A cross-section of the groove is shown in Fig. 2.10.

The strain gauges used were HBM LY11 6 mm long gauges, supplied by Hotting Baldwin Messtechnik, Darmstad, West Germany. After placing the strain gauges in the grooves, these were filled with araldit in order to protect the strain gauges from moisture when casting the concrete. Photo 2.2. shows an example of a bar containing strain gauges in a long groove.

In each S.B.-specimen three out of four longitudinal tensile bars were instrumented with two strain gauges each, one was placed just outside the splice length and the other one was placed outside the concrete. The last bar was instrumented with additional strain gauges. For splice lengths longer than 120 mm, 8 strain gauges were placed along the splice length while for splice lengths 120 mm and 80 mm, 6 respectively 4 strain gauges were used.

Fig. 2.11 and Table 2.9 give the location of the strain gauges along the overlapping splice length in cases where the splice length is longer than 120 mm. In cases of overlapping splice length of 120 mm and 80 mm, Fig. 2.12 respectively Fig. 2.13, illustrates the location of the strain gauges along the splice length.

As will be described in section 2.3.3 the S.B.-specimens were tested in a vertical position compared with that of casting, and bars at the bottom of the specimen (see Fig. 2.11) were always closest to each other. Fig. 2.11 and Table 2.9 give the location of the bar with additional strain gauges of each S.B.-specimen with overlapping splice lengths longer than 120 mm. Table 2.10 gives the location of the bar with additional strain gauges in cases of overlapping splice lengths of 120 mm and 80 mm.

Prior to casting and testing of each S.B.-specimen, all strain gauges in all bars were calibrated in order to achieve load-strain curves. The calibration was conducted in a 60 Mp Mohr and Federhaff AG universal test machine. Using a Hewlett Packard 3947 Data Acquisition/control Unit controlled by a Hewlett Packard 86 Computer. Corresponding values of load and strains of each strain gauge were monitored up to the maximum load of 135 kN.

A typical load-strain curve from one strain gauge is shown in Fig. 2.14. As can be seen from Fig. 2.14 the load-strain curve is not linear and the load-strain curves from each stain gauge were therefore fitted to a quadratic polynomial.

The fitted quadratic polynomial for each strain gauge was used when the actual test was analyzed.

2.3.3 Test-rig and Procedure

2.3.3.1 Test-rig

Fig. 2.15 shows the test-rig. The steel beams in the test-rig consist each of two channels mounted together by several steel cubes and bolts. Yokes and bearings with rotation about one axis were attached on the upper as well as the lower steel beams. The four longitudinal tensile reinforcing bars from the S.B.-specimen were fastened to the beams by yokes and a special anchorage detail. Fig. 2.16 shows the bearing and the placement of it upon the S.B.-specimen, the anchorage detail and the yoke. The test-rig is also shown on photo 2.3.

Load was applied to the upper beam - which is not attached to the steel columns - by an Amsler EPZ 20/10 single acting hydraulic press. As a consequence of the test-rig arrangement the ratio between the compressive load applied to the S.B.-specimen and the tensile load applied to the reinforcing bars is approximately 0.9, i.e. the S.B.-specimen is subjected to nearly pure bending.

2.3.3.2 Procedure

After placing of the S.B.-specimen in the test-rig and fastening of the anchorage detail, a small load was applied by the press. Strain gauges were monitored by the Hewlett Packard system described in section 2.3.2.4 and made it possible to adjust the load to the same value in all four longitudinal bars of S.B.- specimen by use of nuts of the anchorage detail. The anchorage tube was then filled with epoxy thereby ensuring that failure could not take place at the end of the threaded bar where the cross-section was smallest.

The epoxy was sufficient hardened after 24 hours to allow the test to commence. The load was applied by the press to the upper beam in small increments, approximately 2 kN. By monitoring the strain gauges along the splice a new load increment was applied when stable reading from the strain gauges was observed. A complete test took between 30-45 min., depending on the total number of load increments and on how fast a stable strain gauge reading along the splice was obtained.

2.4 EF.-tests

2.4.1 General

The EF.-test specimens in these series are based on the test specimen from Danish Standards DS 2082 [28] which is a standard- ized test procedure made to clarify the specific surface roughness of different kinds of deformed reinforcing bars.

The EF.-test specimen is named after Professor A. Efsen who in collaboration with Dr. H. Krenchel developed spiral sockets for splicing tensile reinforcement. These spiral sockets were, however, not economical in spite of being a logical solution to a splice where the concrete is the medium transferring the stress from steel bar to steel bar. These types of splices can be made so strong that rupture actually occurs outside the splice, see Efsen [5].

These series were designed primarily to study the correlation between the average shear stress as observed in the EF.-tests and the S.B.-tests at failure, and also to study the shear stress distribution along the anchorage length, and the influence, if any, of anchorage length on the average shear stress along the anchorage length at failure.

A total of 96 EF.-specimens were cast, 15 EF.-specimens containing strain gauges along the anchorage length, and anchorage failure was successfully achieved in 84 test specimens.

2.4.2 EF.-specimens

2.4.2.1 Controlled Variables

Concrete compressive strength, f_c, and the anchorage length was the only experimental variable. The following four types of concrete and anchorage lengths were tested:

1) High strength concrete with intended compressive strength at the 90 MPa level and anchorage lengths varying from 192 mm to 80 mm.

2) High strength concrete with intended compressive strength at the 70 MPa level and anchorage lengths varying from 192 mm to 80 mm.

3) Medium strength concrete with intended compressive strength at the 50 MPa level and anchorage lengths varying from 192 mm to 80 mm.

4) Normal strength concrete with intended compressive strength at the 30 MPa level and anchorage lengths varying from 240 mm to 80 mm.

It should be noted that for each intended compressive strength and anchorage length, 6 specimens were cast of which only one specimen contained strain gauges along the anchorage length.

Tables 2.1 and 2.3 summarize the individual values of compressive strength and anchorage length.

2.4.2.2 Specimen Dimension and Reinforcing Details

The test specimen used was concrete prism with 96 mm quadratic cross section and of varying lengths. The prism contained a spiral socket with four longitudinal reinforcing bars of cold stretched Swedish Kam Steel Ks 600 S ø8 mm. The diameter of the

spiral, made from ordinary wire, was 42 mm and the pitch was 30 mm. The diameter of the wire was 3.04 mm and the yield strength was 170 MPa. In the centre of the prism and the spiral socket, two pieces of cold stretched Swedish Kam Steel Ks 600 S ø16 mm were placed end to end.

Fig. 2.17 shows the specimen dimensions and reinforcing details. The lengths l indicates the anchorage length which in these series varied from 240 mm to 80 mm.

As mentioned in section 2.4.2.1 some of the EF.-specimens contained strain gauges along the anchorage length. For this purpose, grooves were therefore cut in the cold stretched Swedish Kam Steel Ks 600 S ø16 mm and strain gauges placed herein prior to placing of the reinforcement in the forms. The geometry of the positioning of strain gauges is described in section 2.4.2.4.

2.4.2.3 Casting and Curing

Casting: EF.-specimens were cast horizontally in a form made of 12 mm thick plywood and capable of producing 6 specimens at the same time. A vibrator table was used to compact the concrete and one placing was completed and the exposed surface was trowelled smooth.

Photo 2.4 shows the form together with the reinforcement.

Curing: After approximately 24 hours the forms were removed and the specimens were cured 7 days in water and 28 days at 20°C and 60 % RH.

2.4.2.4 Instrumentation

Measurement of Reinforcement Strains along the Anchorage Length

The strain gauges placed in the grooves were HBM LY11 6 mm gauges supplied by Hottinger Baldwin Messtechnik, West Germany.

For anchorage lengths from 240 mm to 160 mm, 9 strain gauges were placed along the anchorage length, while for anchorage lengths 120 mm and 80 mm, 7 respectively 5 strain gauges were used.

Fig. 2.18 and Table 2.11 show the geometry of strain gauges placement for anchorage lengths used in these test series.

Prior to placement of the bars in the forms, all bars were calibrated in the same manner as described in section 2.3.2.4.

Measurement of loads

When testing the EF.-specimens with and without strain gauges mounted, the load at failure was read directly from the test machine indicator.

2.4.3 Test Apparatus and Procedure

2.4.3.1 Test Apparatus

A 60 Hp Mohr und Federhaff AG universal test machine was used. The tensile load was applied directly to the two pieces of cold stretched Swedish Kam Steel Ks 600 S ø16 mm. Photo 2.5. shows the testing machine and a test specimen.

2.4.3.2 Procedure

When testing the six EF.-specimens from one batch, the specimens mounted with strain gauges were always tested first. It was then possible to notice the time elapsed before stable readings were observed when the load applied in increments of 2 kN at all load levels. The remaining 5 specimens were tested in the same manner as the first specimens. A complete test took approximately 30 min. depending on the total amount of load increments and when stable strain gauge readings were observed along the splice.

The strain gauges were monitored by the same Hewlett Packard system as described in section 2.3.2.4. The load at failure of all specimens were read directly on the test machine indicator.

2.5 G_F-tests

2.5.1 General

These series were designed primarily to investigate if the fracture energy parameter, G_F, has an effect on the strengths of overlapped splices. A special test-rig was developed in order to determine G_F for the concrete used in this test program and is described in the following sections.

A total of 160 G_F-specimens were tested during the test program.

2.5.2 G_F-specimens

2.5.2.1 Controlled Variables

The only experimental variable in these series was the concrete compressive strength and the following gives a brief summary of the compressive strengths and number of tests.

1) 36 G_F-specimens produced from high strength concrete with intended compressive strength at the 90 MPa level were tested.

2) 40 G_F-specimens produced from high strength concrete with intended compressive strength at the 70 MPa level were tested.

3) 30 G_F-specimens produced of medium strength concrete with intended compressive strength at the 50 MPa level were tested.

4) 45 G_F-specimens produced of normal strength concrete with intended compressive strength at the 30 MPa level were tested.

2.5.2.2 Specimen Dimension

G_F-specimens were shaped like a beam with total length 400 mm, height 60 mm and depth 40 mm. It was necessary to grind the trowelled side of the specimens so that this side and the one opposite were parallel. A notch of 2 mm width and 10 mm depth was cut with a diamond saw in the middle of the specimen in the opposite side to the trowelled side. As a consequence of the grinding of the trowelled side, the height of the G_F-specimens varied when ready for testing. Fig. 2.19 shows the geometry of the G_F-specimens.

2.5.2.3 Casting and Curing

Casting: Specimens were cast in a horizontal position. 6 specimens were cast in one form which was made of 12 mm thick plywood. A vibrator table was used to compact the concrete and once the placing was completed, the exposed side was carefully trowelled to avoid too much grinding later on as described in the previous section.

Curing: Approximately 24 hours later the forms were removed and the specimens were cured 7 days in water and 28 days at 20°C and 60 % RH.

2.5.3 Test-rig and Procedure

2.5.3.1 Test-rig

The G_F-specimens were tested in a three-point bending mode. The measurements were taken as load displacement traces using a closed-loop testing system supplied by Instron Limited, Buckinghamshire, England.

The Instron machine used was of type 6022 and the frame had a maximum load capacity of 10 kN with an axial stiffness of 50 kN/mm. The Instron machine was controlled by an Instron series 6000 Control Console. Special equipment was constructed and mounted on the Instron Three Point Bend Fixture with the anvil assembly connected to the load-cell. This equipment made it possible to mount two extensionmeters so that a deflection controlled test could be accomplished. Fig. 2.20 shows the test-rig and photo 2.6 shows the test-rig and a test specimen.

2.5.3.2 Procedure

Prior to the testing of the G_F-specimen the weight of each specimen was determined. When placed in the test rig, the load cell then carrying the test specimen was adjusted to zero reading, and the test could commence.

All tests were run in a deflection controlled way with a midspan deflection rate of 0.02 mm/min. on the ascending branch of the load-deflection curve, but the rate was changed to 0.04 mm/min. on the descending branch, when the load reading was approximately 20 % of the peak load reading.

The load was measured by the load cell and the mid-span deflections were measured by the two extensiometers. Both values were simultaneously recorded by the Instron series 6000 Control Console and sent to a connected IBM computer.

The area of the alignment was measured after the test was finished, and is defined as the projection of the fracture zone on a plane perpendicular to the beam axis.

3. EXPERIMENTAL RESULTS

3.1 Introduction

The main objectives of this chapter are to present and describe the experimental data so that a discussion of the experimental results can be made in chapter 4.

3.2 S.B.-tests

3.2.1 General

This section presents and describes the experimental data obtained from the S.B.-tests. The test data consists of strain measurements in the tensile bars and converted into load values by the calibration curves determined from each strain gauge as described in section 2.3.2.4.

The experimental data are therefore presented as follows:

1) Load values at failure in the longitudinal tensile reinforcing bars recorded from the strain gauges mounted outside the concrete and just outside the splice.

2) Load distribution along the splice at failure and at 80 %, 60 %, 40 % and 20 % of the failure load.

3) Photos of all S.B.-specimens at failure are shown (photos 3.1 to 3.21).

3.2.2 The Strength of Overlapped Splices

Strain measurements at failure recorded from strain gauges mounted in the tensile bars outside the concrete and just outside the splice is converted, via the calibration curves, into loads. These results are shown in Tables 3.1 and 3.2.

As mentioned in section 2.3.1. problems associated with strain hardening of the four tensile bars of S.B. 70/20 specimen occurred at failure of the specimen. The calibration curve of the strain gauges mounted in the bars outside the concrete and just outside the splice was thereby no longer valid. The calibration curve of each strain gauge was therefore expanded to loads higher than 135 kN following a curve of a shape as the typical strain hardening portion of the non-coldstretched reinforcing bar as shown in Fig. 2.6. It was then possible to convert the strain measurements from the test into loads and evaluate the test results.

Table 3.1 shows that load equilibrium at failure has been accomplished throughout the test series between load in the bars at the top (bars No. 1 and No. 2) and at the bottom (bars No. 3 and No. 4) of the specimens. The ratio between load in the bars at top and bottom of the specimens at failure varied from 0.9 to 1.17 and 1.02 was taken as an average throughout the test series.

Tables 3.1 and 3.2 show that the ratio between the average load at failure recorded in the bars outside the concrete and just outside the overlapped splice, varies from 1.01 to 1.25 and 1.10 was taken as an average throughout the test series.

The fact that the average load in the bars recorded just outside the splice at failure in general seems smaller than the recorded load outside the concrete could be explained by the presence and location of tensile cracks in the concrete just outside the splice.

If tensile cracks in the concrete just outside the splice is not occurring exactly at the strain gauges placed in the bars, there will be stresses in the concrete at the location of the strain gauges. This will result in a smaller recorded load value in the bars just outside the splice compared to the recorded value in the bars outside the concrete.

The presence of tensile stresses in the bars at the location of the strain gauges just outside the splice can be so dominating that the recorded load value at failure is even smaller than the recorded load value along the actual splice. This can be seen many times in the Fig. 3.1 to 3.22.

For the reasons mentioned above, observed results of the strength of overlapping splices determined from the recorded load value at failure in the bars just outside the splice, will be somewhat uncertain. In the following discussions the strength of overlapped splices is therefore determined from the recorded average load value at failure as recorded in the bars outside the concrete.

The strength of overlapped splices in Table 3.1 is expressed not only as an average load value recorded at failure in the bars outside the concrete, but also as an average shear stress at failure along the overlapped splice length, τ_u.

τ_u is determined from the following formula:

$$\tau_u = \frac{P_{ao}}{\pi \cdot d \cdot l_{sp}} \qquad (3.1)$$

where

τ_u : Ultimate average stress along the splice, calculated from the average load recorded at failure in the four tensile reinforcement bars outside the concrete.

P_{ao}: Average load recorded at failure in the four tensile reinforcement bars outside the concrete.

d : Diameter of the cold stretched tensile reinforcement, determined in section 2.2.2.3 to be 15.5 mm.

l_{sp}: The length of the overlapped splice.

3.2.3 Load and Shear Stress Distribution along the Splice Length

The Fig. 3.1 to 3.22 show the load distribution along the splice length in the tensile reinforcing bars of each test. On each figure is shown not only the load distribution at failure, but also the load distribution at 80 %, 60 %, 40 % and 20 % of the failure load recorded by the strain gauges mounted outside the concrete.

As described in section 2.3.2.4 only one of the four tensile reinforcing bars in each test specimen was mounted with strain gauges along the splice except for S.B. 70/15 where two of the four bars had strain gauges mounted along the splice. The results of the load distribution are shown in Fig. 3.12 and 3.13.

Fig. 3.14 shows the load distributions along the splice for the S.B. 70/12.5 specimen, but unfortunately 4 strain gauges placed at the end of the bar to be spliced were damaged during handling of the reinforcing arrangement into the form prior to casting of the concrete.

From the Fig. 3.1 to 3.22 it can be seen that the load recorded from the strain gauge placed just outside the splice in some cases is less than the load recorded from the strain gauge placed at the beginning of the splice. This is most likely caused (as described in section 3.2.2) by the formation of cracks perpendicular to the axis of the tensile bars in the vicinity of the strain gauge placed just outside the splice.

It can be seen from the Fig. 3.1 to 3.22 that the shear stress vary along the splice length, and that the shear variation is very pronounced at low loads, since the load distribution seems far from linear at low load along the splice length. This can be observed in cases of normal strength concrete (Fig. 3.1 to 3.10) as well as high strength concrete (Fig. 3.11 to 3.22). On the other hand the load distribution at failure seems practically linear along the splice length regardless of the concrete compressive strength and the splice length, indicating that the shear stress

are evenly distributed along the splice length. Furthermore, it can be seen from the Fig. 3.1 to 3.22 that the placement of the transverse reinforcement bars does not affect the linear shape of the load distribution at failure along the splice length.

By fitting a 1st degree polynomial expression to the load distribution along the splice length at failure it is possible to study the correctness of assuming an evenly shear stress distribution along the splice length.

Table 3.3 gives the coefficient of variation defined as the ratio between the standard deviation of the recorded values of load compared to the fitted curve and the average recorded load along the splice length.

From Table 3.3 it can be seen that the coefficient of variation varies from 3.32 % to 22.0 %. The high value of the coefficient of variation obtained from the S.B. 90/07.5 test result is caused by insufficient shear stresses at the beginning of the splice (see Fig. 3.21). As a result the load distribution curve at failure in the case of S.B. 90/07.5 test is far from linear, causing the high value of the coefficient of variation. The cause was that the araldit used to fill the grooves covered not only the grooves but also the entire surface of the bar so that the surface becomes very smooth.

From Table 3.3 the coefficient of variation taken as an average is 8.2 % excluding the test result from the S.B. 90/07.5 specimen.

The above observations suggest that the shear stress at failure for most practical purposes can be considered evenly distributed along the splice regardless of the concrete compressive strength. It seems, however, that the even distribution of shear stress along the overlapped splice length is more distinct the longer the splice. This is illustrated in Fig. 3.23 where the coefficient of variation is shown as a function of the overlapped splice length.

From Fig. 3.23 it can be seen that the coefficient of variation seems to decrease as the overlapped splice length increases regardless of the concrete compressive strength level.

3.3 EF.-tests

3.3.1 General

This section presents and describes the experimental data obtained from the EF.-tests. The test data consists of failure load recorded from the indicator of the testing machine and strain measurements along the anchorage length in the tensile reinforcing bar. The strain measurements in the bar are converted into loads by the calibration curve as described in section 2.4.2.4.

The experimental data is presented as follows:

1) Failure load of all test specimens recorded from the indicator of the test machine

2) Load distribution along the anchorage length at failure and 80 %, 60 %, 40 % and 20 % of the failure load.

3.3.2 The Anchorage Strength

The average load applied at failure of six identical EF.-specimens by the testing machine is given in Table 3.4 together with the calculated ultimate average shear stress, τ_u, along the anchorage length. The ultimate average shear stress is calculated by the following formula:

$$\tau_u = \frac{P_a}{\pi \cdot d \cdot l_a} \qquad (3.2)$$

where

P_a: Average load applied at failure by the testing machine.

d : Diameter 15.5 mm of the steel used in the anchoring, see section 2.2.2.3

l_a: Anchorage length.

As noted in Table 3.4 no results are given from the EF. 90/12 and EF. 70/12 test series since the anchorage strength exceeded that of the tensile reinforcing bar. Furthermore, it can be observed that two series of EF. 90/10 and EF. 70/10 are carried out due to damaged strain gauges in the first series.

3.3.3 Load and Shear Stress Distribution along the Anchorage Length

Fig. 3.24 to 3.34 show the load distribution along the anchorage length in the tensile reinforcing bar. On each figure is shown not only the load distribution at failure, but also the load distribution at 80 %, 60 %, 40 % and 20 % of the failure load, all recorded on the strain gauge placed outside the concrete.

It can be seen from the Fig. 3.24 to 3.34 that the shear stress varies along the anchorage length, and that the shear variation is very pronounced at low loads as the load distribution seems far from linear at low loads. This is observed in cases of normal strength concrete (Fig. 3.24 to 3.29) as well as high strength concrete (Fig. 3.30 to 3.34).

At failure the load distribution along the anchorage length seems practically linear regardless of the compressive strength of the concrete and of the anchorage length. Two tests do not show this linear shape of the load distribution at failure, EF. 50/10 and EF. 90/07.5, an explanation has not been found.

In order to study the correctness of assuming evenly shear stress distribution along the anchorage length at failure, a 1st degree polynomial expression was fitted to the load distribution curve. In Table 3.5 is given the coefficient of variation defined in section 3.2.3. Taken as an average throughout the test series, this coefficient is 7.64 %.

It must therefore be reasonable to conclude that the shear stress can be considered evenly distributed along the anchorage length regardless of the anchorage length and concrete compressive strength.

Fig. 3.35 shows the coefficient of variation as a function of the anchorage length and the intended compressive strength. From the figure it can be seen that the coefficient seems to decrease as the anchorage length increases.

3.4 G_F-Tests

3.4.1 General

This section presents and describes the experimental data obtained from the G_F-tests. The test data consists of load-deflection curves for each test and from these the fracture energy G_F is calculated. The calculation of the fracture energy is described in the following section while the experimental results are described in section 3.4.3.

3.4.2 The Fracture Energy G_F of Concrete

The fracture energy G_F is calculated by the following formula derived by considering the test-rig arrangement and using Hillerborg [20] and Petersson [29].

$$G_F = (W_o + m_t \cdot g - \delta_o)/A_{lign} \qquad (3.3)$$

where

W_o: Area below the recorded load-deflection curve

m_t: Weight of the test specimen

g: Acceleration due to gravity, 9.81 m/s^2

δ_o: Central deflection of test specimen when the applied load has descended to 0 and final rupture occurs.

A_{lign}: Area of the alignment, defined as the projection of the fracture zone on a plane perpendicular to the beam axis.

3.4.3 G_F and Corresponding Concrete Strength

Fig. 3.36 to 3.68 show the load-deflection curves of all tests. Using the above mentioned formula, the average fracture energy G_F of each batch is calculated and given in Table 3.6 together with the standard deviation.

Fig. 3.69 shows the average value of the fracture energy G_F and corresponding compressive strength value of the concrete for each batch. Also shown in Fig. 3.69 is a tendency curve which is a fitted quadratic polynomial using regression analysis. From Fig. 3.69 it can be seen that an increase in concrete compressive strength results in an increase of the fracture energy, G_F, up to 70 MPa. The favourable influence of the concrete compressive strength is then lost and even becomes negative.

Fig. 3.70 shows the average value of the fracture energy G_F and corresponding splitting strength values of the concrete for each batch. A tendency line obtained by regression analysis of a quadratic polynomial is also shown. From Fig. 3.70 it can be seen that an increasing concrete splitting strength has a favourable influence on the fracture energy G_F up to the 5 MPa level and then appears to become negative.

Based on experimental results from a large number of investigations, Hillerborg [21] concluded that the value of G_F depends on the size of the test specimen, composition of concrete, curing conditions, age etc. in a way which so far is not known in detail. The experimental results of the fracture energy presented in this report is based on test-specimens, test-rig and procedure not similar to previous investigations. As a consequence of this and the conclusions by Hillerborg [21], the present test results are therefore not compared to other investigations.

4. DISCUSSION OF THE EXPERIMENTAL RESULTS

4.1 Introduction

Based on the experimental results of the strength of overlapped tensile splices, the effects of increasing concrete strength and splice length are discussed in the following sections. The experimental results are also compared to the empirical formula of Orangun et al. [23], the theoretical model of Andreasen [24] and the Danish Code DS 411 [25] in order to study the application of these on splices in high strength concrete.

Furthermore, the effects of increasing concrete strength and anchorage lengths on the anchorage strengths observed from the recorded pull-out tests are also discussed. The theory of plasticity is applied to the experimental results from the pull-out tests in order to develop a model capable of estimating the anchorage strength.

Finally, a comparison between the S.B.-tests and EF.-tests is made in the last section.

4.2 S.B.-tests

4.2.1 Discussion of Parameter Effects

Fig. 4.1 shows the experimental results illustrated by τ_u/f_c as a function of l_{sp}/d. From this figure it can be seen that τ_u/f_c appears to increase for decreasing l_{sp}/d-values regardless of the concrete compressive strength level. Furthermore, it appears that the concrete compressive strength taken to the first power does not seem to be a governing parameter for the strength of overlapped splices as the different compressive strength levels are very clearly divided in the τ_u/f_c - l_{sp}/d illustration.

This result supports a large experimental investigation carried out by Tepfers [13] who conducted beam tests with overlapped splices in normal strength concrete. Tepfers found that τ_u/f_c-values decrease as l_{sp}/d-values increase and explained this phenomenon by unevenly shear stress distribution along especially short splices. The present investigation supports the explanation of Tepfers and is shown in Fig. 3.23 where an assumption of evenly shear stress distribution along an overlapped splice at failure becomes more justified as the splice length increases.

Another illustration of the experimental results is shown in Fig. 4.2 where τ_u/f_{sp} is given as a function of l_{sp}/d. As shown in Fig. 4.2 - which also could be seen in Fig. 4.1 τ_u/f_c-values increase as l_{sp}/d-values decrease regardless of the concrete compressive strength.

By comparing Fig. 4.1 and Fig. 4.2 it is seen that the concrete splitting strength taken to the first power appears to be a more governing property to the strength of overlapped splices than the concrete compressive strength because the different concrete compressive strength levels are divided to a smaller degree shown in Fig. 4.2 than shown in Fig. 4.1.

This result is consistent with the common assumption that bond strength varies with $\sqrt{f_c}$, see Chinn et al. [9] and Chamberlin [11].

A third illustration of the experimental results is shown in Fig. 4.3 where τ_u/G_F is shown as a function of l_{sp}/d. From Fig. 4.3 it seems clear that the influence of l_{sp}/d-values on τ_u/G_F- values shows the same characteristics as in Fig. 4.1 and Fig. 4.2.

Furthermore, Fig. 4.3 shows that the fracture energy of concrete taken to the first power appears to be a property of concrete governing the strength of overlapped splices to a considerably larger degree than the concrete compressive strength and the concrete splitting strength.

In conclusion, the fracture energy of concrete appears to be a property which has not only a strong influence on the anchorage strengths of bars in pull-out tests as indicated by Olsson [22], but also a strong influence of the strength of overlapped splices in normal as well as high strength concrete.

4.2.2 Comparison of the Test Results with the Theoretical Model of Andreasen [24]

The theory of plasticity is used by Andreasen [24] to develop expressions from which the strength of overlapped splices can be estimated. The material properties of concrete do, however, not fulfill the conditions of the plasticity theory and therefore modification factors known as factors of effectiveness are introduced.

The factors of effectiveness are introduced in such a way the that concrete is considered to be a material having plastic strengths instead of the normal strengths. The plastic strengths are reduced in proportion to the normal strengths by factors of effectiveness. The plastic uniaxial compression and tensile strengths can then be written as

$$f_{cp} = \nu \cdot f_c \tag{4.1}$$

$$f_{tp} = \rho \cdot f_c \tag{4.2}$$

where

f_c: Uniaxial compressive strength measured by a standard compression test on a cylinder.

f_{cp}: Plastic uniaxial compressive strength of concrete.

f_{tp}: Plastic uniaxial tensile strength of concrete.

ν: Factor of effectiveness for compression.

ρ: Factor of effectiveness for tension.

Andreasen [24] has suggested a simple formula for estimating the strength of overlapped splices in which the ratio ρ/ν is set to 0.1 and where ν is a function of the concrete compressive strength. The following formula is suggested by Andreasen:

$$\nu = 2.9/\sqrt{f_c} \qquad (4.3)$$

The simple formula for estimating the strength of overlapped splices consists of three parts:

- Local failure immediately around the reinforcing bar
- Failure in the surroundings
- Complete failure which includes all bars in the section

Two in principle different types of local failure may occur, named failure shape 1 and failure shape 2. The decisive failure shape is determined by the surroundings and the geometry of the deformations on the reinforcement. The two dimensionless rib parameters, D and F, are of importance. They are given by:

$$D = \frac{(d+h_d)\cdot h_d}{2\cdot d\cdot a} \tag{4.4}$$

$$F = \frac{1}{2} + \frac{h_d}{d} \tag{4.5}$$

where the symbols are explained in Fig. 4.4.

The expression for the local failure is given below:

$$\frac{\tau_u}{f_c} = \text{min of} \begin{cases} \frac{D\cdot\nu}{4}\cdot\left[3\cdot\left[1+\frac{C\cdot\nu}{D\cdot\nu}\right]+5\cdot\sqrt{1+2\cdot\frac{C}{D\cdot\nu}}\right] \\ \frac{F\cdot\nu}{40}\cdot\left[1+\sqrt{1+2400\cdot\frac{C}{F\cdot\nu}}\right] \end{cases} \tag{4.6}$$

where the upper expression is valid for failure shape 1 and the lower is valid for failure shape 2. τ_u is the ultimate average shear stress along the overlapped splice, ν is the effectiveness factor, and C is the dimensionless internal work from the surroundings.

For $\frac{F}{D}$ less than 8 the expression for failure shape 2 should be used while for $\frac{F}{D}$ larger than 8, the smaller of the expression must be used.

The dimensionless internal works from the surroundings are in Andreasen [24] suggested to be based on a mechanism named plate mechanism which yields a satisfactory agreement when compared to existing test results mainly with concrete in normal strength range. The expression can be written:

$$C = \frac{1}{2\cdot\pi\cdot n_{sp}}\cdot\left[\nu\cdot\frac{b\cdot s}{d\cdot l_{sp}} + n_{ss}\cdot\psi\right] \tag{4.7}$$

The geometrical parameters, b, s, d and l_{sp} are shown in Fig. 4.5. n_{sp} is the number of overlapped splices in the section, n_{ss} is the number of stirrups, and ψ is the reinforcement degree of the surrounding reinforcement. ψ is defined as:

$$\psi = \frac{\frac{\pi}{4} \cdot d_s^2 \cdot f_{ys} \cdot n_s}{d \cdot l_{sp} \cdot f_c} \qquad (4.8)$$

where d_s is the diameter of the surrounding reinforcement, f_{ys} is the yield strength of the surrounding reinforcement, and ns is the number of stirrups over the overlapped length. The above simple expression for estimating the strength of overlapped splices has been compared by Andreasen [24] to 333 test results with and without surrounding reinforcement. The tests used for the comparison cover the following range of the parameters:

$\frac{s}{d} \in [0.81;6.50]$, $\frac{b}{d} \in [4.8;44.0]$

$\psi \in [0.0;1.978]$, $\frac{l_{sp}}{d} \in [8.3;\ 82.5]$

$D \in [0.030;0.089]$, $\frac{\tau_u}{f_c} \in [0.038;0.533]$

$F \in [0.54;0.61]$, $f_c \in [6.00;94]$ MPa

$\tau_u \in [1.0;8.5]$ MPa , $n_{sp} \in [1;6]$

$n_{ss} \in [0;12]$

Fig. 4.6 - 4.9 show the achieved τ_u/f_c-values from the tests presented in this report and calculated τ_u/f_c-values using the above described expression where D and F for the coldstretched reinforcement has been measured to be 0.089 and 0.59, respectively.

From the Fig. 4.6 - 4.7 it is seen that in case of high strength concrete the original theory of Andreasen [24] seems to overestimate the value of τ_u/f_c, i.e. the strength of the overlapped splice. While in use of normal strength concrete (Fig. 4.8 - 4.9), the calculated values of τ_u/f_c seem to be a reasonable good estimate.

Based on the above comparison between test results and estimated values of τ_u/f_c it can now be concluded that the expressions suggested by Andreasen [24] need to be modified in cases of overlapped splices in high strength concrete.

It should be noted that the expressions suggested by Andreasen are based on tests where only 4.2 % are tests with concrete compressive strengths larger than 50 MPa and that these tests originate from Tepfers [13] who used large quantities of cement and no superplasticizer to produce higher strength concrete which is uncommon in todays production of high strength concrete.

Assuming that $\rho/\nu = 0.1$ is a reasonable estimate also for high strength concrete, a new expression for estimating the value ν is now suggested below for concrete compressive strengths larger than 50 MPa and based on the experimental results presented in this report.

$$\nu = \begin{cases} 2.9/\sqrt{f_c} \ , & f_c < 50 \text{ MPa} \\ 0.65 - 0.0048 \cdot f_c \ , & 50 \text{ MPa} \leq f_c < 100 \text{ MPa} \end{cases} \qquad (4.9)$$

The above suggested ν-expression for concrete compressive strength larger than 50 MPa is based on the assumption that $\nu = k_1 + k_2 \cdot f_c$.

The values of k_1 and k_2 are obtained by requiring continuity to the original ν-expression for f_c = 50 MPa and correspondence between test and theory using the load ratio test/theory as a measure of correspondence. The mean value and the standard deviation on the ratio test/theory for 13 tests with f_c > 50 MPa are found to be 1.006 and 0.088, respectively.

The correspondence between test and theory is satisfactory as can be seen in Fig. 4.10 which shows the correspondence for all 21 tests.

Fig. 4.11 - 4.14 show the obtained τ_u/f_c estimates using the suggested modification of the ν-expression. As can be seen in the Fig. 4.11 - 4.14 the modification of the ν-expression gives satisfactory estimates of the τ_u/f_c-values in case of concrete compressive strength larger than 50 MPa.

4.2.3 Comparison of the Test Results with the Empirical Formula of Orangun et al. [23]

An empirical equation has been developed by Orangun et al. [23] for calculating the strength of overlapped splices of deformed bars. The equation is based on a non-linear regression analysis of tests results obtained in the United States. The empirical formula reflects the effect of the overlapped length, concrete cover, spacing between bars, bar diameter, concrete compressive strength and transverse reinforcement.

The best fitting curve was found by Orangun et al. to be:

$$\frac{\tau_u}{\sqrt{f_c}} = 0.1 + 0.27\cdot\frac{c_{min}}{d} + 4.4\cdot\frac{d}{l_{sp}} + \frac{1}{41.5}\cdot\frac{A_{tr}\cdot f_{ys}\cdot n_s}{l_{sp}\cdot d} \qquad (4.10)$$

where

τ_u: The ultimate uniformly distributed shear stress along the splice.

f_c: Uniaxial concrete compressive strength of ø150 mm cylinders measured in MPa.

c_{min}: The minimum of (1) the clear bottom cover or (2) half the clear spacing between the next adjacent splice.

d: Nominal bar diameter.

l_{sp}: Splice length.

A_{tr}: Cross sectional area of the transverse reinforcement which has an angle of 90 degrees with the failure surface.

f_{ys}: Yield strength of the transverse reinforcement.

n_s: The number of transverse reinforcing bars over the splice length.

Using the empirical equation of Orangun et al. on the present tests makes it possible to compare computed τ_u-values with experimentally obtained values. This comparison is shown in Fig. 4.15 where it can be seen that the computed values seem to be conservative in case of normal strength concrete, but slightly unconservative in the case of high strength concrete with compressive strength in the range of 86 - 99 MPa.

In Orangun et al. [23] the empirical equation was compared to a major experimental study reported by Tepfers [13]. Results of the comparison showed that the average ratio between measured and computed ultimate shear stresses for 92 tests were 1.18. This was explained by the deformed bars used in the tests by Tepfers which differed from those normally used in the United States.

The deformed bars used in the experimental tests reported in this report are very similar to the deformed bars used by Tepfers.

Taking the above into account and considering Fig. 4.15 it can be concluded that the equation of Orangun et al. seems to overestimate the ultimate shear stress capacity of overlapped splices in high strength concrete.

4.2.4 Comparison of the Test Results with the Danish Code DS 411

In the Danish code of practice for the structural use of concrete, DS 411 [25], the length of overlapped splices of deformed reinforcing bars is determined by:

$$\frac{l_{sp}}{d} \geq \begin{cases} \dfrac{0.09 \cdot f_{ys}}{\zeta \cdot f_t} & \text{Rule 1} \\ \dfrac{30}{\zeta} & \text{Rule 2} \end{cases} \qquad (4.11)$$

where the greater of the two values of l_{sp}/d should be taken. In the formulas d is the diameter of the bar, ζ is the anchorage factor, f_{ys} is the yield or 0.2 per cent proofstress of the reinforcement and f_t is the tensile strength of the concrete. The above formula can be rewritten:

$$\tau_u \leq \begin{cases} \dfrac{\zeta \cdot f_t}{0.36} & \text{Rule 1} \\ \dfrac{\zeta \cdot f_{ys}}{120} & \text{Rule 2} \end{cases} \qquad (4.12)$$

In DS 411 [25] a relationship between f_t and f_c is given to be

$$f_t = \sqrt{f_c/10} \qquad (4.13)$$

where f_t and f_c are measured in MPa.

Assuming that $\zeta = 0.8$ which conforms to an anchorage factor for ribbed hot-rolled high yield bars and assuming that $f_{ys} = 649$ MPa conforming to the yield stress of the spliced reinforcement of the tests, the formulas for calculating τ_u-values according to DS 411 can now be written as:

$$\tau_u \leq \begin{cases} 0.703 \cdot f_t & \text{Rule 1} \\ 4.33 \text{ MPa} & \text{Rule 2} \end{cases} \qquad (4.14)$$

It should be mentioned that the smaller of the two values of τ_u should be taken in the design and that the Danish code of practice assumes that the splice is provided with a certain amount of transverse reinforcement in order to ensure a sufficient capacity of the splice.

In DS 411 the amount of transverse reinforcement is given by the distance, s, between stirrups along the overlapped length. The Danish code states that:

$$s \leq 55 \cdot \frac{d_s^2}{d} \qquad (4.15)$$

where

d_s: Diameter of the stirrup bar.

d: Diameter of the bars being spliced.

In the test presented in this report the amount of transverse reinforcement conforms to the amount suggested in the Danish code of practice. It is therefore possible to compare computed values from DS 411 with experimentally obtained results.

Fig. 4.16 - 4.19 show τ_u-values obtained from the tests and computed values from DS 411. As can be seen from the figures the test results are always larger than the computed τ_u-values and that the values found by rule 2 is the smallest except for the S.B 30/30 test.

Taking the above into account and considering Fig. 4.20 it can now be concluded that using the Danish code for the design of overlapped splices in high strength concrete will yield more conservative results than in case of normal strength concrete.

Fig. 4.21 shows the ratio between test τ_u-values and τ_u-values computed from DS 411, rule 1, as a function of l_{sp}/d. From this figure it can be seen that using DS 411 rule 1 yields τ_u-values which seem to be slightly unconservative in case of overlapped splices in high strength concrete when comparing to normal strength concrete.

4.3 EF.-Tests

4.3.1 Discussion of Parameter Effects

In Fig. 4.22, 4.23 and 4.24 the experimental results are illustrated by τ_u/f_c, τ_u/f_{sp} and τ_u/G_F-values as a function of l_a/d.

From Fig. 4.23 it appears that τ_u/f_{sp}-values decrease as the l_a/d-values increase regardless of the concrete compressive strength which is consistent with the result obtained from the S.B.-tests, but to a smaller degree (see Fig. 4.2). The same tendency appears, however, doubtful in case of τ_u/f_c-values and τ_u/G_F-values as illustrated in Fig. 4.22 and 4.24.

By comparing the Fig. 4.22, 4.23 and 4.24 it seems difficult to reach a clear conclusion regarding which material property is the most covering property on the τ_u-values in EF.-tests.

This may be explained by the spiral sockets used in the EF.-test specimens as transverse reinforcement. The spiral sockets provide a very good confinement of the concrete which surrounds the anchored reinforcing bar. The confined concrete in the EF.-test specimens may be the cause for the above mentioned inconsistency of the obtained experimental results.

4.3.2. The Theory of Plasticity applied to the Test Results

The theory of plasticity has been applied in this section to the EF.-test results in order to develop an expression that estimates the anchorage strength of bars in EF.-specimens. The principles of developing an expression conform to the principles used by Andreasen [24].

The expression consists of the following three parts:

- Local failure immediately around the reinforcing bar
- Failure in the surroundings
- Complete failure

The same two in principle different types of local failure as suggested by Andreasen [24] are used. These are named failure shape 1 and failure shape 2 and are given in (4.16).

$$\frac{\tau_u}{f_c} = \min \text{ of } \begin{cases} \frac{D\cdot\nu}{4}\cdot\left[3\cdot\left[1+\frac{C\cdot\nu}{D\cdot\nu}\right]+5\cdot\sqrt{1+2\cdot\frac{C}{D\cdot\nu}}\right] \\ \frac{F\cdot\nu}{40}\cdot\left[1+\sqrt{1+2400\cdot\frac{C}{F\cdot\nu}}\right] \end{cases} \quad (4.16)$$

where the upper expression is valid for the failure shape 1 and the lower expression is valid for failure shape 2.

τ_u is the ultimate average shear stress along the anchorage length and ν is the effectiveness factor for compression. D and F are the dimensionless rib parameters described in section 4.2.2. and C is the dimensionless internal work from the surroundings.

Based upon the observed failure modes of the EF.-test specimens the following failure mechanism is suggested to calculate the dimensionless internal work C.

Fig. 4.25 illustrates the suggested failure mechanism. Using the symbols shown in Fig. 4.25 the following expression for the internal work is obtained:

$$W_i = 2\cdot a\cdot l_a\cdot\rho\cdot f_c\cdot 2 + 2\cdot f_{ys}\cdot A_{ss}\cdot n_s\cdot\cos(\beta)$$

where

ρ: Factor of effectiveness for tension

f_c: Concrete compressive strength

f_{ys}: Yield strength of the spiral reinforcement

A_{ss}: Cross sectional area of spiral reinforcement

n_s: Number of spirals over the anchorage length.

According to Andreasen [24] the dimensionless work, C, is then defined as:

$$C = \frac{W_i}{\pi \cdot d \cdot l_a} = \frac{1}{\pi} \cdot \left[4 \cdot \frac{a}{d} \cdot \rho + 2 \cdot \psi \cdot \cos(\beta) \right] \qquad (4.17)$$

where

$$\psi = \frac{f_{ys} \cdot A_{ss} \cdot n_s}{d \cdot l_a} \qquad (4.18)$$

By assuming that $\rho/\nu = 0.1$ and $\nu = k/\sqrt{f_c}$ which conforms to Andreasen [24]. The expression for C can be written as:

$$C = \frac{1}{\pi} \cdot \left[0.4 \cdot \frac{a}{d} \frac{k}{\sqrt{f_c}} + 2 \cdot \psi \cdot \cos(\beta) \right] \qquad (4.19)$$

where ν is the effectiveness factor for compression and k is a constant.

The test results are compared to the above theory in order to obtain the value of k using the load ratio test/theory as a measure of correspondence. The comparison of theory and test results showed that using

$$\nu = 3.47/\sqrt{f_c}\ , \quad 19\ \text{MPa} \leq f_c < 94\ \text{MPa}$$

yields a satisfactory agreement between theory and tests as indicated in Fig. 4.26. The mean value and the standard deviation on the ratio test/theory for 14 tests are found to be 1.0001 and 0.054, respectively. The satisfactory agreement between theory and test results is also illustrated in the Fig. 4.27 - 4.31.

The above relationship between ν and f_c corresponds to what is found in many other cases where concrete structures are treated by using the theory of plasticity, see Andreasen [24], section 2.2.

4.4 S.B.-tests compared to EF.-tests

Fig. 4.31 shows the test results obtained from the EF.-tests and S.B.-tests. As can be seen in Fig. 4.31 the τ_u-values from the EF.-tests are considerably larger than the corresponding τ_u-values from the S.B.-tests.

The reason for this is partly the surrounding spiral reinforcement in the EF.-test specimens which confines the concrete around the anchored bar to a higher degree than the strirrups in the S.B.-test specimens and that the failure mechanism is completely different in the EF.-tests compared to the S.B.-tests. This is reflected in the theoretical models described in sections 4.2.2 and 4.3.2 where different formulas are suggested to calculate the total dimensionless internal work, C, which consists of contributions from concrete and surrounding reinforcement.

Fig. 4.32 shows for all EF.-tests and S.B.-tests the calculated values of τ_u/f_c and the corresponding total dimensionless internal work, C. As can be seen in Fig. 4.32 the values of C in case of EF.-tests are generally larger than S.B.-tests and results in the larger τ_u/f_c-values.

5. CONCLUSION

The following conclusions can be made from the investigation presented in this report:

1) The compressive strength of normal - and high strength concrete has been determined by ø100 x 200 mm and ø150 x 300 mm cylinders. The ratio between compressive strength determined from ø150 and ø100 mm cylinders appears to be 0.95 regardless of the concrete compressive strength level.

2) The formula $f_{sp} = 0.527 \cdot \sqrt{f_c}$ which estimates the concrete splitting strength in case of normal strength concrete seems to underestimate the concrete splitting strength in case of high strength concrete.

3) Corresponding values of concrete compressive strength, splitting strength and fracture energy, G_F, have been obtained for normal - and high strength concrete. The test results indicate that an increase in compressive strength results in an increase of the fracture energy up to the 70 MPa level. The favourable influence of the concrete compressive strength was then lost and even became negative. The same tendency was also observed when comparing corresponding splitting strength and fracture energy where the favourable influence of increasing splitting strength was present only up to the 5 MPa level.

4) Tests with overlapped tensile splices in normal- and high strength concrete in regions of pure bending have been carried out. These tests indicate that shear stress at failure for most practical purposes may be considered as evenly distributed along the splice length, regardless of the concrete compressive strength. It appears, however, that even distribution of shear stress along the splice at failure becomes more di-

stinct the longer the splice. Furthermore, the tests indicated that the fracture energy of concrete appears to be a more governing property to the strength of splices than the compressive strength and splitting strength.

5) τ_u/f_c-values from the tests with overlapped tensile splices in normal - and high strength concrete have been compared to estimated values from a theoretical model developed by Andreasen [24] which is based on the theory of plasticity and tests with concrete in the normal strength range. The comparison showed that the model developed by Andreasen overestimates the τ_u/f_c-values in case of high strength concrete. A modification to the ν-expression used in the model is suggested and given below:

$$\nu = \begin{cases} 2.9/\sqrt{f_c} \ , & f_c < 50 \text{ MPa} \\ 0.65 - 0.0048 \cdot f_c \ , & 50 \text{ MPa} \leq f_c < 100 \text{ MPa} \end{cases}$$

6) $\tau_u/\sqrt{f_c}$-values from the tests with overlapped tensile splices have also been compared to estimated values using an empirical formula developed by Orangun et al. [23]. The comparison showed that the empirical formula overestimated the $\tau_u/\sqrt{f_c}$- values for splices in high strength concrete.

7) The results from the tests with overlapped splices have been compared to the Danish code of practice for the structural use of concrete, DS 411. The comparison showed that using the Danish code for the design of overlapped splices in high strength concrete will yield more conservative results than in case of normal strength concrete.

8) Pull-out tests of tensile reinforcement in spiral sockets in normal - and high strength concrete have been carried out. Just like the tests with overlapped splices theses tests indicated that shear stress at failure for most practical purposes

may be considered as evenly distributed along the anchorage length regardless of the concrete strength, and that even distribution for shear stress becomes more distinct the longer the anchorage length.

9) No clear conclusion could be reached from the pull-out tests regarding which concrete property (compressive strength, splitting strength and fracture energy) is the most governing property on the anchorage strength. This may be explained by the spiral sockets which provide a very good confinement of the concrete which surrounds the anchored bar.

10) A model is suggested for calculating the anchorage strength of tensile reinforcement in spiral sockets in normal - and high strength concrete, and is based on the theory of plasticity and the principles suggested by Andreasen [24]. The model which yields satisfactory results in case of normal - and high strength concrete reflects a suggested failure mechanism of the pull-out test specimen and the following ν-expression:

$$\nu = 3.47/\sqrt{f_c},\ 19\ \text{MPa} \leq f_c < 94\ \text{MPa}$$

11) τ_u-values obtained from the tests with overlapped splices and the pull-out tests are compared. The comparison indicates that τ_u-values from pull-out tests are considerably larger than corresponding τ_u-values from tests with overlapped splices regardless of the concrete compressive strength. The reaso for this is partly the surrounding spiral reinforcement in the pull-out test specimens which confine the concrete around the anchored bar and that the failure mechanism is completely different in the pull-out tests when compared to the tests with overlapped splices.

6. REFERENCES

[1] "Utilization of High Strength Concrete", Proceedings from symposium held in Stavanger, Norway, June 15/18 1987, Tapir Publishers 1987

[2] ACI Committee 363, "State-of-the-Art Report on High Strength Concrete", ACI Journal, Proceedings V. 811, No. 4, July-August 1984, pp. 364-411

[3] Hoff, A., "Materialeegenskaber og konstruktiv opførsel. Et "State-of-the-Art" studie, Report No. STF65 A83033, Cement and Concrete Research Institute (SINTEF div. FCB), Trondheim-NTH, May 1983, pp. 36 (in Norwegian)

[4] Tomaszewicz, A., "Heftforsøk", Report No. STF65 A86086, Cement and Concrete Research Institute (SINTEF div. FCB), Trondheim-NTH, December 1986, pp. 42 (in Norwegian)

[5] Efsen, A., "Spiral Socket Splices for Deformed Bars", Bygningsstatiske Meddelelser, Nr. 1, 1957. (in Danish)

[6] Ferguson, P.M., and Thompson, J.N., "Development Length of High Strength Reinforcing Bars in Bond", Journal of the American Concrete Institute. Proc. Vol. 59-2, 1962, pp. 887-917.

[7] Ferguson, P.M., and Thompson, J.N., "Development Length for Large High Strength Reinforcing Bars", Journal of the American Concrete Institute, Proc. Vol. 62-1, 1965, pp. 71-93.

[8] Østlund, R., "Studium av förankrings- og sprickproblem hos balkar armerade med Ks 60", Institutionen för Byggnadsteknik, CtH, Göteborg, 1962. (in Swedish)

[9] Chinn, H., Ferguson, P.M., and Thompson, J.N., "Lapped Splices in Reinforced Concrete Beams", Journal of the American Concrete Institute, Proc. V. 52, October 1955

[10] Ferguson, P.M., and Breen, J.E., "Lapped Splices for High Strength Reinforcing Bars", Journal of the American Concrete Institute, Proc. Vol. 62, September 1965

[11] Chamberlin, S.J., "Spacing of Spliced Bars in Beams", Journal of the American Concrete Institute, Proc. Vol. 54, February 1958.

[12] Ferguson, P.M., and Krishnaswamy, C.N., "Tensile Lap Splices - Part 2: Design Recommendations for Retaining Wall Splices and Large Bar Splices", Research Report 113-3, Center for Highway Research, The University of Texas at Austin, April 1971.

[13] Tepfers, R., "A Theory of Bond applied to Overlapped Tensile Reinforcement Splices for Deformed Bars", Publication 73:2, Division of Concrete Structures, Chalmers Teknisk Högskola (Chalmers University of Technology), Göteborg, Sweden

[14] Mains, R.M., "Measurement of the Distribution of Tensile and Bond Stress along Reinforcement Bars", Journal of the American Concrete Institute, Proc. Vol. 48, 1952, pp. 225-252.

[15] Matley, R.G., and Watstein, D., "Investigation of Bond in Beam and Pull-Out Specimens with High-Yields-Strength Deformed Bars", Journal of the American Concrete Institute, Vol. 57-2, 1961, pp. 1071-1080.

[16] Perry, E.S., and Thompson, J.N., "Bond Stress Distribution of Reinforcing Steel in Beams and Pull-Out Specimens", Journal of the American Concrete Institute, Vol. 63-2, 1966, pp. 865-875

[17] Jensen, J.H., "Forkammede Armeringsstængers Forankring Specielt ved Vederlag", 2. Del, Serie R No. 155, Department of Structural engineering, Technical University of Denmark, 1982

[18] Rathkjen, A., "Forankringsstyrke af Armeringsjern ved Bjælkeunderstøtninger", Rap. 7203, DIA-B, Aalborg, 1972 (in Danish)

[19] Thompson, M.A., Jirsa, J.O., Breen, J.E., and Meinheit, D.F., "The Behavior of Multiple Lap Splices in Wide Sections", Research Report 154-1, Center for Highway Research, The University of Texas at Austin, February 1975

[20] Hillerborg, A., "The Theoretical Basis of a Method to Determine the fracture Energy G_F of Concrete", Materiaux et Constructions, Vol. 18, No. 106, 1985

[21] Hillerborg, A., "Results of Three Comparative Test Series to Determine the Fracture Energy G_F of Concrete", Materiaux et Constructions, Vol. 18. No. 107, 1985

[22] Olsson, R.-Å., "A Fracture Mechanics and Experimental Approach on Anchorage Splitting", Nordic Concrete Research, Publikation No. 4, The Nordic Concrete Federation, 1985

[23] Orangun, C.O., Jirsa, J.O., and Breen, J.E., "A reevaluation of Test Data on Development Length and Splices", Journal of the American Concrete Institute, March 1977

[24] Andreasen, B.S., "Anchorage of Deformed Reinforcing Bars", Report Series R. No. 238, Department of Structural Engineering, Technical University of Denmark

[25] DS 411, "Dansk Ingeniørforenings norm for betonkonstruktioner", Teknisk Forlag, Normstyrelsens publikationer, NP-169-N, 1984 (in Danish)

[26] Blanks, R.F. and McNamara, C.C., "Mass Concrete Tests in Large Cylinders", Journal of the American Concrete Institute, Jan-Feb 1935, pp. 280 - 303

[27] "Beton-Bogen", Aalborg Portland, Cementfabrikkernes tekniske Oplysningskontor, 1979 (in Danish)

[28] Dansk Standard DS 2082, "Armeringsstål: Prøvning af forankringsevnen", Dansk Standardiseringsråd, (in Danish)

[29] Petersson, P.E., "Crack Growth and Formation of Fracture Zones in Plain Concrete and Similar Materials", Division of Building Materials, Lund Institute of Technology, Report No. TVBM-1006, 1981

[30] Comite Euro-International du Beton, "Bond Action and Bond Behavior of Reinforcement", State-of-the-Art-Report, Bulletin No. 151, April 1982.

7. TABLES

Batch No.	EF. No.	Number of ø150 x 300 mm cylinders	Number of G_F-specimens
90/15	90/12	-	4
70/20	70/12	-	5
50/20	50/12	-	4
30/30	30/15	4	5
90/05	90/05	6	6
70/05	70/05	6	4
50/10	50/05	6	5
30/10	30/05	7	5
90/10	90/10	5	5
70/10	70/10	5	5
30/20	30/10	-	5
70/15	-	8	6
90/12.5	90/10	3	11
90/07.5	90/07.5	5	10
70/12.5	70/10	4	11
70/07.5	-	7	9
	50/10		
50/15		7	9
	50/07.5		
50/12.5	-	6	8
50/07.5	-	7	13
30/12.5	-	6	14
30/07.5	-	5	16

Table 2.1 Correlation between EF. No. and Batch No. as well as the number of G_F-specimens and ø150 x 300 mm cylinders produced from each batch.

Intended Compressive Strength in MPa	90	70	50	30
Portland Rapid Cement	390	310	260	230
Silica Fume	39	31	-	-
Fly Ash	-	-	105	-
Superplasticizer	21	16.7	14.3	4.2
Sand (0-8 mm)	872	925	896	959
Gravel (4-8 mm)	372	406	390	419
Gravel (8-16 mm)	610	595	579	618
Water	102	102	109	120
Units	kg/m^3	kg/m^3	kg/m^3	kg/m^3

Table 2.2 Mixing proportions for the concrete

	Compressive Tests				Splitting Tests	
	ø100 x 200 mm		ø150 x 300 mm		ø100 x 200 mm	
Batch No.	Mean Value	Standard Deviation	Mean Value	Standard Deviation	Mean Value	Standard Deviation
90/15	89.7	5.6	-	-	5.693	0.935
70/20	75.4	7.0	-	-	4.912	0.666
50/20	49.6	3.0	-	-	3.890	0.149
30/30	20.5	1.2	25.9	3.2	1.763	0.089
90/05	98.6	6.3	74.9	3.2	4.845	0.391
70/05	85.1	7.0	75.1	3.6	4.692	0.615
50/10	46.5	1.9	43.3	4.4	3.141	0.410
30/10	42.3	2.2	37.2	2.8	3.384	0.080
90/10	87.7	9.1	78.9	3.8	6.398	0.602
70/10	81.3	10.9	81.0	7.0	5.422	0.786
30/20	41.7	1.0	-	-	2.992	0.651
70/15	81.5	6.8	78.8	4.1	5.688	0.554
90/12.5	95.1	8.1	83.9	4.5	6.212	1.015
90/07.5	86.1	9.1	77.4	5.1	5.434	0.470
70/12.5	79.1	6.1	74.8	11.4	5.424	1.232
70/07.5	89.4	10.3	81.6	3.9	5.868	0.658
50/15	58.3	2.4	52.5	2.3	4.417	0.599
50/12.5	56.9	3.4	49.1	5.9	4.466	0.472
50/07.5	48.2	1.4	50.2	1.8	3.769	0.489
30/12.5	48.4	4.3	51.1	4.9	3.909	0.441
30/07.5	44.9	1.5	45.3	4.1	3.228	0.550

Table 2.3 Concrete compressive strength and splitting strength in MPa.

	Number of Tests	Mean Value	Standard Deviation	Maximum Value	Minimum Value
E	5	11096	1001	11857	10000
T_y	44	34.00	0.47	34.50	32.00
T_u	44	41.35	0.24	41.70	40.80

Table 2.4 Modulus of elasticity, E in kN, yield load, T_y in kN, and ultimate load, T_u in kN of Swedish Kam Steel KS 600 S ø8 mm used as stirrups in the S.B.-specimens.

	Number of Tests	Mean Value	Standard Deviation	Maximum Value	Minimum Value
E	11	6468	73	6536	6369
$T_{0.2}$	11	14.49	0.31	14.90	14.10
T_u	37	19.68	0.24	20.10	19.20

Table 2.5 Modulus of elasticity, E in kN, load at which the sustained deformation is 0.2 %, $T_{0.2}$ in kN, and ultimate load, T_u in kN for Danish Kam Steel KS 410 S ø6 mm.

	Number of Tests	Mean Value	Standard Deviation	Maximum Value	Minimum Value
E	4	4001	164	4211	3810
$T_{0.2}$	4	11.66	0.11	11.80	11.50
T_u	5	13.10	0.08	13.20	13.00

Table 2.6 Modulus of elasticity, E in kN, load at which the sustained deformation is 0.2 %, $T_{0.2}$ in kN, and ultimate load, T_u in kN, for Danish Profiled Steel W 4301 ø5 mm.

	Number of Tests	Mean Value	Standard Deviation	Maximum Value	Minimum Value	Units
E	9	40792	2817	44444	39683	kN
T_y	29	130.5	1.94	134.0	127.5	kN
d	44	15.48	0.06	15.61	15.35	mm
T_u	29	160.6	1.43	163.0	157.0	kN

Table 2.7 Modulus of elasticity, E, and yield load, T_y, of the Swedish Kam Steel KS 600 S ø16 mm and the diameter and ultimate load, d, respectively, T_u, of the cold stretched steel.

	Number of Tests	Mean Value	Standard Deviation	Maximum Value	Minimum Value
E	6	11397	263	11765	11111
T_y	41	34.05	0.23	34.50	33.50
T_u	41	41.25	0.42	43.50	40.8

Table 2.8 Modulus of elasticity, E, yield load, T_y, and the and the ultimate load, T_u, of Swedish Kam Steel KS 600 S ø8 mm in kN.

S.B.-specimen No.	l (mm)	l_1 (mm)	l_2 (mm)	a (mm)	b (mm)	Bar No. with 8 strain-gauges along the splice
90/15	240	530	146	30	45	2
70/20	320	490	186	40	55	1
50/20	320	490	186	40	55	4
30/30	480	410	266	60	75	4
50/10	160	570	106	20	35	4
30/10	160	570	106	20	35	2
90/10	160	570	106	20	35	4
70/10	160	570	106	20	35	3
30/20	320	490	186	40	55	4
70/15	240	530	146	30	45	4+1
90/12.5	200	550	126	25	40	3
70/12.5	200	550	126	25	40	2
50/15	240	530	146	30	45	4
50/12.5	200	550	126	25	40	2
30/12.5	200	550	126	25	40	2

Table 2.9 Geometry of arrangement of strain gauges, when 8 gauges are placed along the splice

Specimen No.	Bar No. with more than 2 strain gauges along the splice
90/12	4
70/05	3
90/07.5	1
70/07.5	1
50/07.5	2
30/07.5	2

Table 2.10 Arrangement of reinforcing bar with 6 or 4 strain gauges along the splice

EF.-specimen No.	l (mm)	a (mm)
90/12	192	25
70/12	192	25
50/12	192	25
30/15	240	30
70/10	160	20
30/10	160	20
90/10	160	20
50/10	160	20

Table 2.11 Geometry of strain gauge arrangement in EF.-specimens with anchorage length longer than 120 mm

S.B No.	Load in bar No.1 (kN)	Load in bar No.2 (kN)	Load in bar No.3 (kN)	Load in bar No.4 (kN)	Average load (kN)	Standard deviation (kN)	τ_u (MPa)
90/15	117.36	122.15	127.14	110.49	119.28	7.09	10.21
70/20	146.53	155.26	150.23	151.00	150.76	3.58	9.68
50/20	131.00	134.94	127.09	128.20	130.31	3.50	8.37
30/30	122.46	122.23	125.76	129.87	125.08	3.58	5.36
90/05	61.40	55.32	57.19	55.66	57.39	2.79	14.75
70/05	56.19	53.48	54.71	52.67	54.26	1.53	13.95
50/10	78.57	88.62	78.48	85.30	82.74	5.06	10.63
30/10	76.21	-	68.03	68.77	71.00	4.52	9.12
90/10	85.59	95.72	86.74	84.76	88.20	5.08	11.34
70/10	86.55	88.69	93.65	86.41	88.83	3.38	11.41
30/20	114.95	115.85	114.47	119.30	116.14	2.18	7.46
70/15	123.52	124.79	120.27	123.59	123.04	1.94	10.54
90/12.5	-	94.00	-	104.96	99.48	7.75	10.23
90/07.5	62.22	63.04	64.88	60.79	62.73	1.71	10.75
70/12.5	100.22	102.51	101.52	90.84	98.77	5.37	10.16
70/07.5	68.48	65.52	68.21	71.46	68.42	2.43	11.72
50/15	110.35	117.47	114.63	112.75	113.80	3.01	9.75
50/12.5	95.23	92.03	89.08	91.74	92.02	2.52	9.46
50/07.5	59.65	61.24	63.53	54.86	59.82	3.67	10.25
30/12.5	87.28	90.11	91.33	-	89.57	2.08	9.21
30/07.5	46.12	52.86	42.05	-	47.01	5.46	8.06

Table 3.1 Load at failure determined from strain gauges outside the concrete and calculated average shear stress, τ_u, along the overlapped splice in MPa.

S.B No.	Load in bar No.1 (kN)	Load in bar No.2 (kN)	Load in bar No.3 (kN)	Load in bar No.4 (kN)	Average load (kN)	Standard deviation (kN)
90/15	111.51	98.51	105.72	109.56	106.33	5.74
70/20	142.65	143.71	142.02	145.80	143.55	1.65
50/20	-	119.62	123.88	121.30	121.60	2.15
30/30	119.64	119.70	119.82	118.43	119.40	0.65
90/05	49.40	53.88	47.05	57.58	51.98	4.69
70/05	52.53	50.55	32.08	38.36	43.38	9.80
50/10	74.76	83.36	77.18	82.10	79.35	4.06
30/10	71.46	61.13	59.99	59.53	62.53	6.09
90/10	82.86	79.14	79.95	77.64	79.90	2.19
70/10	77.56	75.52	76.65	81.02	77.69	2.37
30/20	119.61	111.70	113.20	114.13	114.66	3.45
70/15	119.92	116.62	106.30	106.13	112.24	7.09
90/12.5	90.81	-	95.06	88.41	91.43	3.36
90/07.5	59.63	58.56	46.75	46.23	52.79	7.29
70/12.5	88.61	93.47	82.00	88.40	88.12	4.70
70/07.5	64.78	50.05	60.69	53.73	57.31	6.65
50/15	110.19	105.17	-	103.33	106.23	3.55
50/12.5	95.85	86.22	85.13	77.73	86.23	7.44
50/07.5	52.56	46.26	56.21	-	51.68	5.03
30/12.5	80.05	80.02	84.17	83.54	81.95	2.22
30/07.5	41.78	51.77	41.57	47.65	45.69	4.94

Table 3.2 Load at failure determined from strain gauges just outside the splice.

S.B. No.	Coefficient of Variation (%)
90/15	7.92
70/20	3.83
50/20	7.77
30/30	4.27
90/05	9.17
70/05	11.60
50/10	11.10
30/10	11.70
90/10	7.57
70/10	13.20
30/20	3.98
70/50*	4.13
70/15**	10.68
90/12.5	6.12
90/07.5	22.00
70/07.5	7.71
50/15	8.28
50/12.5	9.41
50/07.5	12.78
30/12.5	9.34
30/07.5	3.32

* Bar No. 1 ** Bar No. 4

Table 3.3 Coefficient of variation of a 1st degree polynomial fitted to the load distribution along the splices at failure for S.B.-tests.

EF. No.	Average Load (kN)	Standard Deviation (kN)	Anchorage Length (mm)	Average Shear Stress (MPa)
50/12	156.33	3.63	192	16.72
30/15	138.67	1.47	240	11.87
90/05	79.70	3.07	80	20.46
70/05	72.17	3.39	80	18.53
50/05	64.43	1.16	80	16.54
30/05	56.27	1.53	80	14.46
90/10	151.67	5.35	160	19.47
70/10	153.17	4.46	160	19.66
30/10	107.33	3.83	160	13.78
90/10	153.08	4.58	160	19.65
90/07.5	112.45	6.05	120	19.24
70/10	152.00	2.12	160	19.51
50/10	129.58	3.93	160	16.63
50/07.5	99.75	3.05	120	17.07

Table 3.4 Average load at failure, the standard deviation, the anchorage length and the calculated average shear stress along the splice anchorage of all EF.-tests.

EF. No.	Coefficient of Variation (%)
30/15	3.04
30/10	5.62
30/05	11.47
50/12	2.50
50/10	9.00
50/05	4.71
70/10	4.54
70/05	11.56
90/10	3.73
90/07.5	16.09
90/05	11.79

Table 3.5 Constants and coefficient of variation of a 1st degree polynomial fitted to the load distribution along the anchorage lengths at failure for EF.-tests.

Batch No.	Fracture Energy G_F (N/m)	Standard Deviation (N/m)	Number of Test Specimens
30/30	133.21	30.33	5
30/20	139.46	11.16	5
30/12.5	163.91	29.26	14
30/10	163.48	20.22	5
30/07.5	145.61	24.12	16
50/20	180.56	43.43	4
50/15	196.23	37.39	9
50/12.5	156.81	27.90	8
50/10	178.66	40.21	5
50/07.5	175.99	28.84	13
70/20	195.23	32.53	4
70/15	168.27	10.61	6
70/12.5	180.25	24.86	11
70/10	157.33	12.23	6
70/07.5	179.27	27.61	9
70/05	169.94	20.56	4
90/15	170.70	11.38	4
90/12.5	151.66	25.90	11
90/10	181.99	32.85	5
90/07.5	175.82	35.36	10
90/05	179.93	23.54	6

Table 3.6 Average fracture energy, G_F, of the concrete in each batch

8. FIGURES

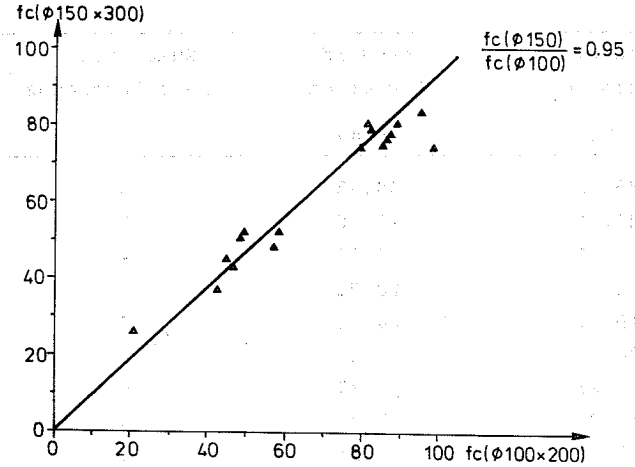

Fig. 2.1 Comparison of compressive strength, in MPa, obtained on cylinders with sizes of ø150 mm x 300 mm and ø100 x 200 mm.

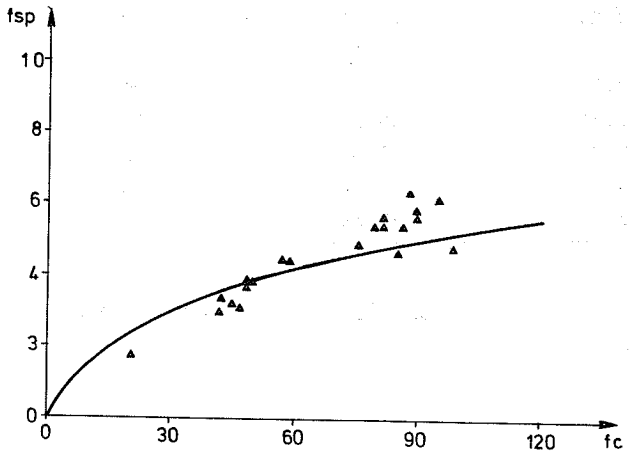

Fig. 2.2 Comparison of compressive strength and splitting strength, in MPa, obtained on cylinders, ø100 mm x 200 mm.

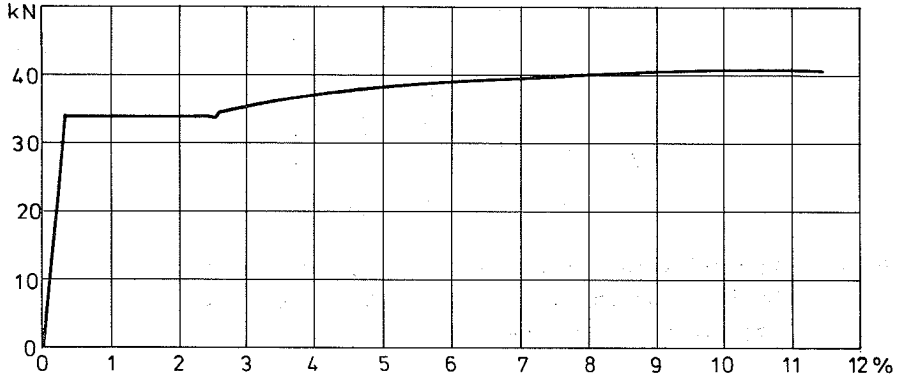

Fig. 2.3 Typical relation between load and strain of Swedish Kam Steel Ks 600 S ø8 mm used as stirrups and compression steel in S.B.-specimens.

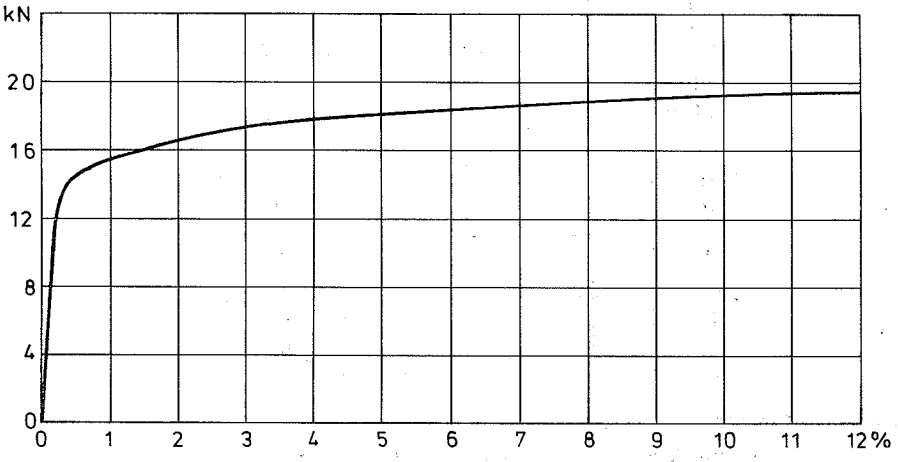

Fig. 2.4 Typical relation between load and strain of Danish Kam Steel Ks 410 S ø6 mm used as stirrups in S.B.-specimens.

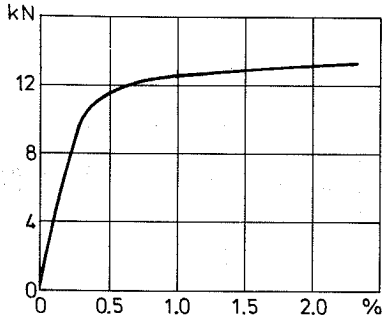

Fig. 2.5 Typical relation between load and strain of Danish Profiled Steel W 4301 ø5mm used as stirrups in S.B.-specimens.

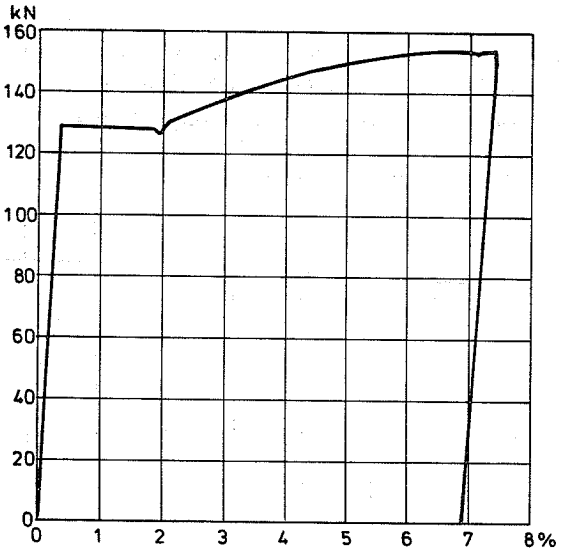

Fig. 2.6 Typical relation between load and strain of Swedish Kam Steel Ks 600 S ø16 mm, when cold stretching the bar.

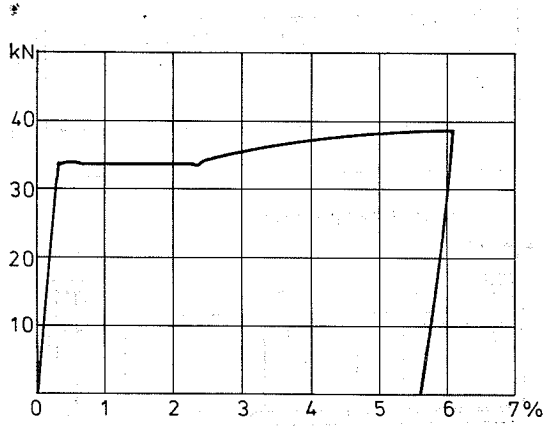

Fig. 2.7 Typical relation between load and strain of Swedish Kam Steel Ks 600 S ø8 mm, when cold streching the bar.

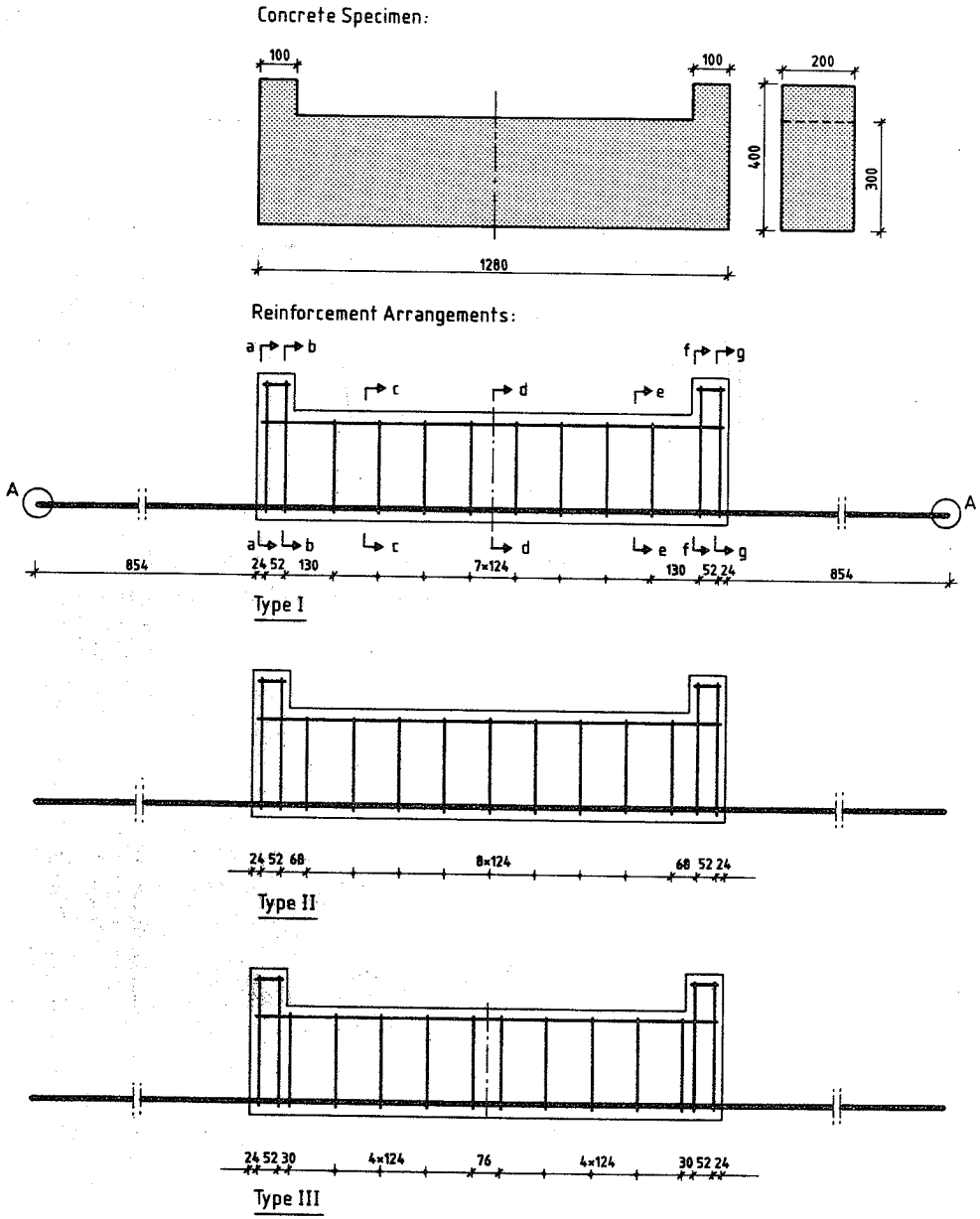

Fig. 2.8 S.B.-specimen dimensions and reinforcement arrangements.

Fig. 2.9 Stirrups used in the S.B.-specimens and detail A from Figure 2.8.

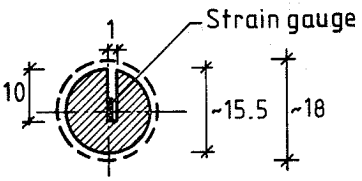

Fig. 2.10 Gross section of the groove cut in the longitudinal tensile reinforcing bar.

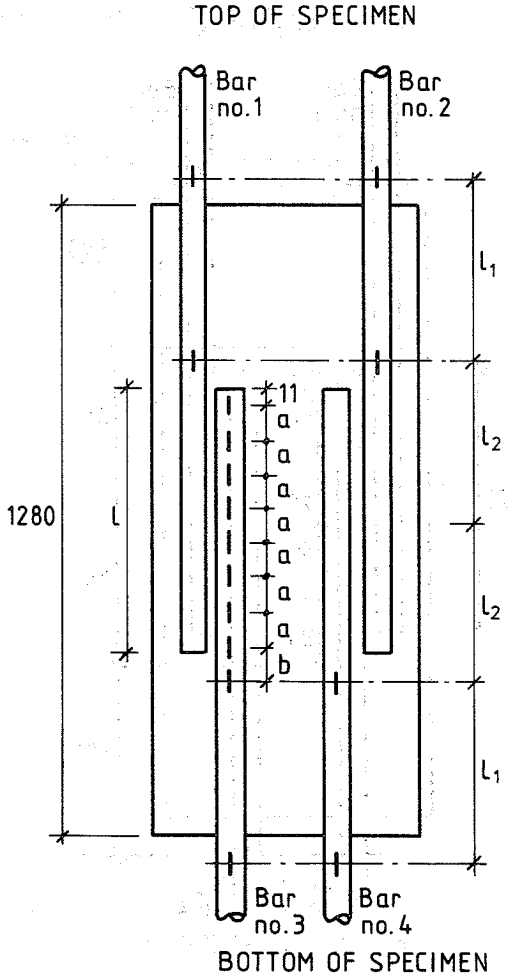

Fig. 2.11 Arrangement of strain gauges in the S.B.-specimen along the splice length for splice lengths longer than 120 mm.

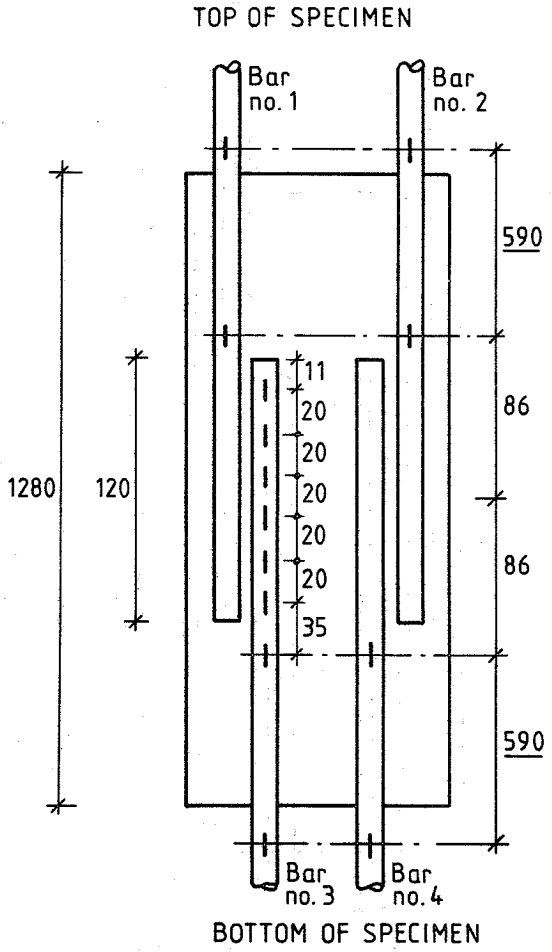

Fig. 2.12 Arrangement of strain gauges in the S.B.-specimen along the splice length, when the splice length is 120 mm.

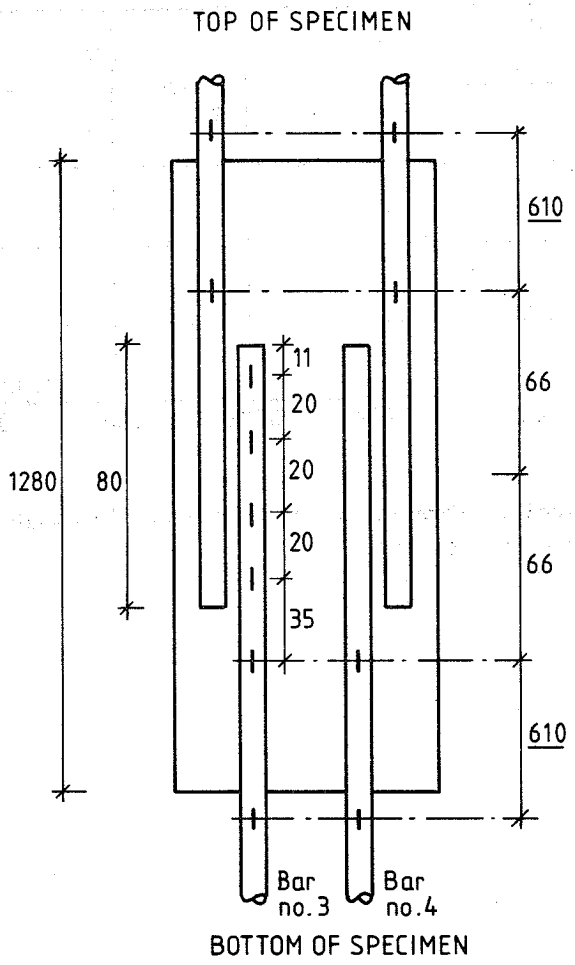

Fig. 2.13 Arrangement of strain gauges in the S.B.-specimen along the splice length, when the splice length is 80 mm.

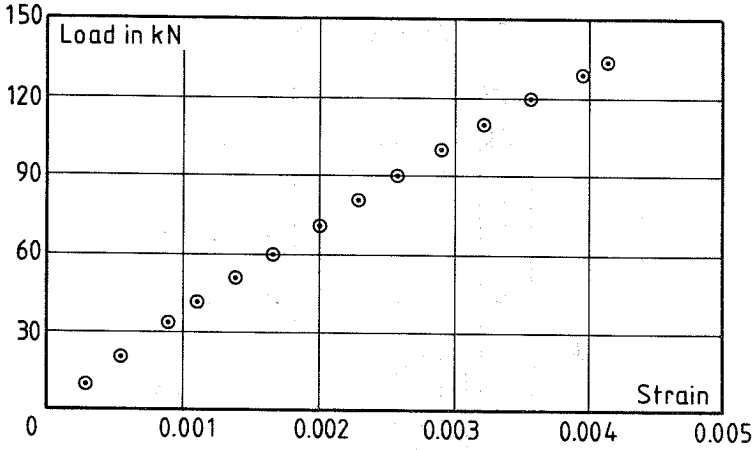

Fig. 2.14 Typical calibration curve of one strain gauge placed in a groove.

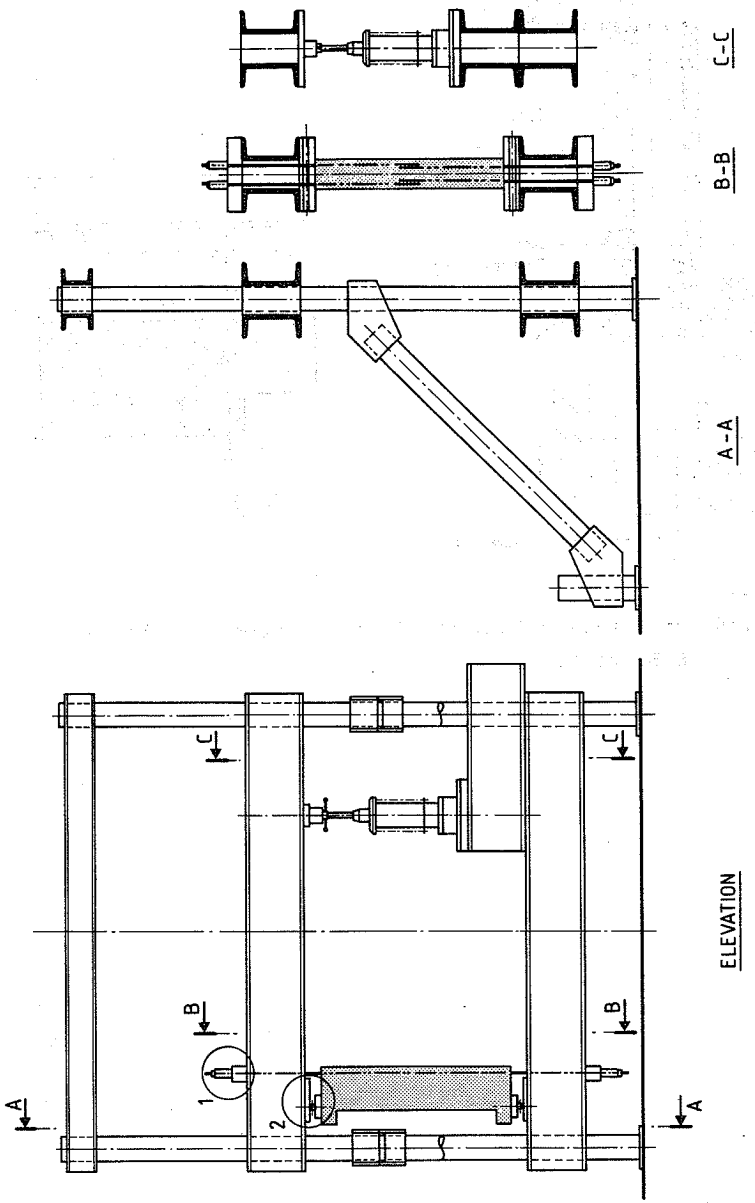

Fig. 2.15 Test-rig for the S.B.-specimens.

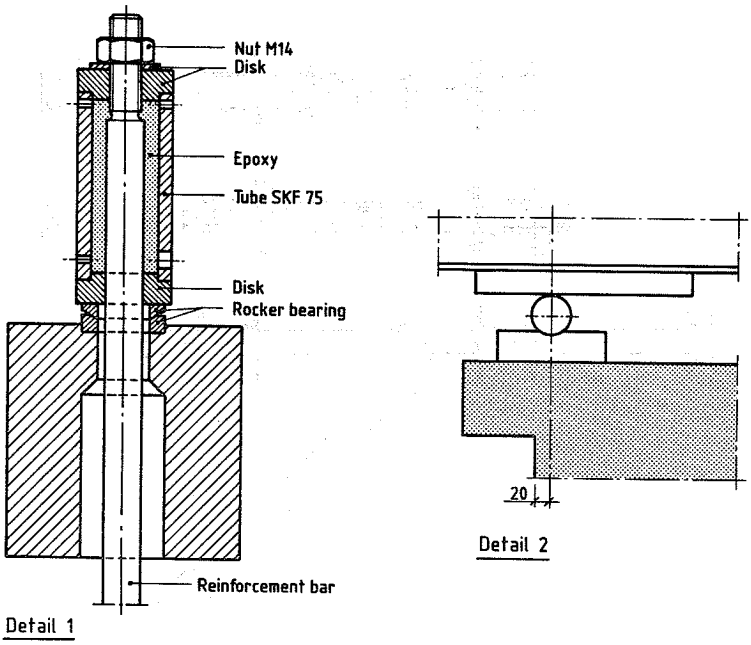

Fig. 2.16 Anchorage detail and bearings used for the S.B.-tests.

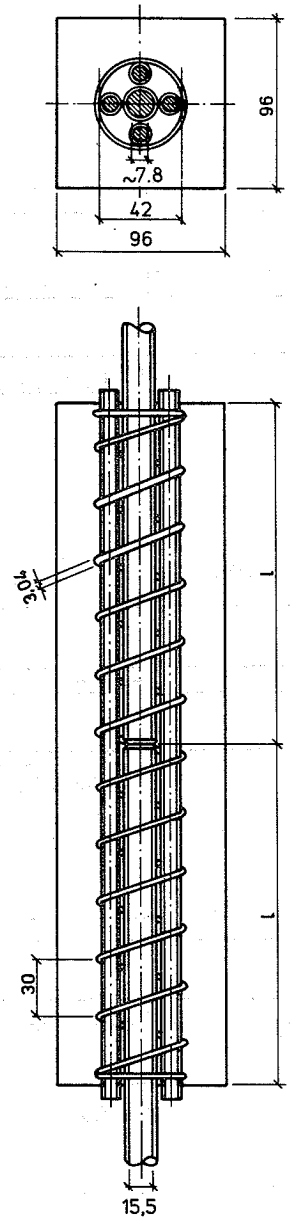

Fig. 2.17 EF.-specimen dimensions and reinforcement arrangements.

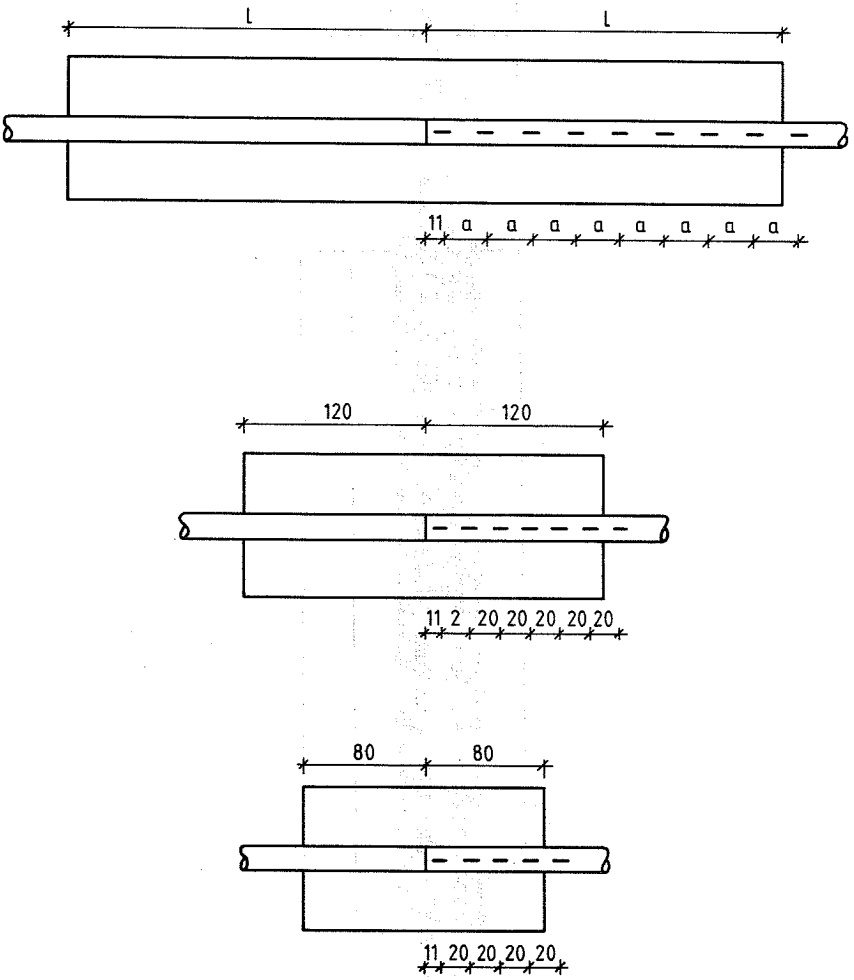

Fig. 2.18 Arrangement of strain gauges in the EF.-specimens.

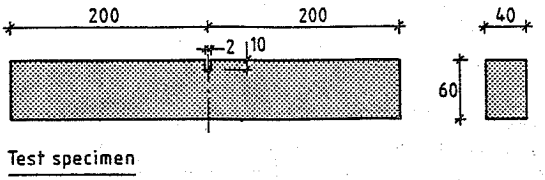

Fig. 2.19 Geometry of the G_F-specimens.

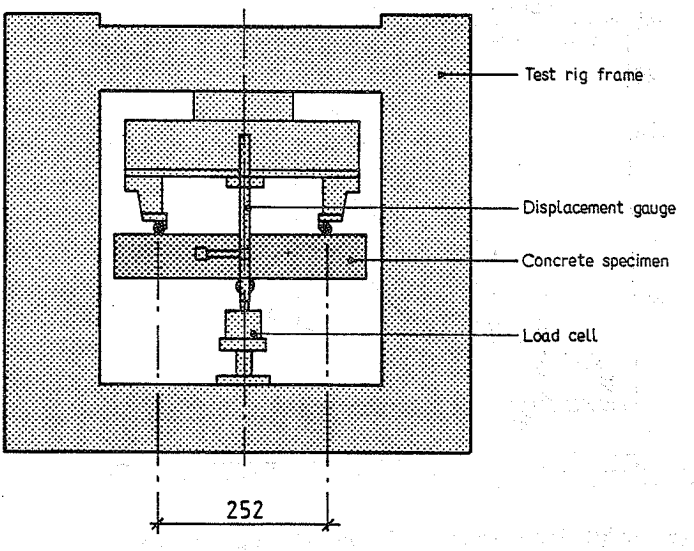

Fig. 2.20 Test-rig for the G_F-specimens.

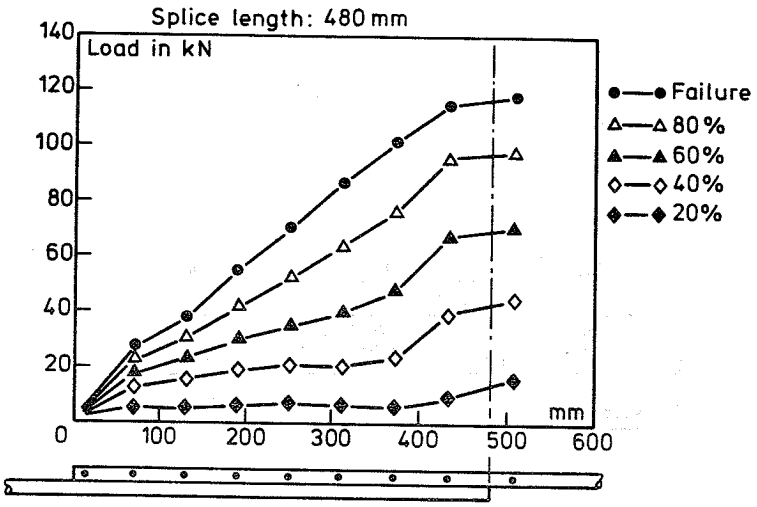

Fig. 3.1 Load distribution along the splice length in S.B. 30/30.

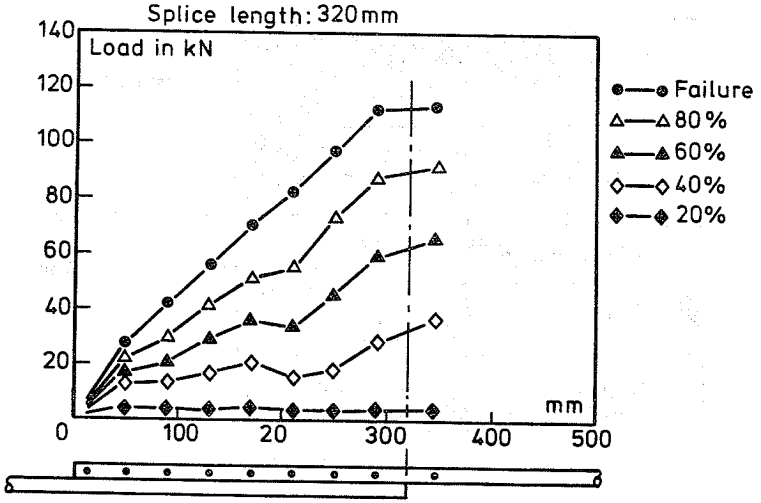

Fig. 3.2 Load distribution along the splice length in S.B. 30/20.

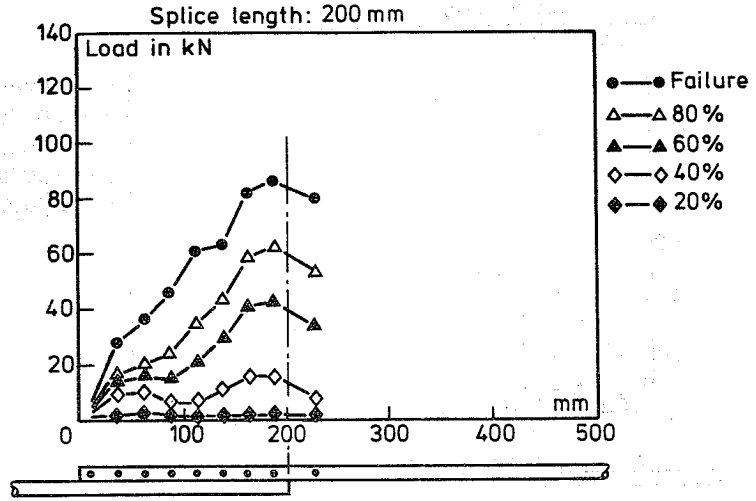

Fig. 3.3 Load distribution along the splice length in S.B. 30/12.5.

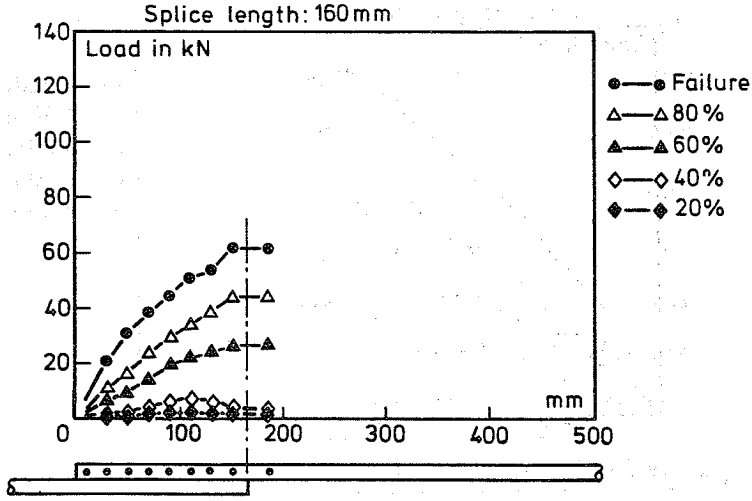

Fig. 3.4 Load distribution along the splice length in S.B. 30/10.

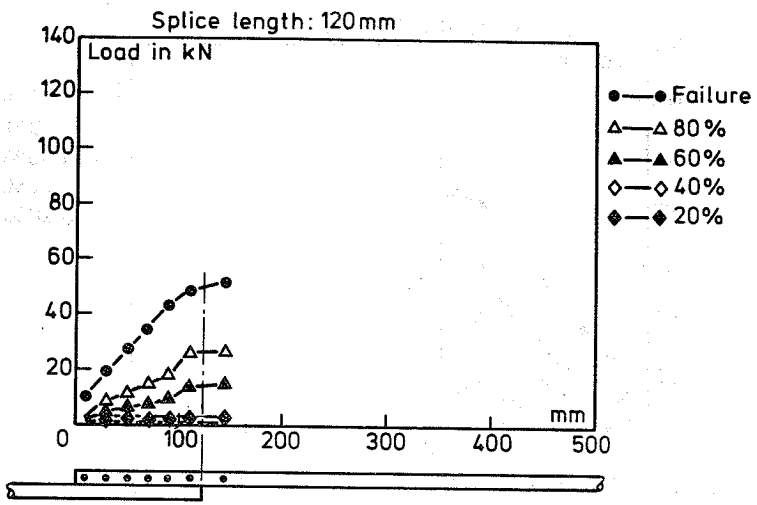

Fig. 3.5 Load distribution along the splice length in S.B. 30/07.5.

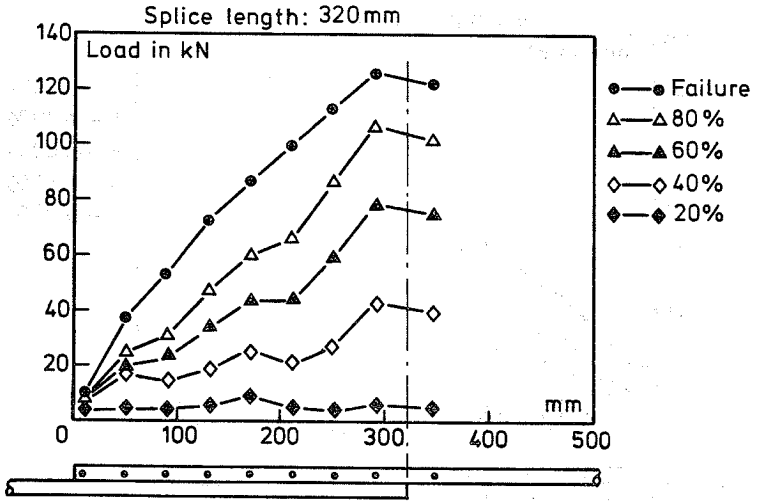

Fig. 3.6 Load distribution along the splice length in S.B. 50/20.

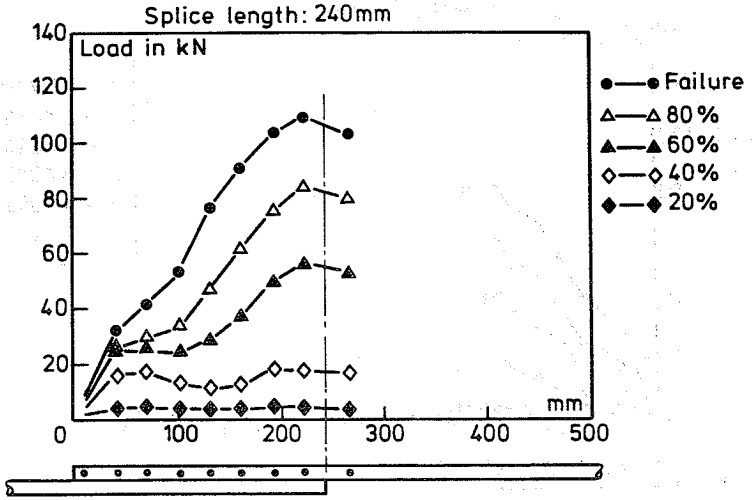

Fig. 3.7 Load distribution along the splice length in S.B. 50/15.

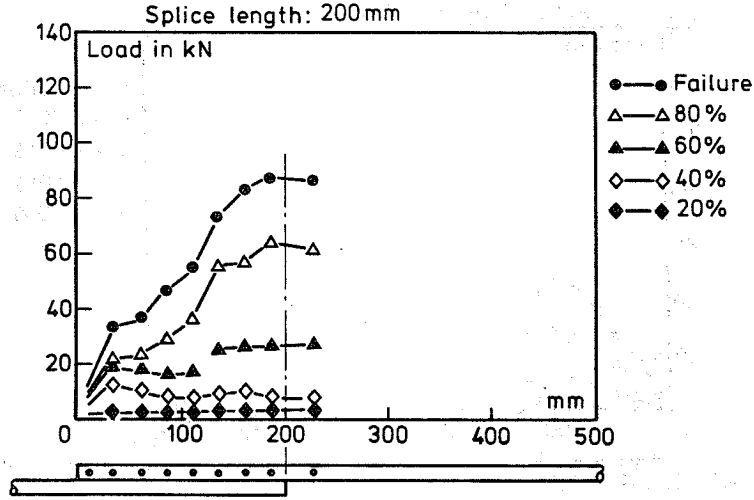

Fig. 3.8 Load distribution along the splice length in S.B. 50/12.5.

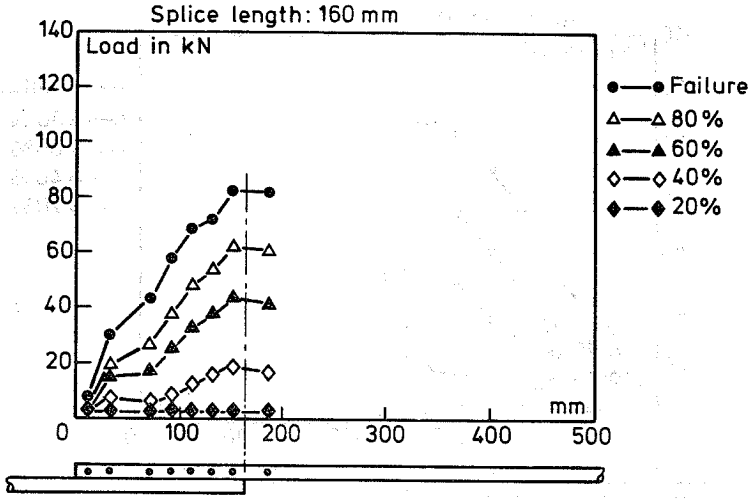

Fig. 3.9 Load distribution along the splice length in S.B. 50/10.

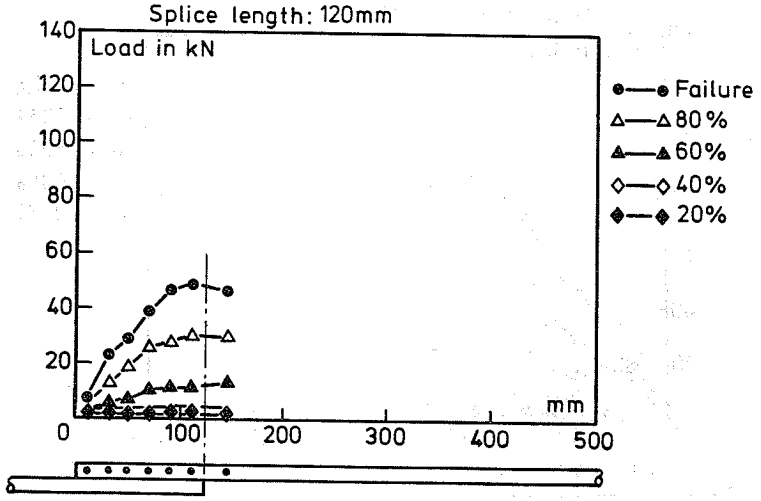

Fig. 3.10 Load distribution along the splice length in S.B. 50/07.5.

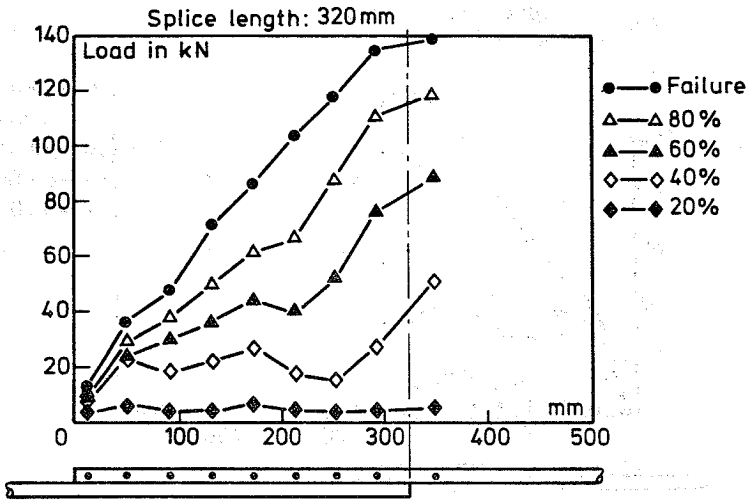

Fig. 3.11 Load distribution along the splice length in S.B. 70/20.

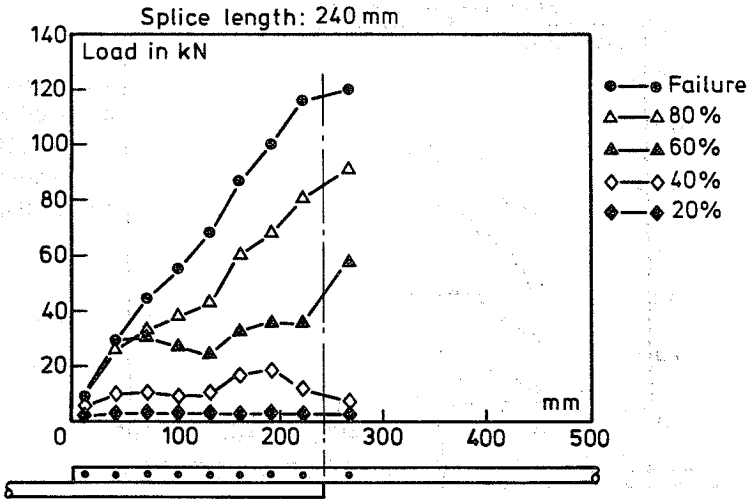

Fig. 3.12 Load distribution along the splice length in S.B. 70/15, Bar No. 1.

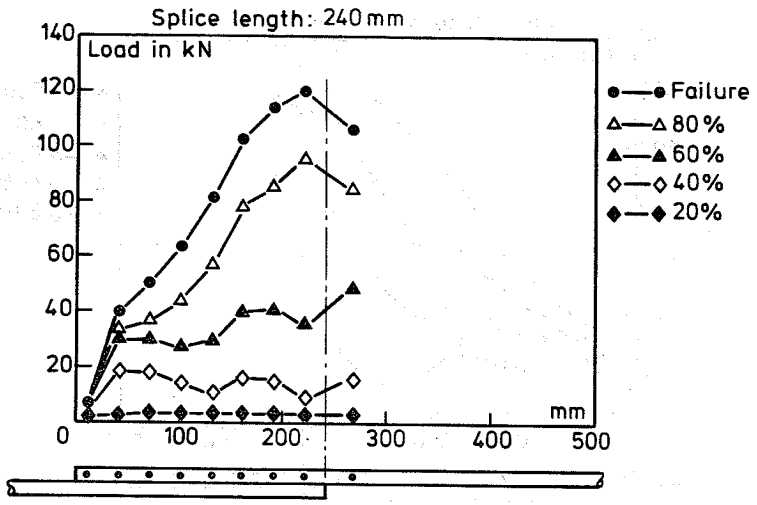

Fig. 3.13 Load distribution along the splice length in S.B. 70/15, Bar No. 4.

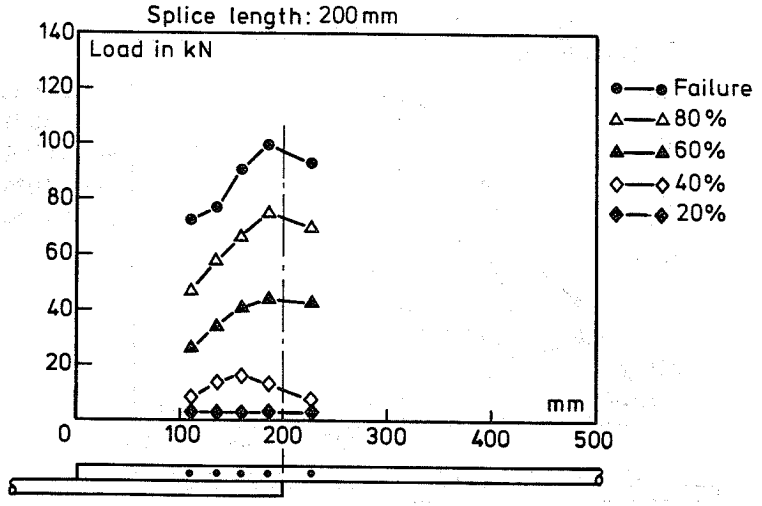

Fig. 3.14 Load distribution along the splice length in S.B. 70/12.5.

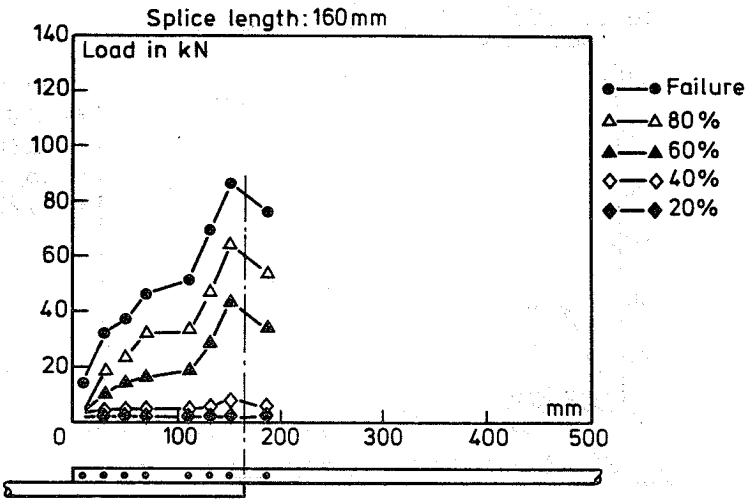

Fig. 3.15 Load distribution along the splice length in S.B. 70/10.

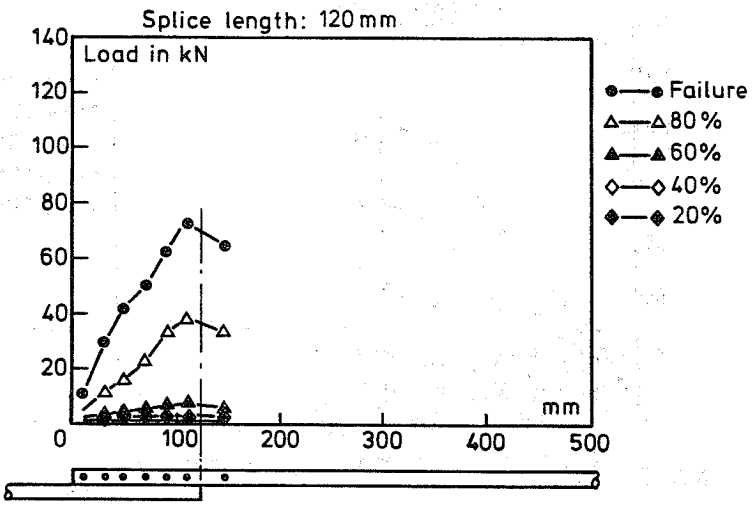

Fig. 3.16 Load distribution along the splice length in S.B. 70/07.5.

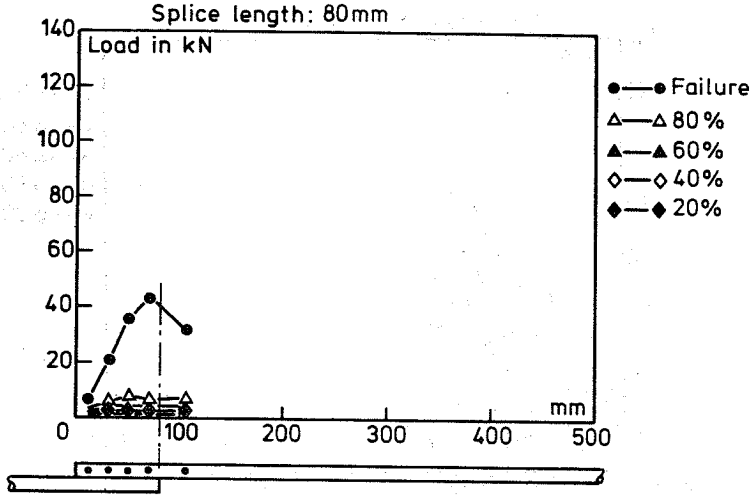

Fig. 3.17 Load distribution along the splice length in S.B. 70/05.

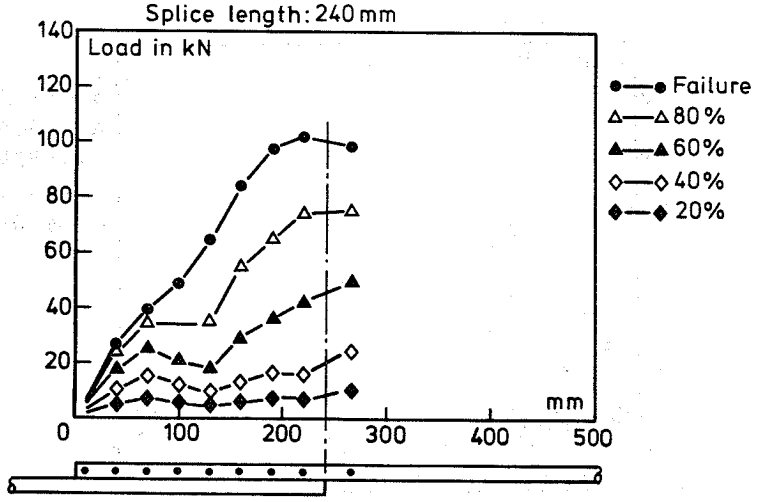

Fig. 3.18 Load distribution along the splice length in S.B. 90/15.

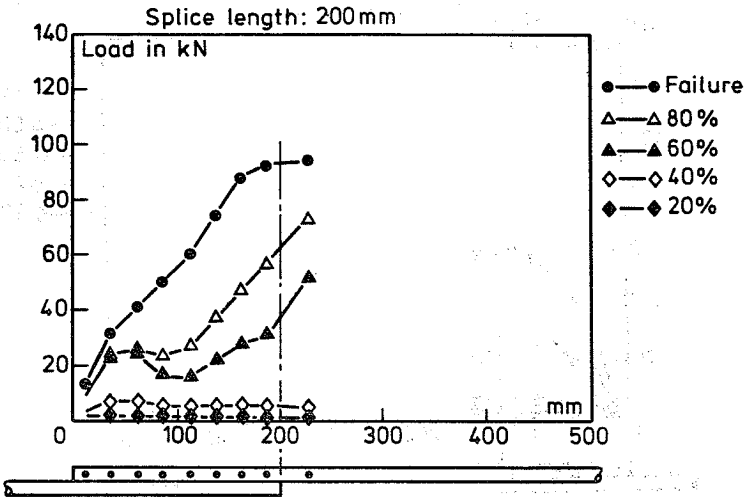

Fig. 3.19 Load distribution along the splice length in S.B. 90/12.5.

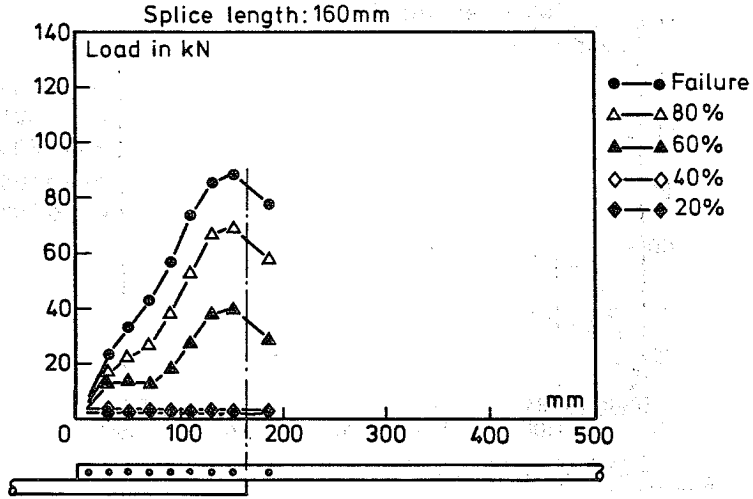

Fig. 3.20 Load distribution along the splice length in S.B. 90/10.

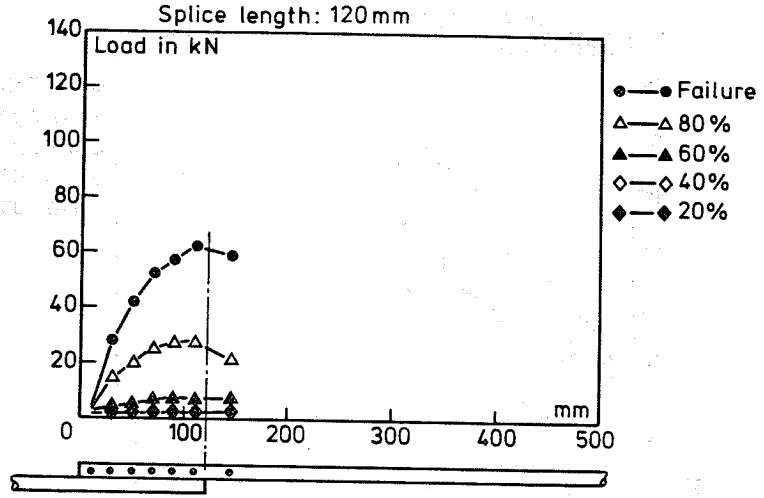

Fig. 3.21 Load distribution along the splice length in S.B. 90/07.5.

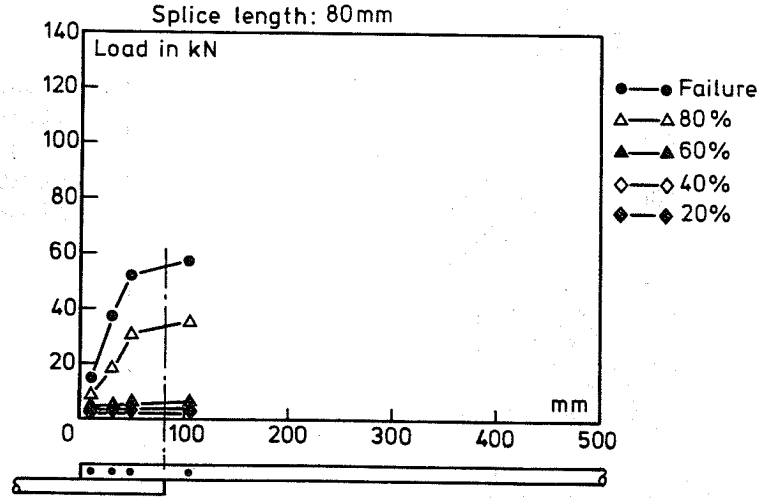

Fig. 3.22 Load distribution along the splice length in S.B. 90/05.

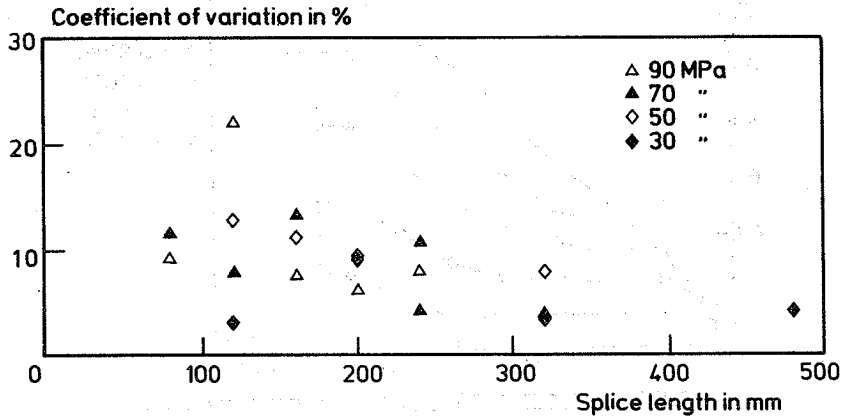

Fig. 3.23 Coefficient of variation assuming evenly distribution of shear stress along the splice length.

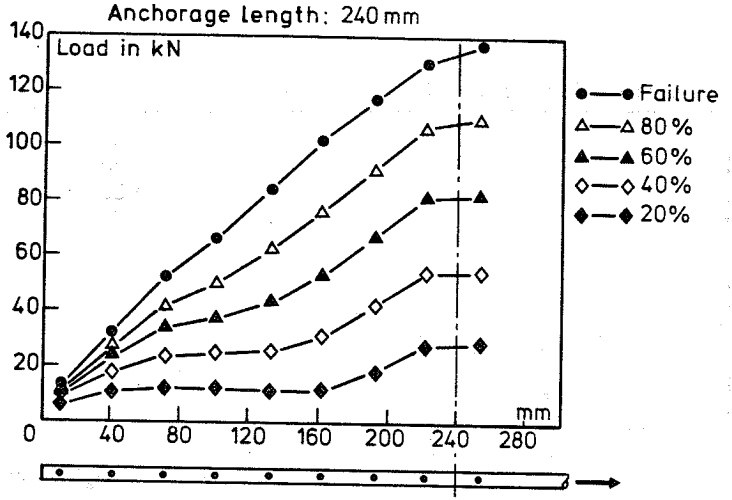

Fig. 3.24 Load distribution along the anchorage length in EF.30/15.

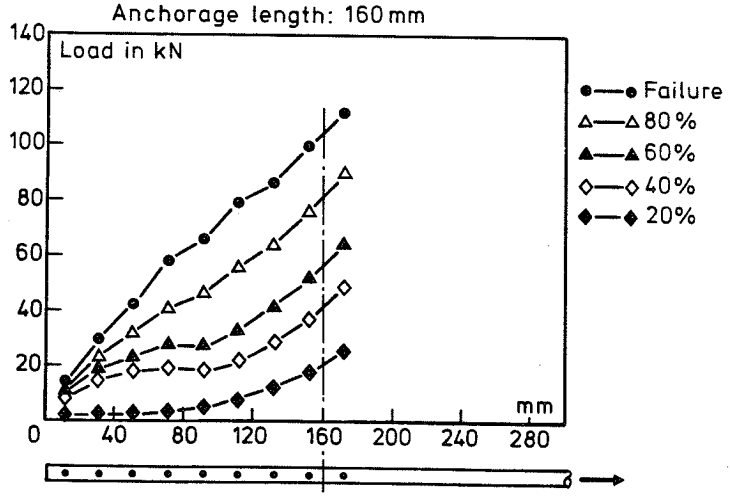

Fig. 3.25 Load distribution along the anchorage length in EF.30/10.

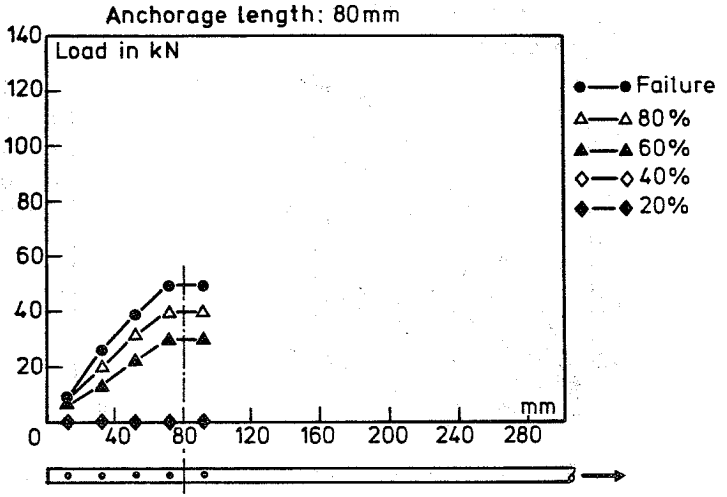

Fig. 3.26 Load distribution along the anchorage length in EF.30/05.

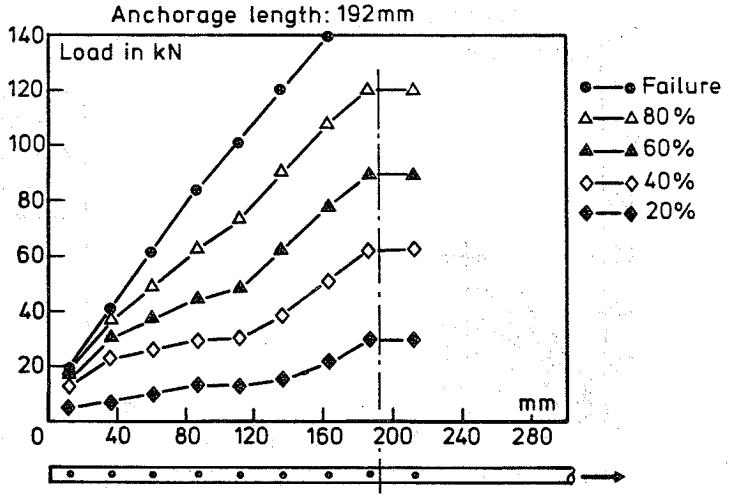

Fig. 3.27 Load distribution along the anchorage length in EF.50/12.

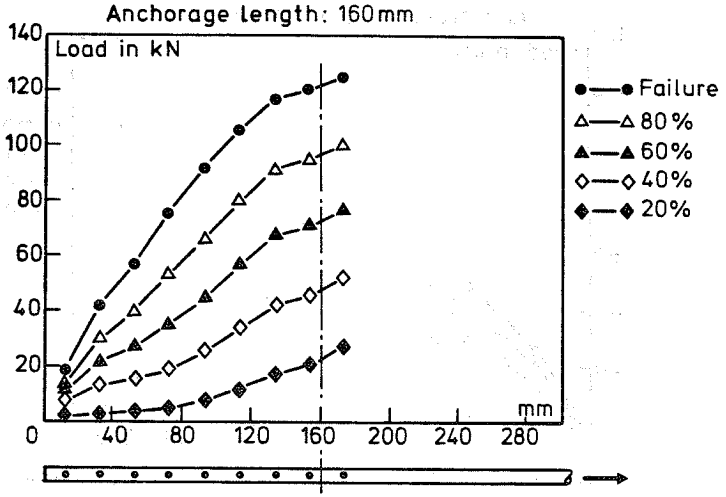

Fig. 3.28 Load distribution along the anchorage length in EF.50/10.

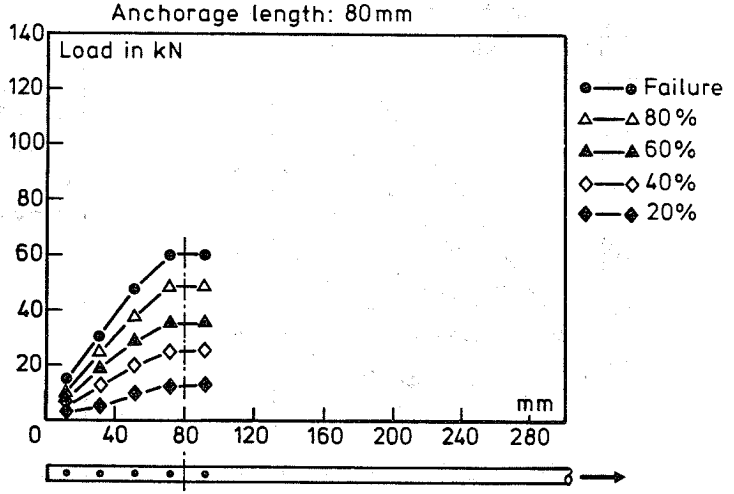

Fig. 3.29 Load distribution along the anchorage length in EF.50/05.

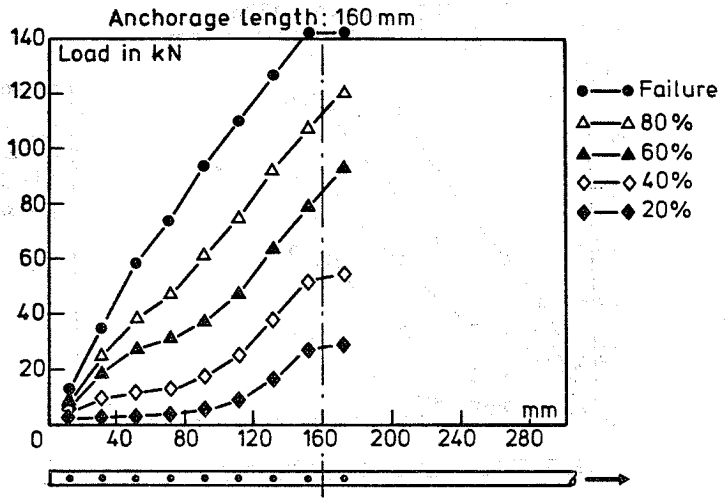

Fig. 3.30 Load distribution along the anchorage length in EF.70/10.

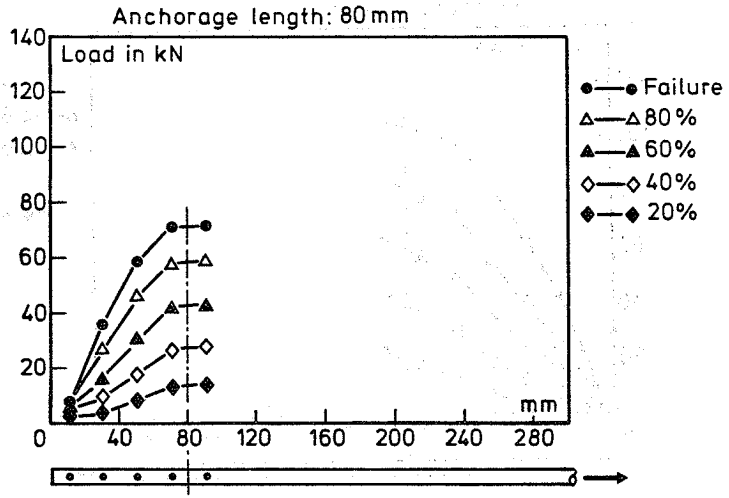

Fig. 3.31 Load distribution along the anchorage length in EF.70/05.

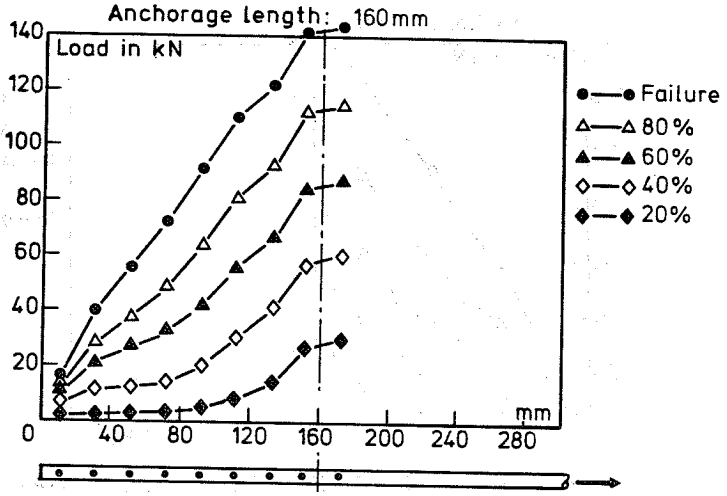

Fig. 3.32 Load distribution along the anchorage length in EF.90/10.

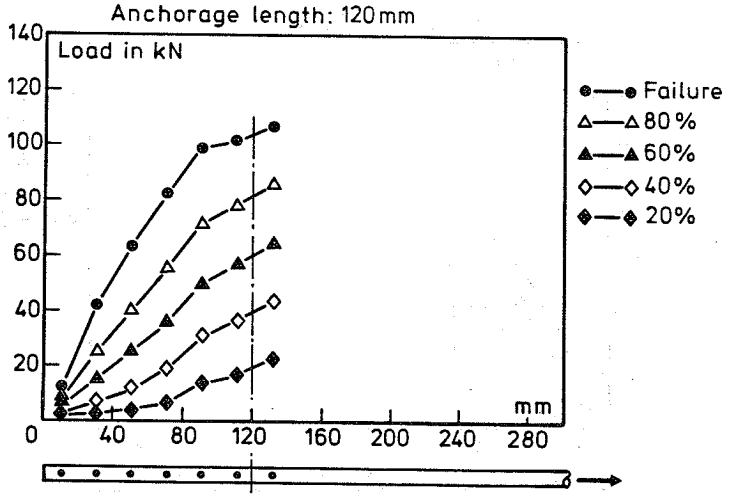

Fig. 3.33 Load distribution along the anchorage length in EF.90/07.5.

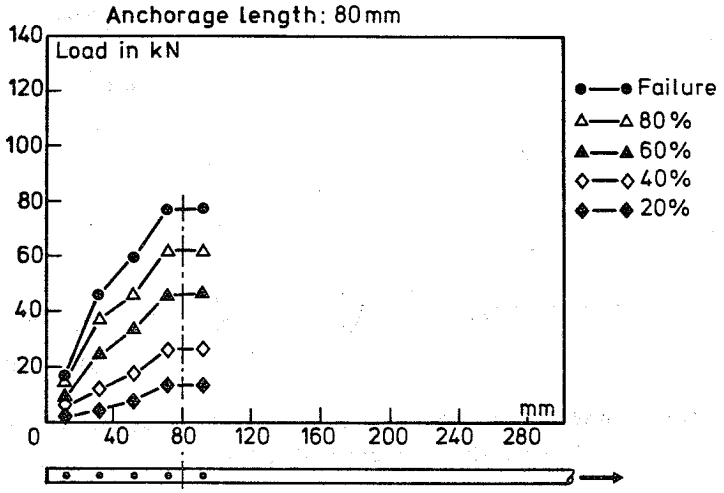

Fig. 3.34 Load distribution along the anchorage length in EF.90/05.

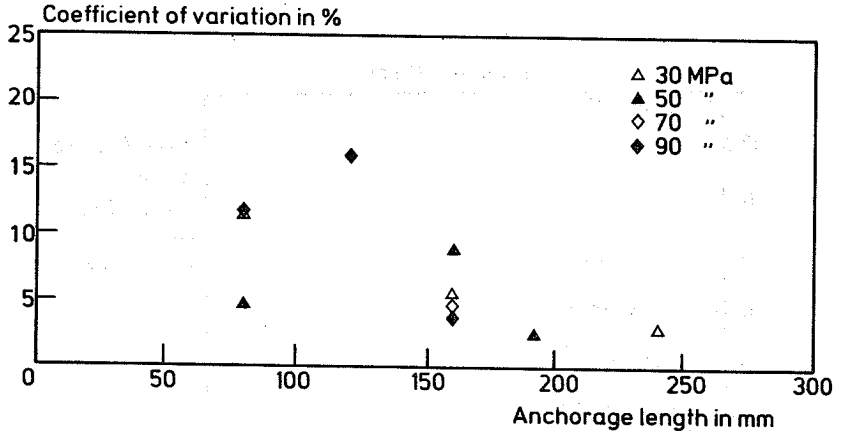

Fig. 3.35 Coefficient of variation assuming evenly distribution of shear stress along the anchorage length.

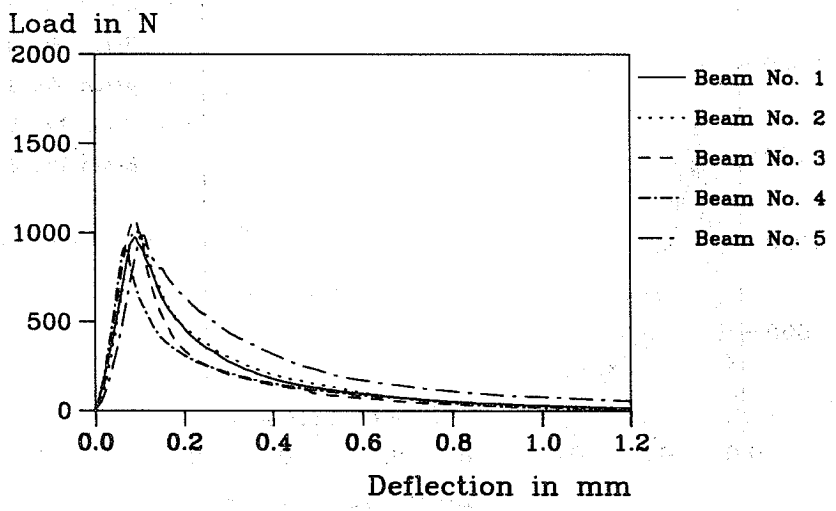

Fig. 3.36 Load-deflection curves from G_F-tests.
Batch No. 30/30.

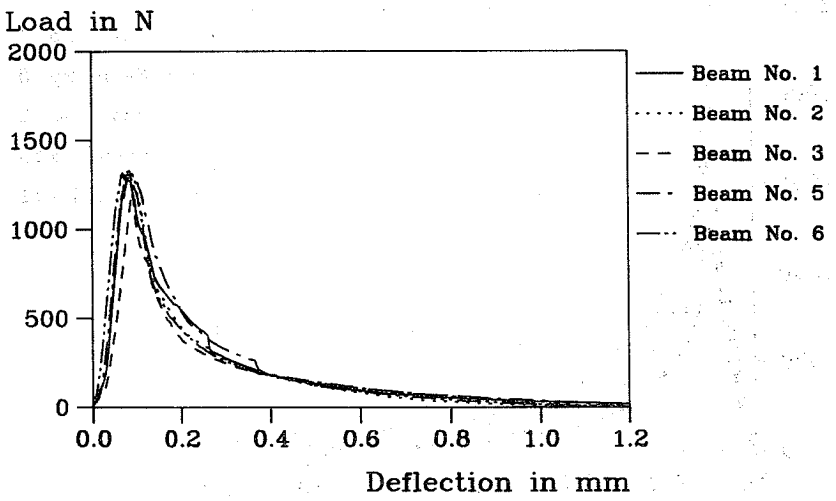

Fig. 3.37 Load-deflection curves from G_F-tests.
Batch No. 30/20.

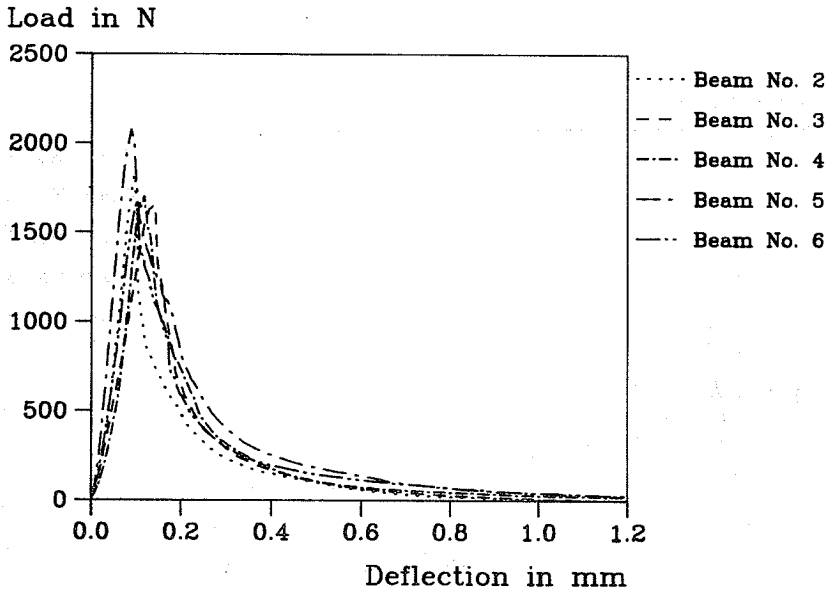

Fig. 3.38 Load-deflection curves from G_F-tests. Batch No. 30/12.5.

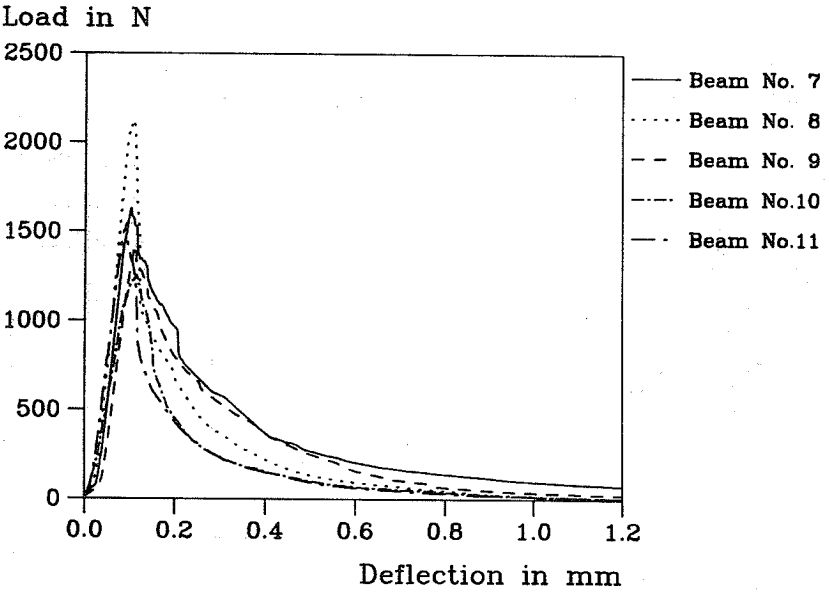

Fig. 3.39 Load-deflection curves from G_F-tests. Batch No. 30/12.5.

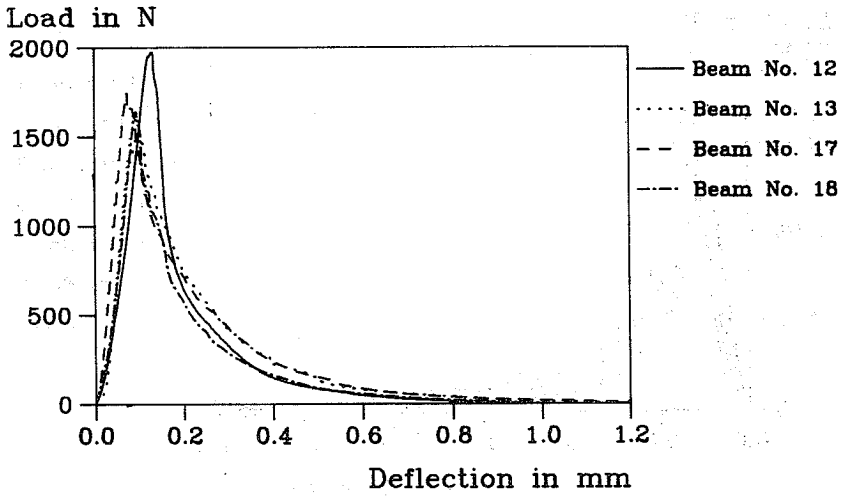

Fig. 3.40 Load-deflection curves from G_F-tests.
Batch No. 30/12.5.

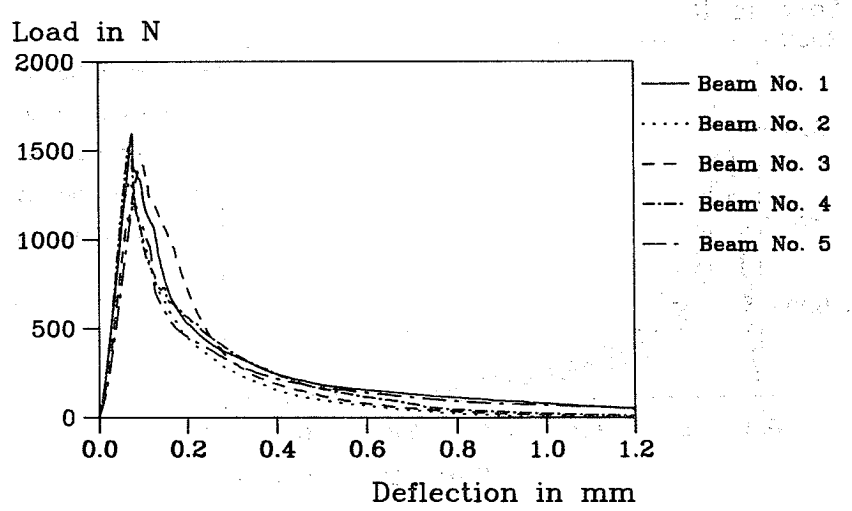

Fig. 3.41 Load-deflection curves from G_F-tests.
Batch No. 30/10.

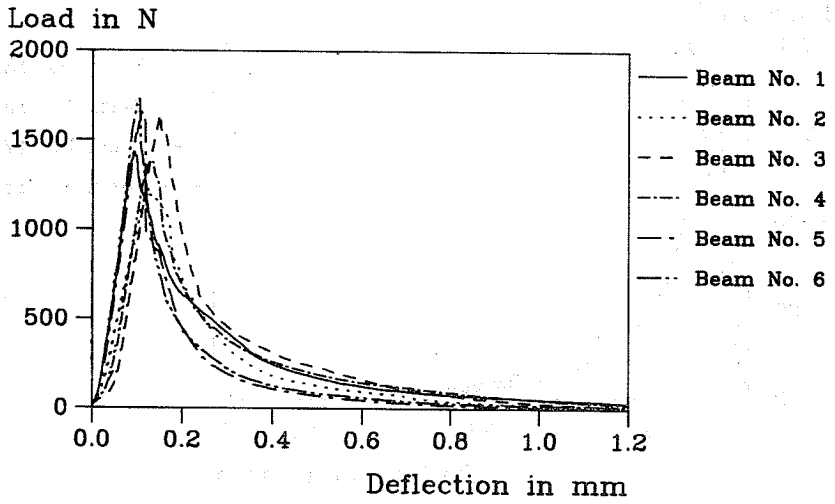

Fig. 3.42 Load-deflection curves from G_F-tests.
Batch No. 30/07.5.

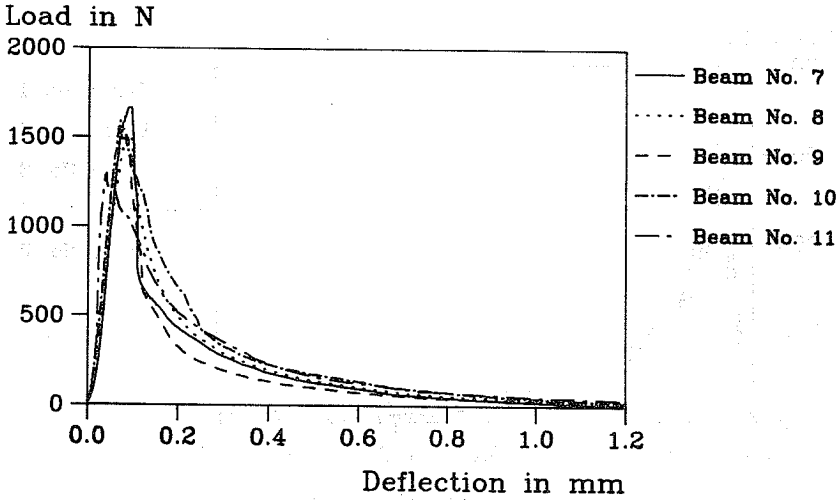

Fig. 3.43 Load-deflection curves from G_F-tests.
Batch No. 30/07.5.

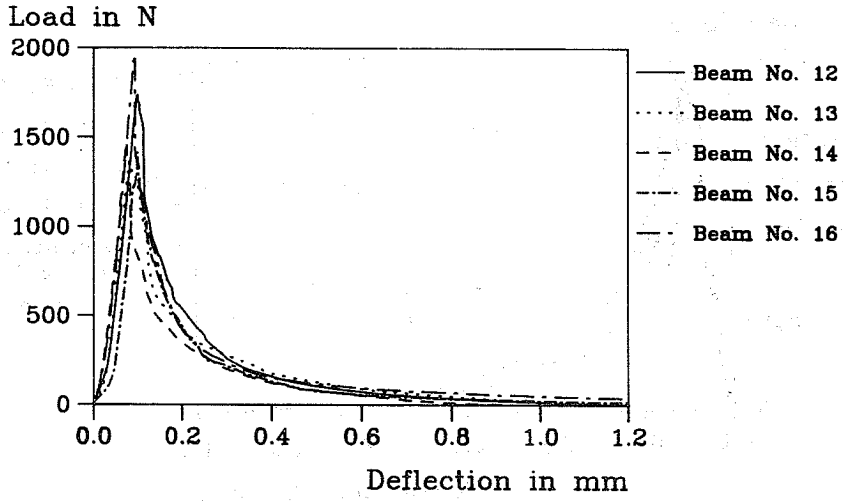

Fig. 3.44 Load-deflection curves from G_F-tests.
Batch No. 30/07.5.

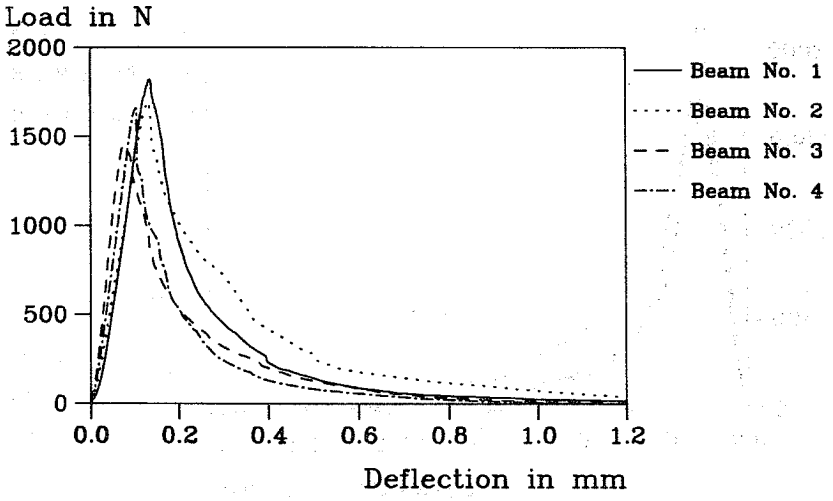

Fig. 3.45 Load-deflection curves from G_F-tests.
Batch No. 50/20.

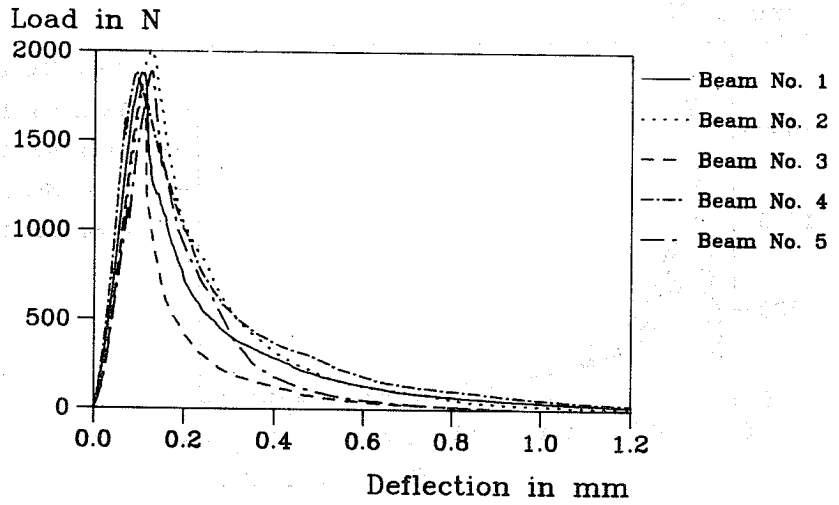

Fig. 3.46 Load-deflection curves from G_F-tests. Batch No. 50/15.

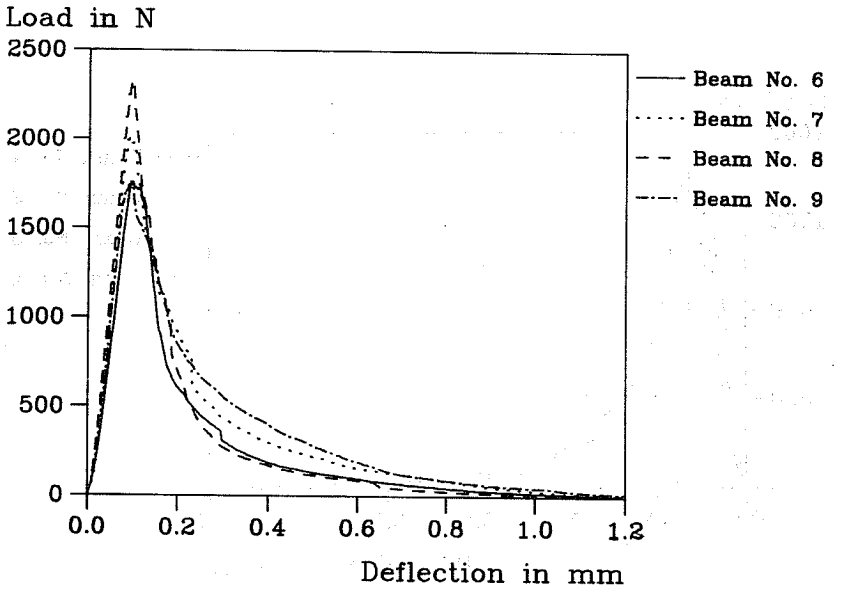

Fig. 3.47 Load-deflection curves from G_F-tests. Batch No. 50/15.

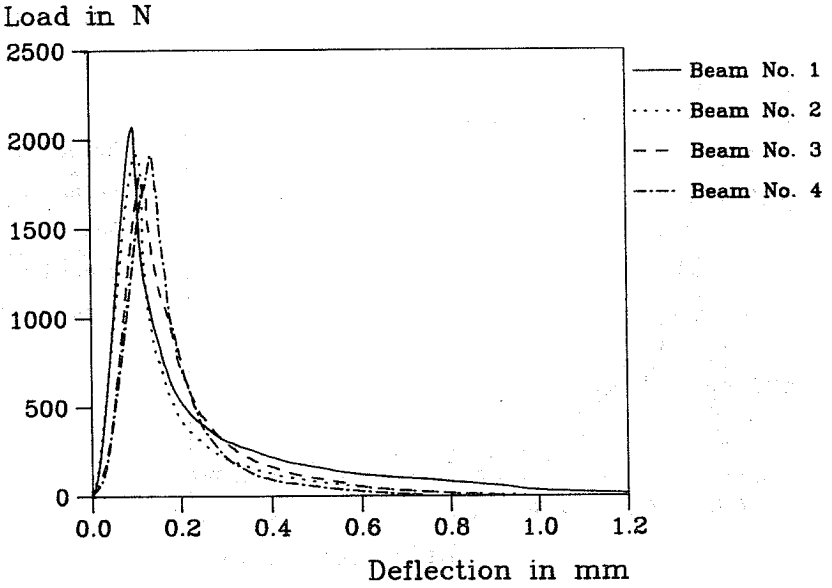

Fig. 3.48 Load-deflection curves from G_F-tests.
Batch No. 50/12.5.

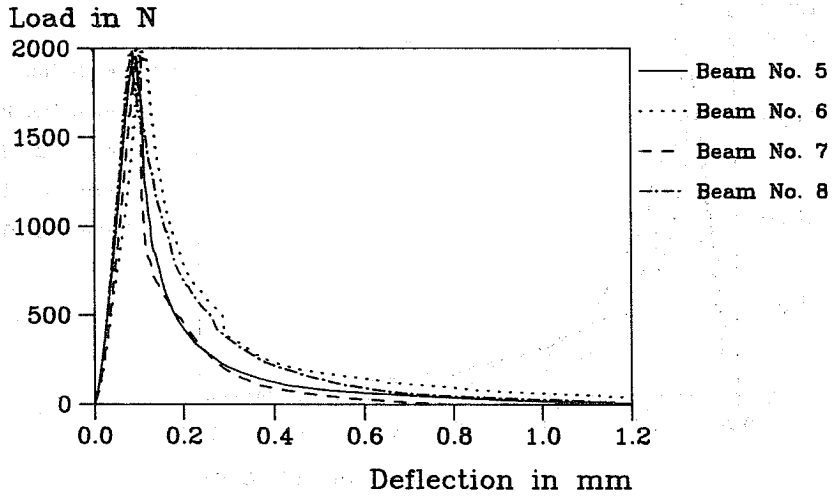

Fig. 3.49 Load-deflection curves from G_F-tests.
Batch No. 50/12.5.

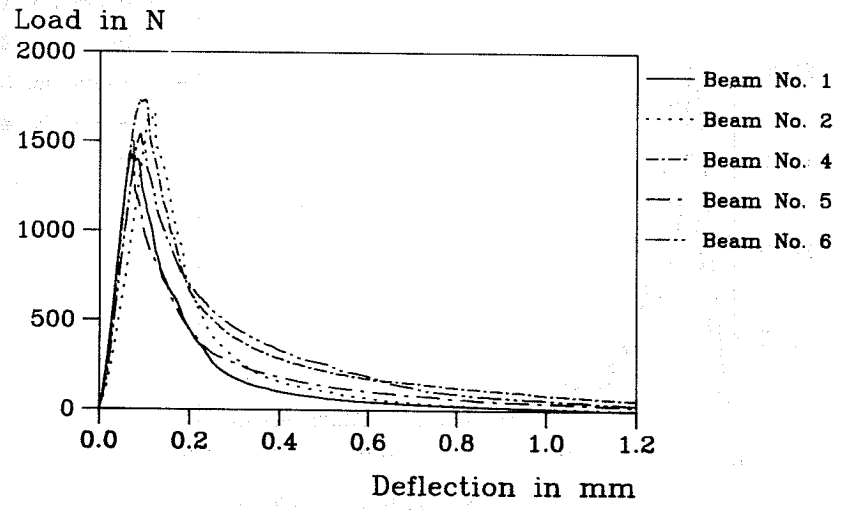

Fig. 3.50 Load-deflection curves from G_F-tests. Batch No. 50/10.

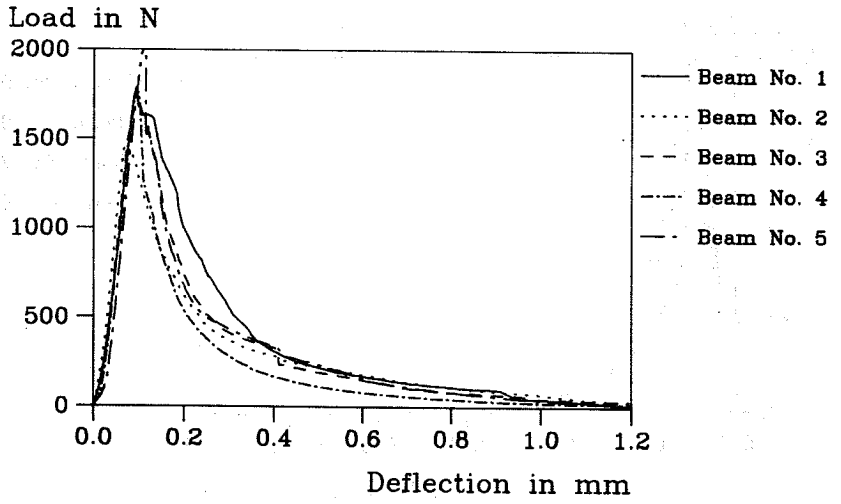

Fig. 3.51 Load-deflection curves from G_F-tests. Batch No. 50/07.5.

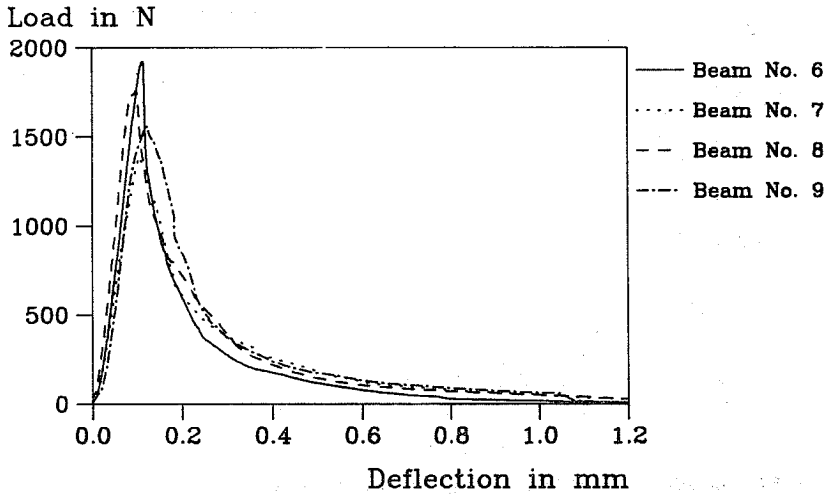

Fig. 3.52 Load-deflection curves from G_F-tests.
Batch No. 50/07.5.

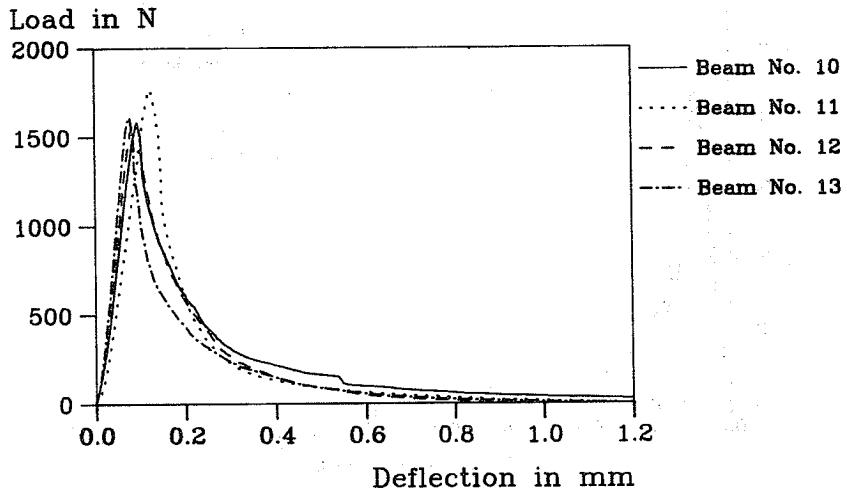

Fig. 3.53 Load-deflection curves from G_F-tests.
Batch No. 50/07.5.

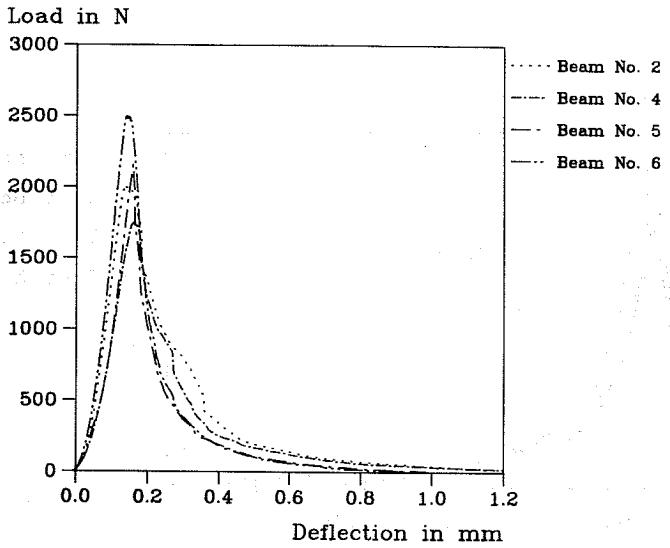

Fig. 3.54 Load-deflection curves from G_F-tests. Batch No. 70/20.

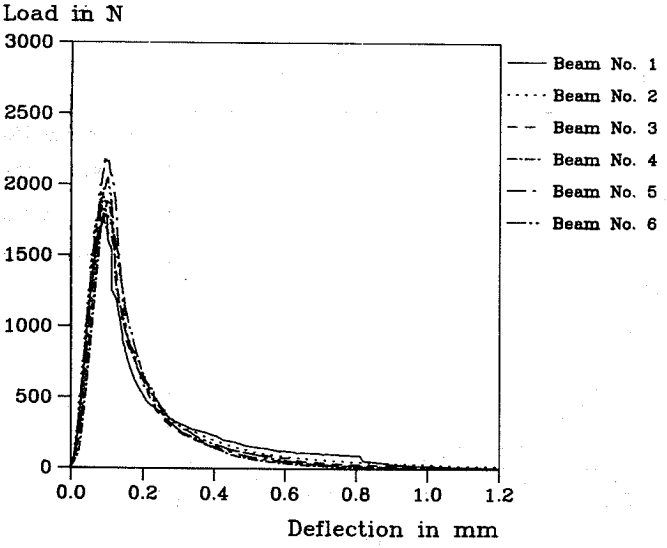

Fig. 3.55 Load-deflection curves from G_F-tests. Batch No. 70/15.

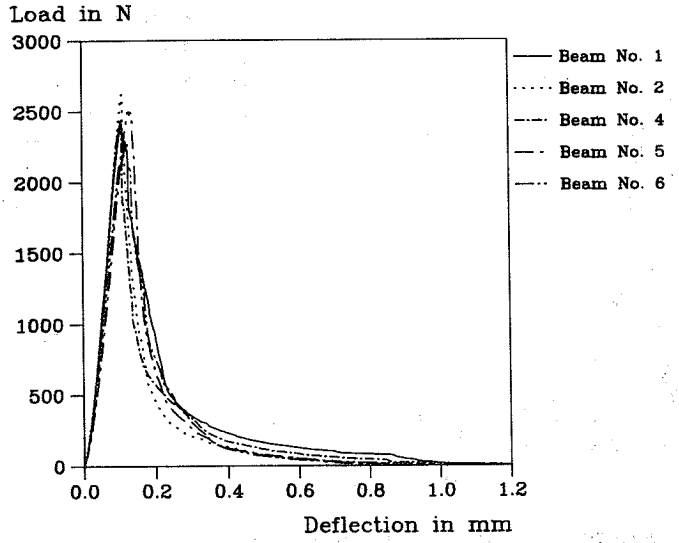

Fig. 3.56 Load-deflection curves from G_F-tests. Batch No. 70/12.5.

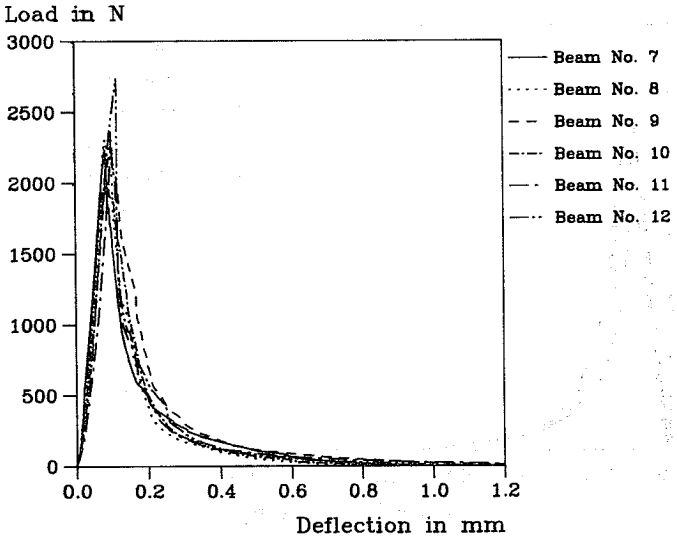

Fig. 3.57 Load-deflection curves from G_F-tests. Batch No. 70/12.5.

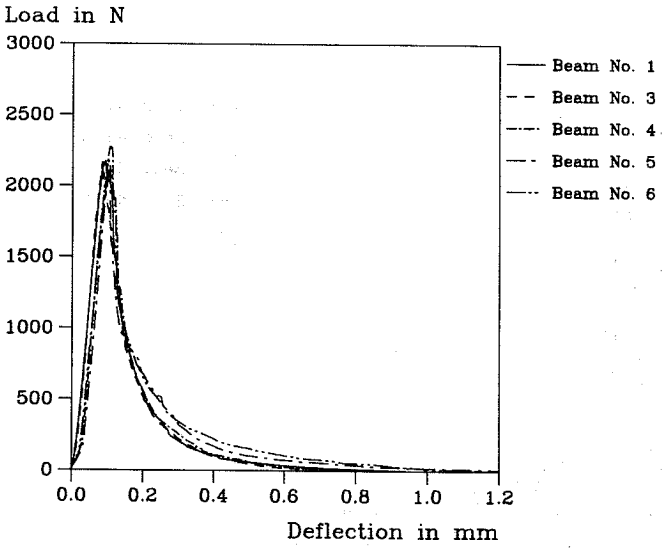

Fig. 3.58 Load-deflection curves from G_F-tests.
Batch No. 70/10.

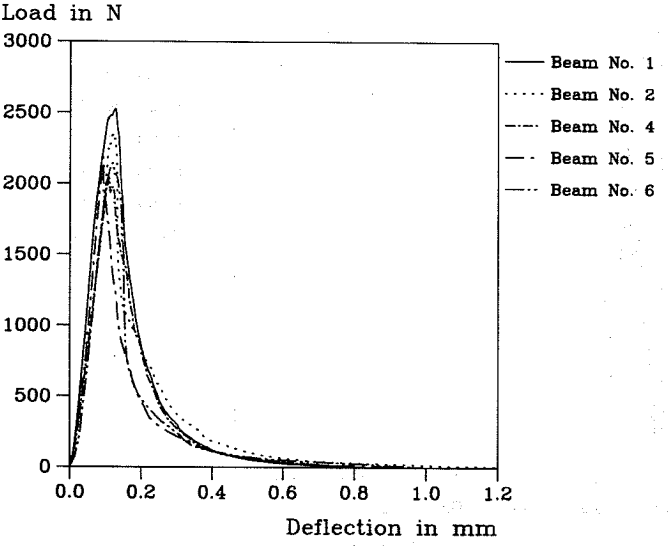

Fig. 3.59 Load-deflection curves from G_F-tests.
Batch No. 70/07.5.

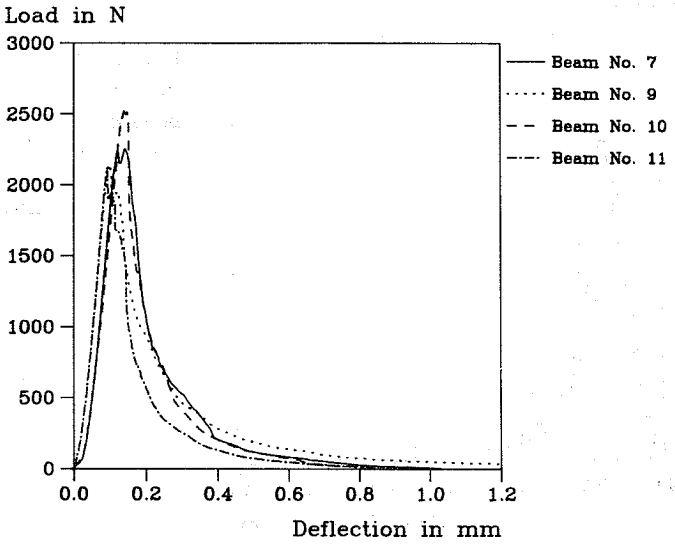

Fig. 3.60 Load-deflection curves from G_F-tests.
Batch No. 70/07.5.

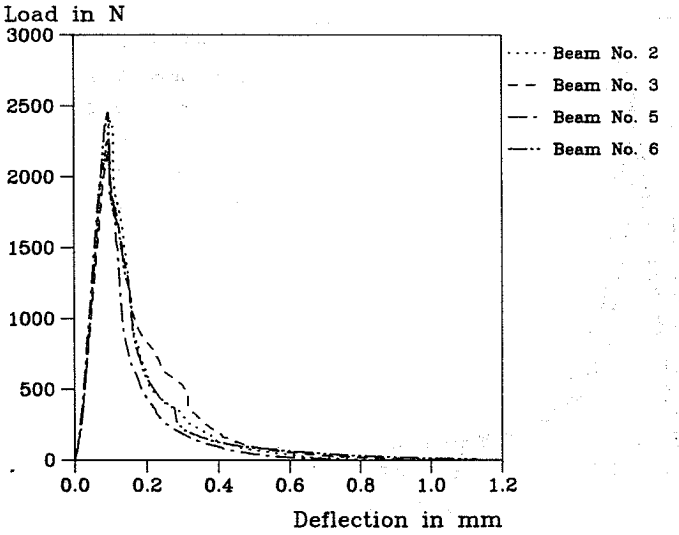

Fig. 3.61 Load-deflection curves from G_F-tests.
Batch No. 70/05.

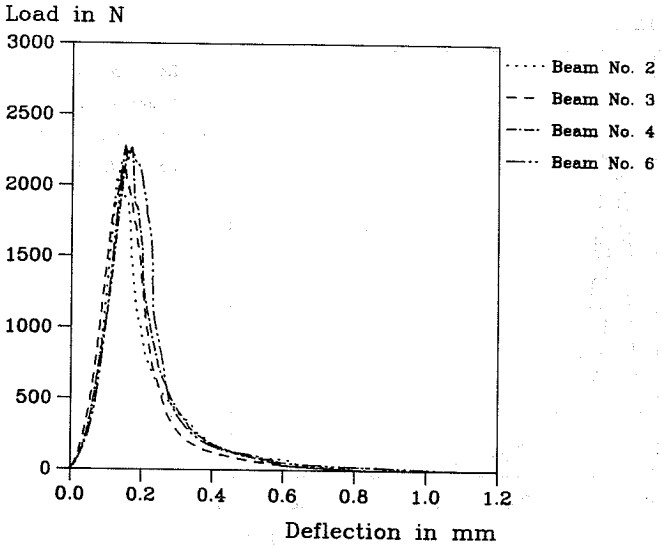

Fig. 3.62 Load-deflection curves from G_F-tests.
Batch No. 90/15.

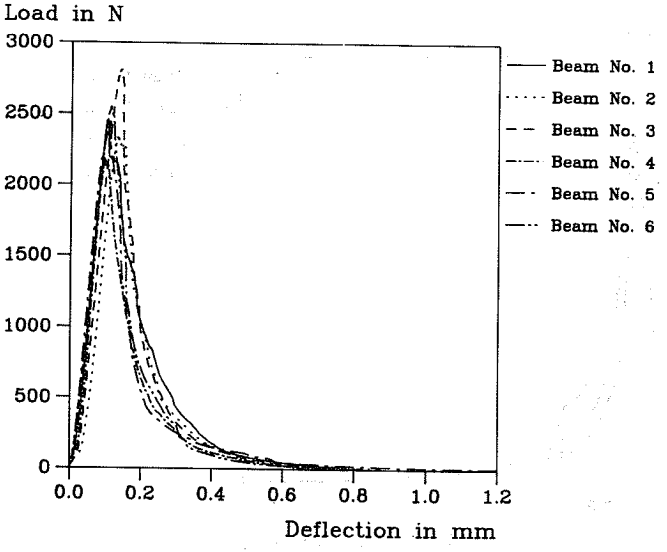

Fig. 3.63 Load-deflection curves from G_F-tests.
Batch No. 90/12.5.

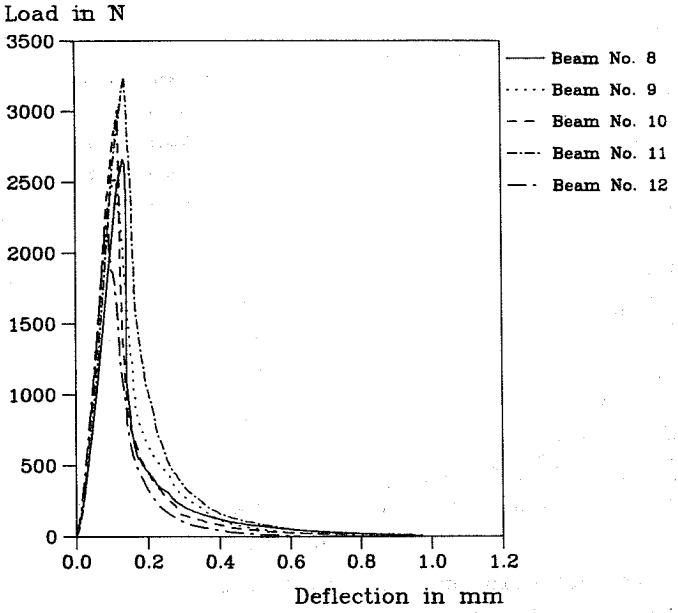

Fig. 3.64 Load-deflection curves from G_F-tests. Batch No. 90/12.5.

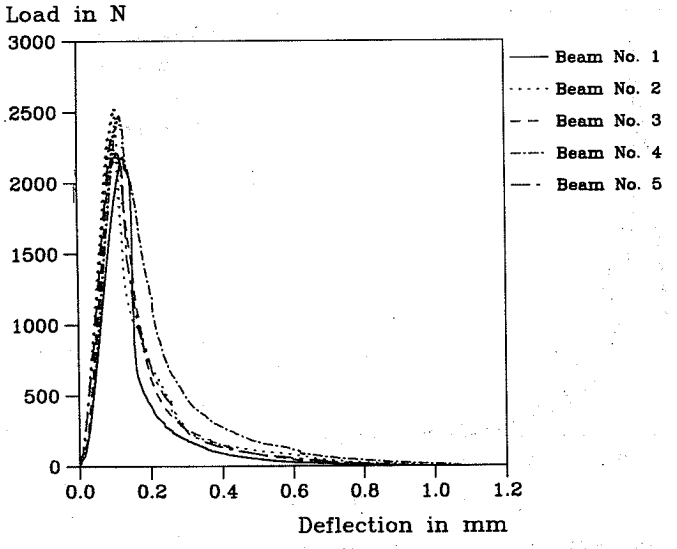

Fig. 3.65 Load-deflection curves from G_F-tests. Batch No. 90/10.

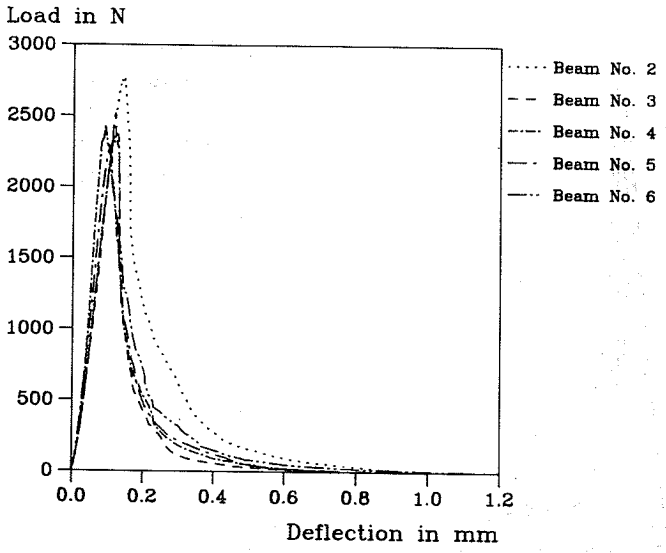

Fig. 3.66 Load-deflection curves from G_F-tests.
Batch No. 90/07.5.

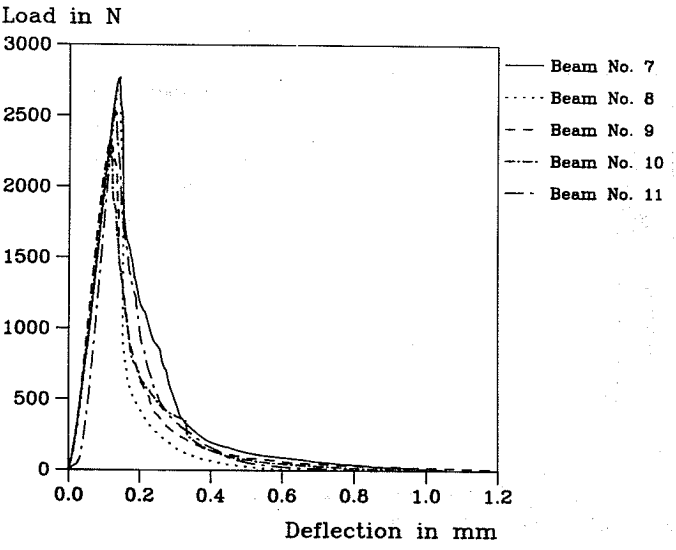

Fig. 3.67 Load-deflection curves from G_F-tests.
Batch No. 90/07.5.

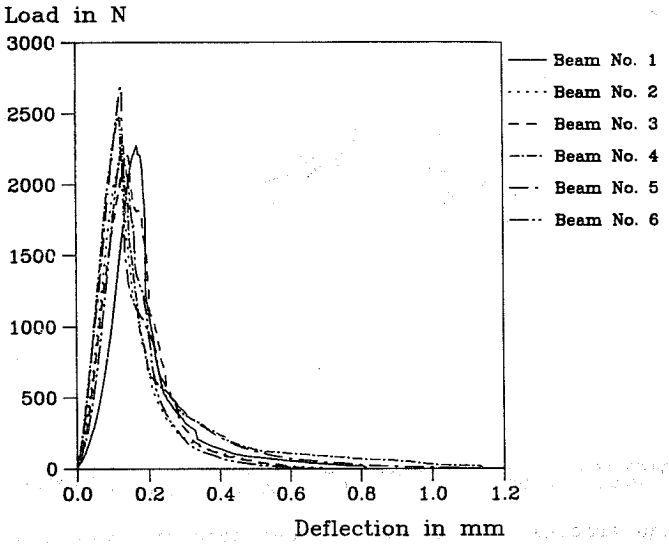

Fig. 3.68 Load-deflection curves from G_F-tests. Batch No. 90/05.

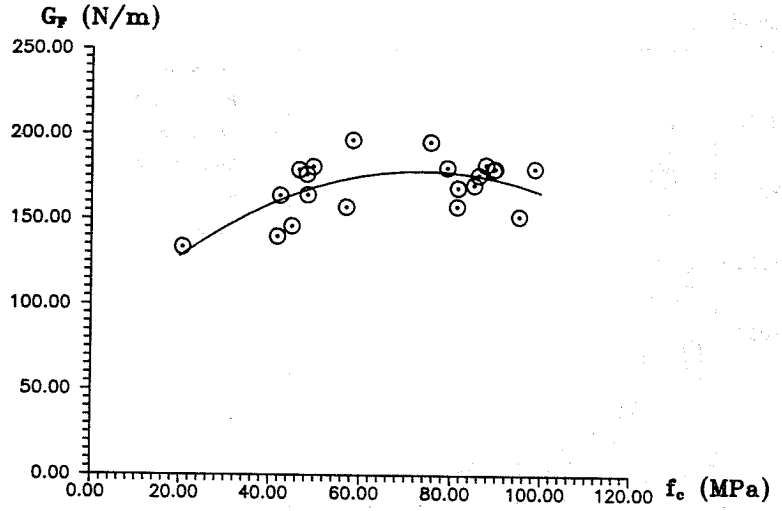

Fig. 3.69 The fracture energy, G_F, versus concrete compressive strength.

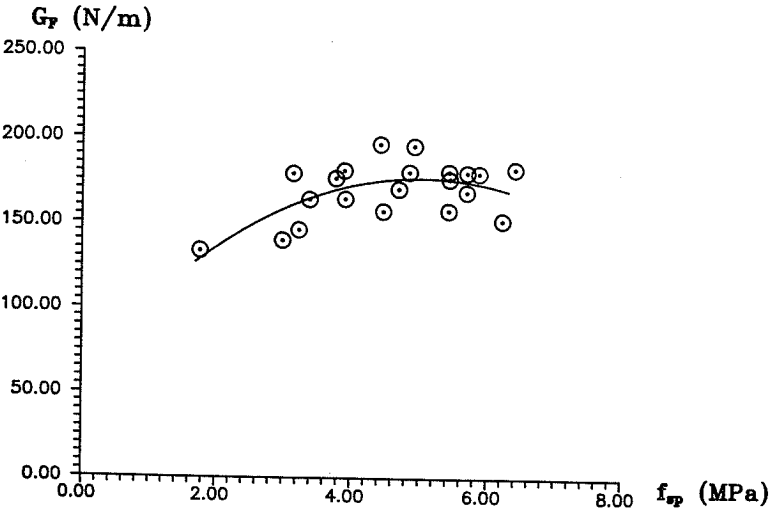

Fig. 3.70 The fracture energy, G_F, versus concrete splitting strength.

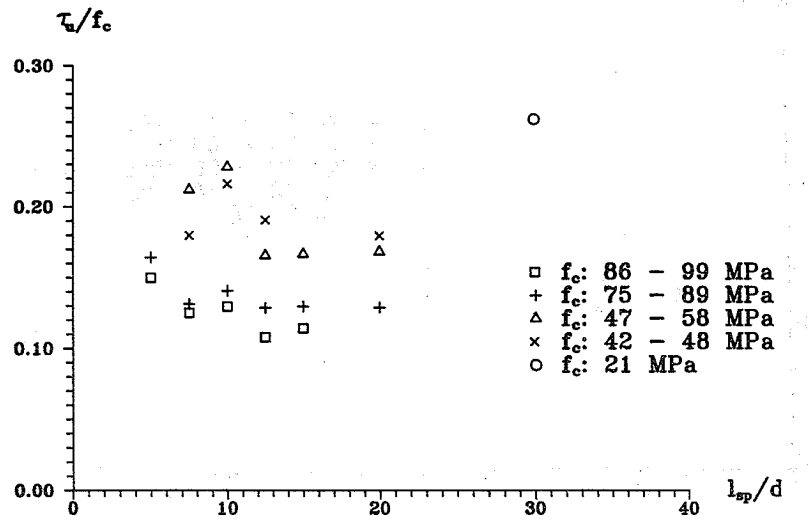

Fig. 4.1 τ_u/f_c - l_{sp}/d illustration of the experimental results from the S.B.-tests.

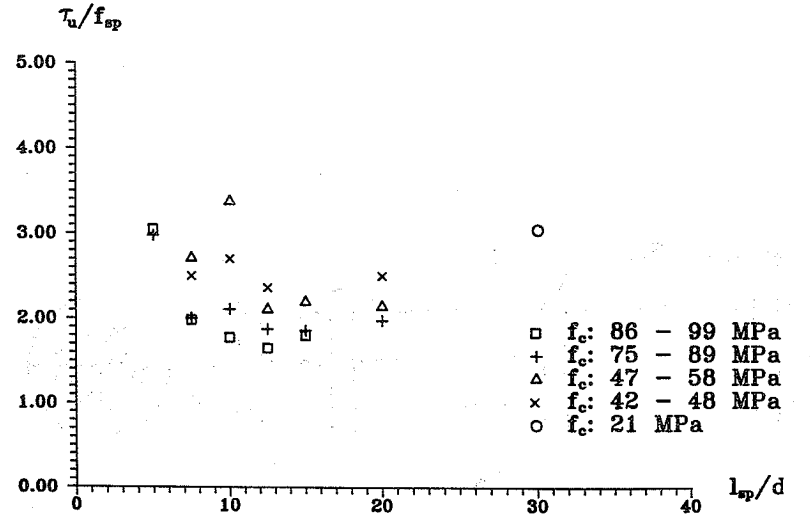

Fig. 4.2 τ_u/fsp - l_{sp}/d illustration of the experimental results from the S.B.-tests.

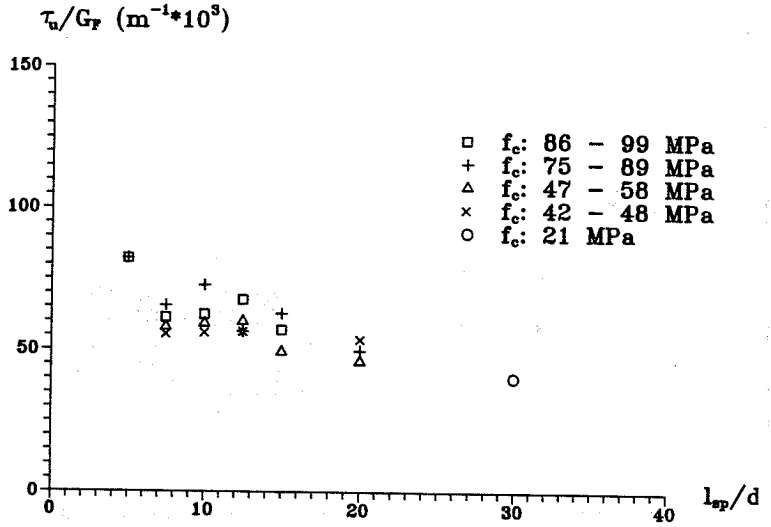

Fig. 4.3 τ_u/G_F - l_{sp}/d illustration of the experimental results from the S.B.-tests.

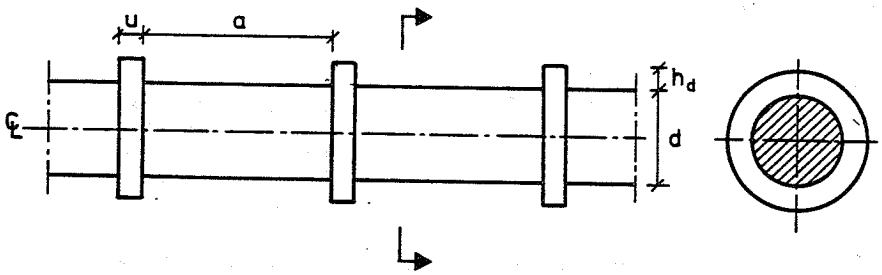

Fig. 4.4 Rib geometry of a deformed reinforcing bar.

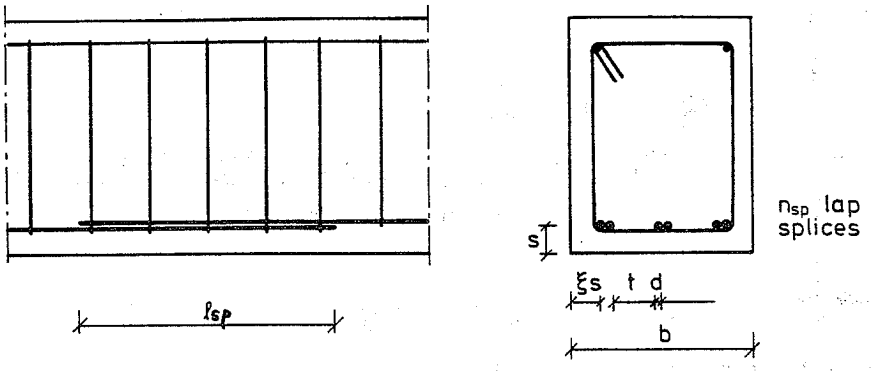

Fig. 4.5 Geometrical parameters for lap splices.

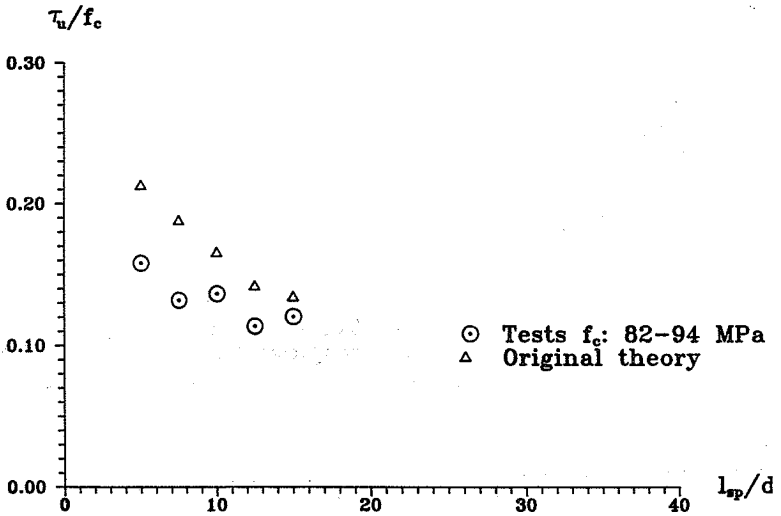

Fig. 4.6 Test results and estimated values of τ_u/f_c using the original theory of Andreasen [24] for f_c: 82-94 MPa.

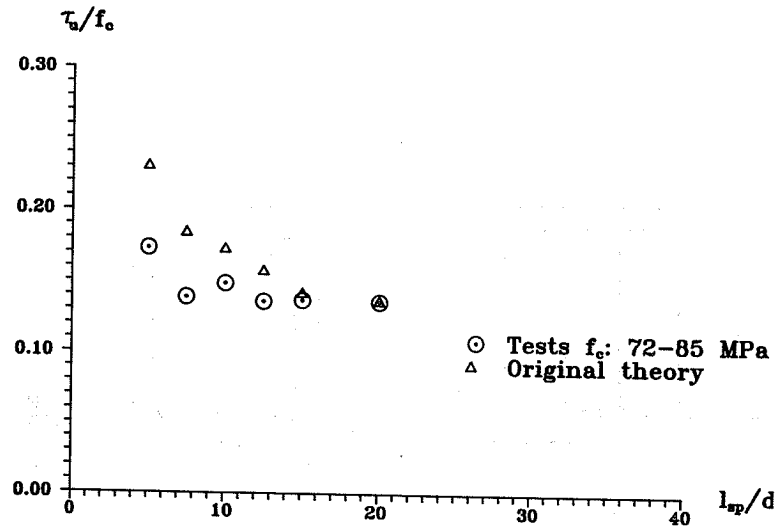

Fig. 4.7 Test results and estimated values of τ_u/f_c using the original theory of Andreasen [24] for f_c: 72-85 MPa.

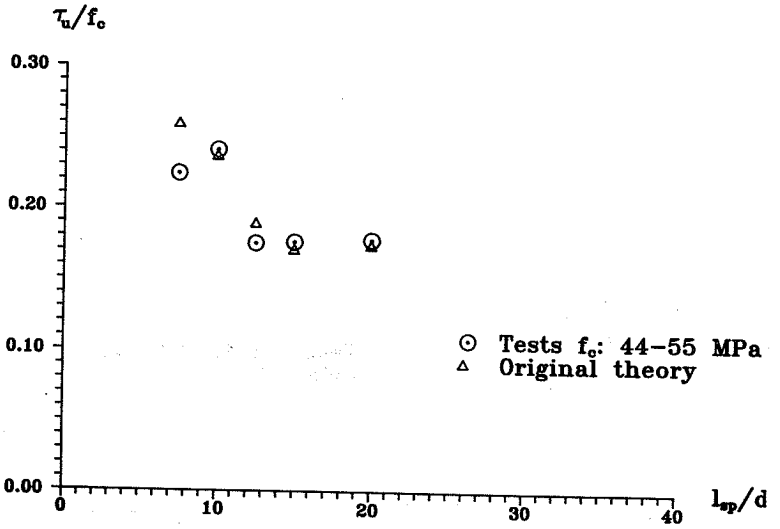

Fig. 4.8 Test results and estimated values of τ_u/f_c using the original theory of Andreasen [24] for f_c: 44-55 MPa.

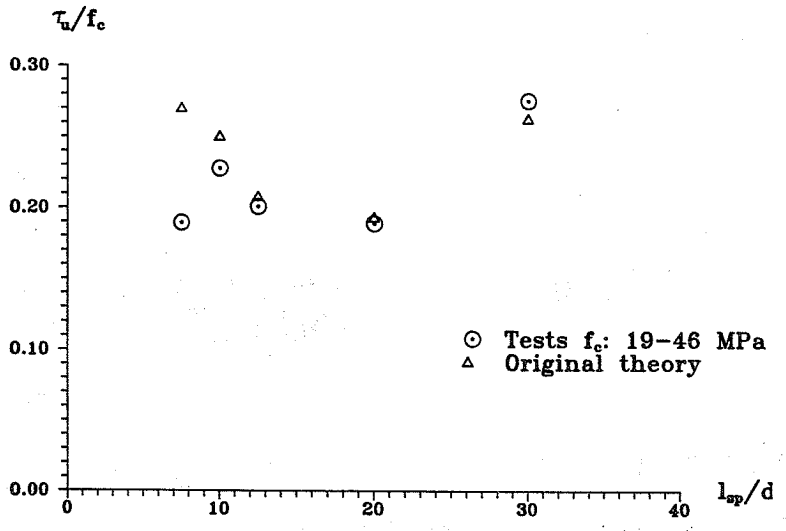

Fig. 4.9 Test results and estimated values of τ_u/f_c using the original theory of Andreasen [24] for f_c: 19-46 MPa.

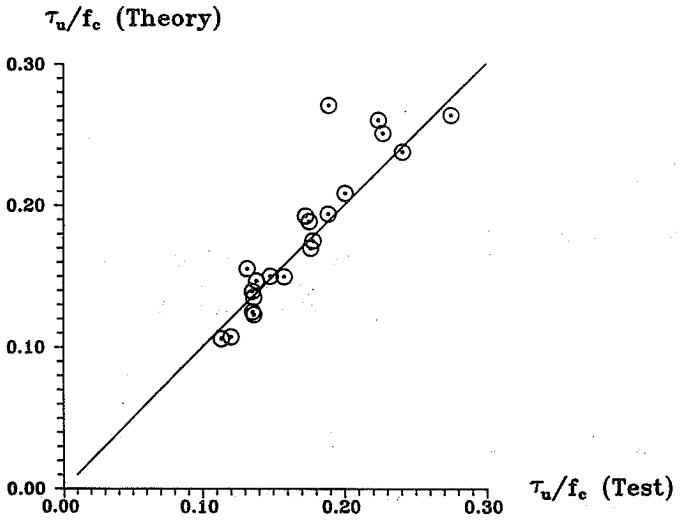

Fig. 4.10 Correspondence between the S.B.-tests and the theory which includes the new ν-expression.

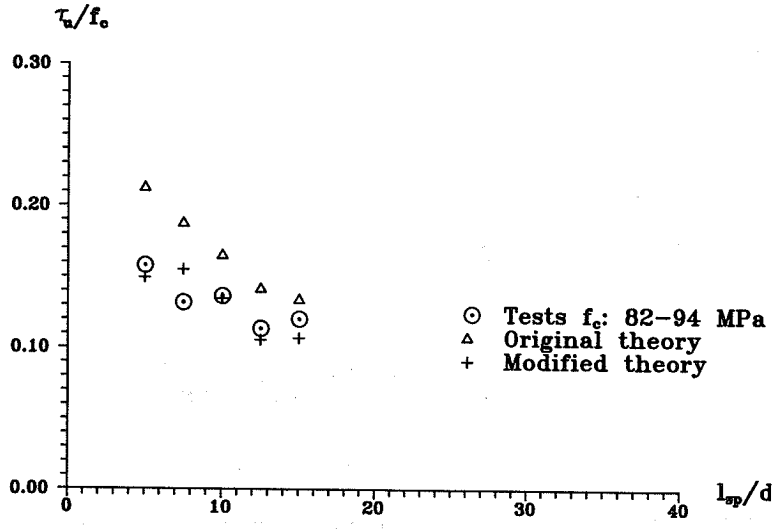

Fig. 4.11 Test results and estimated values of τ_u/f_c using the original theory of Andreasen [24] and a modification of the ν-expression for f_c: 82-94 MPa.

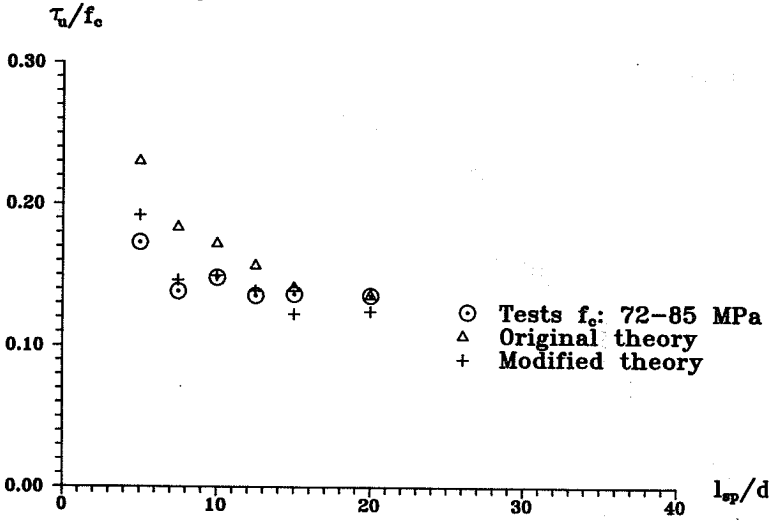

Fig. 4.12 Test results and estimated values of τ_u/f_c using the original theory of Andreasen [24] and a modification of the ν-expression for f_c: 72-85 MPa.

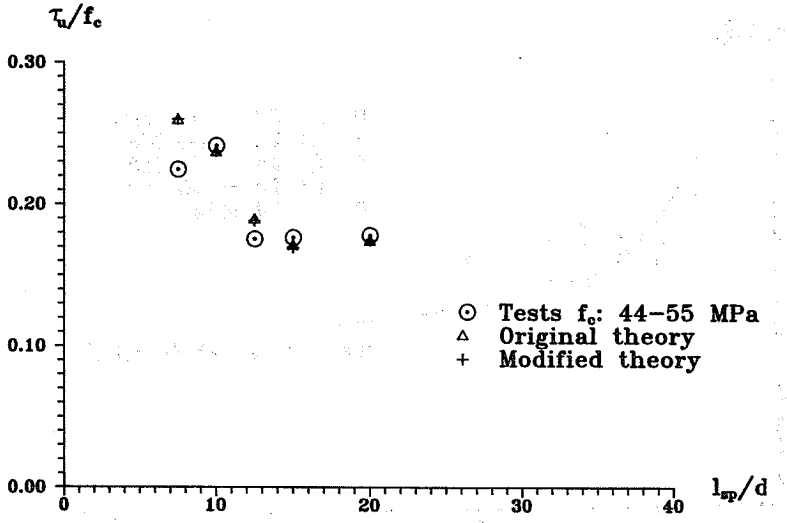

Fig. 4.13 Test results and estimated values of τ_u/f_c using the original theory of Andreasen [24] and a modification of the ν-expression for f_c: 44-55 MPa.

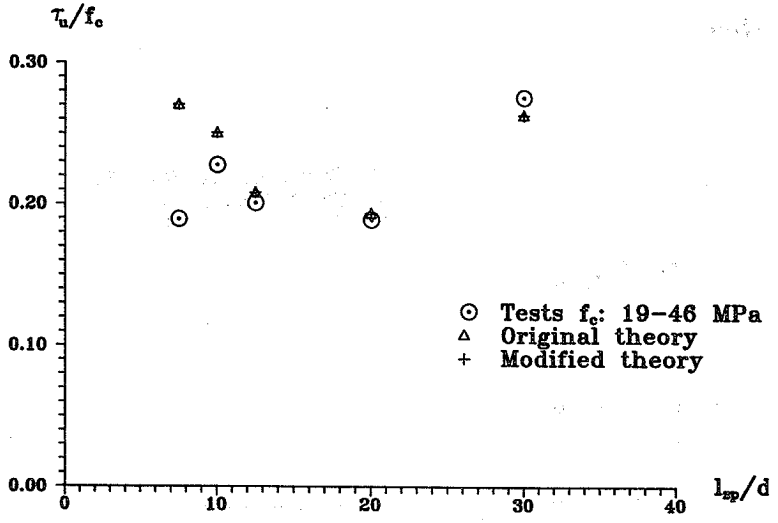

Fig. 4.14 Test results and estimated values of τ_u/f_c using the original theory of Andreasen [24] and a modification of the ν-expression for f_c: 19-46 MPa.

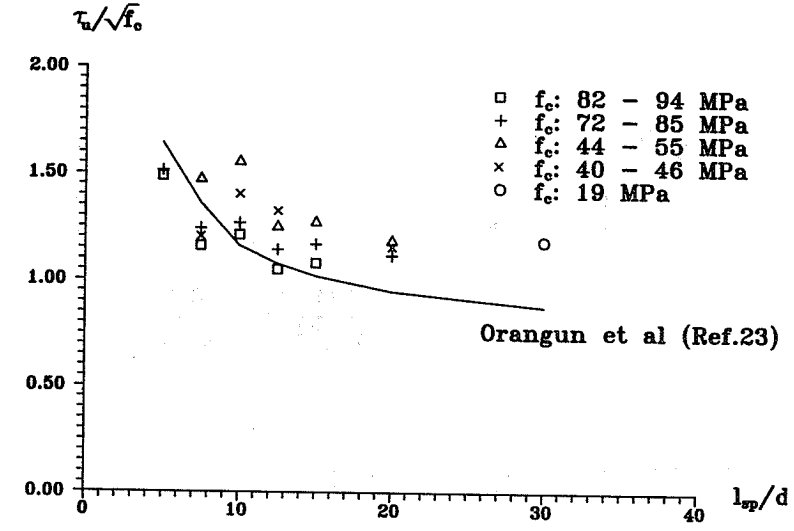

Fig. 4.15 Experimental results compared to Orangun et al. [23].

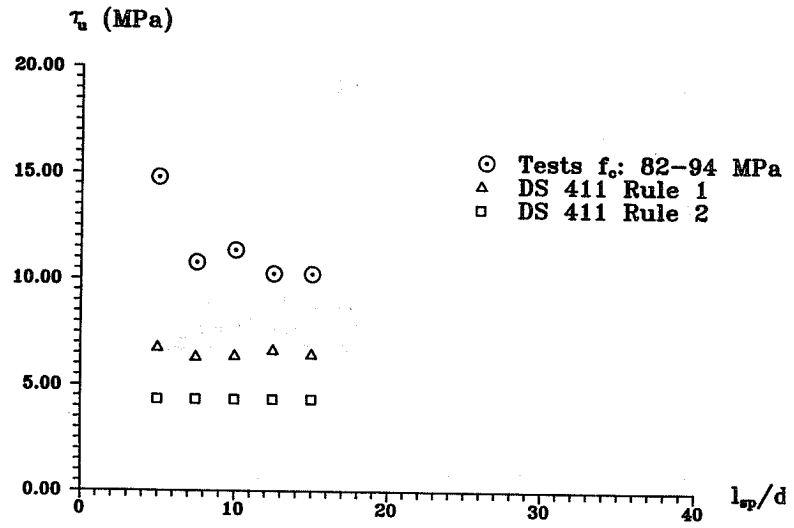

Fig. 4.16 τ_u-values from the tests and computed values using DS 411 in case of high strength concrete, for f_c: 82-94 MPa.

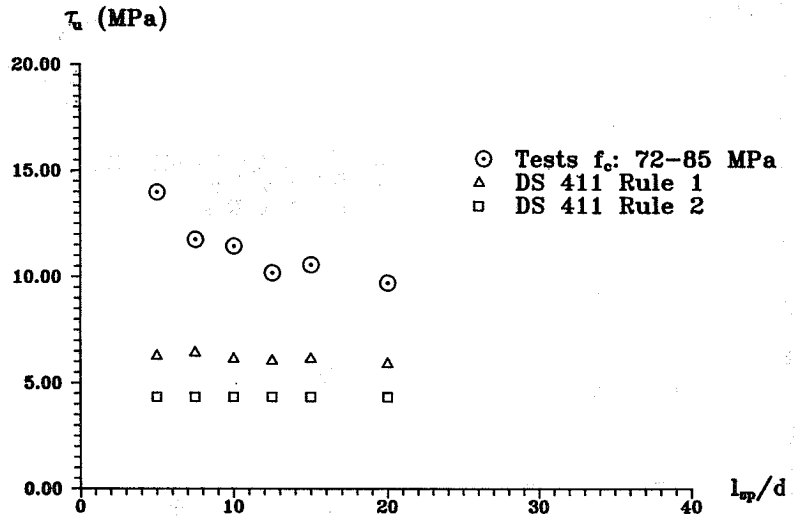

Fig. 4.17 τ_u-values from the tests and computed values using DS 411 in case of high strength concrete, for f_c: 72-85 MPa.

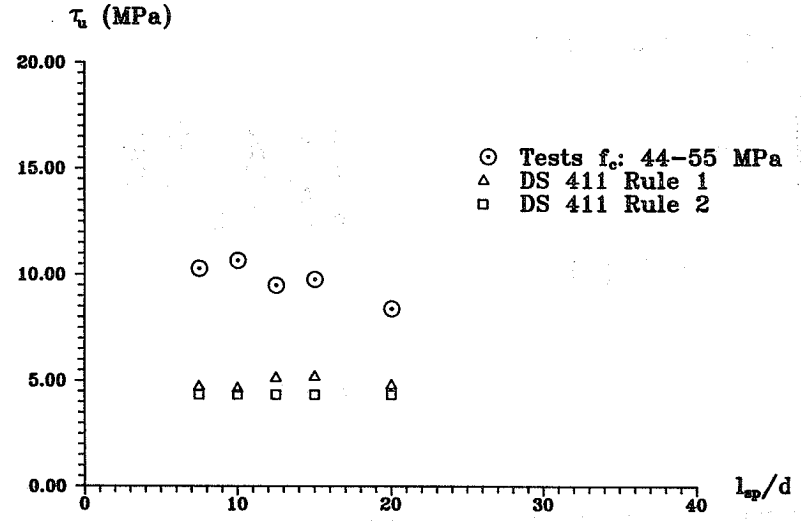

Fig. 4.18 τ_u-values from the tests and computed values using DS 411 in case of normal strength concrete, for f_c: 44-55 MPa.

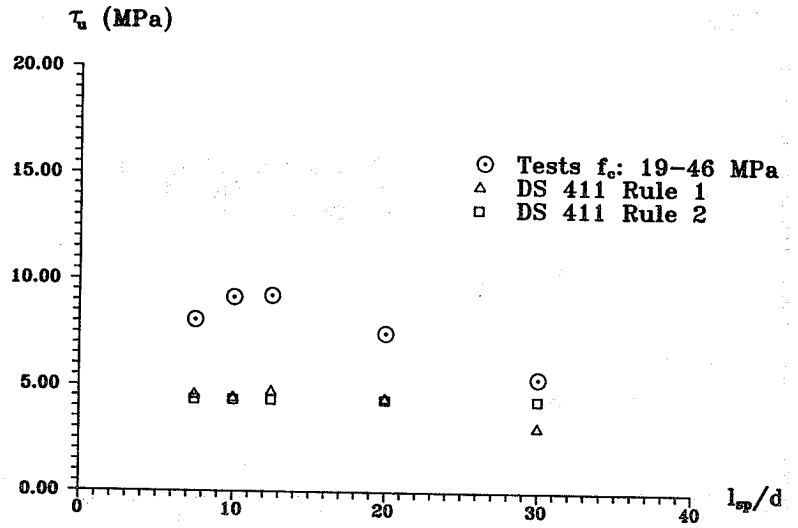

Fig. 4.19 τ_u-values from the tests and computed values using DS 411 in case of normal strength concrete, for f_c: 19-46 MPa.

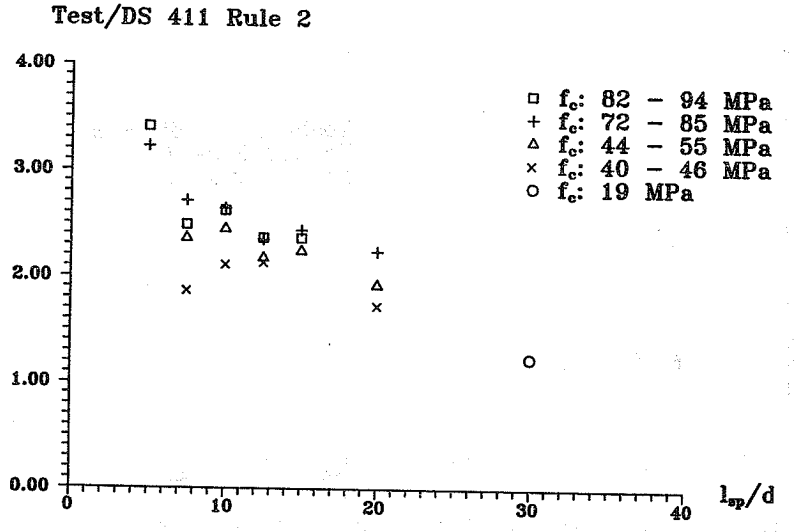

Fig. 4.20 Ratio between τ_u-values from the tests and computed values from DS 411 rule 2.

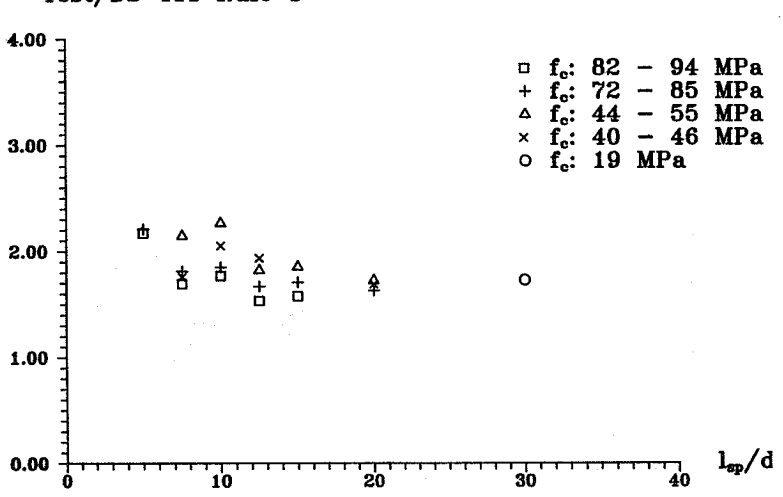

Fig. 4.21 Ratio between τ_u-values from the tests and computed values from DS 411 rule 1.

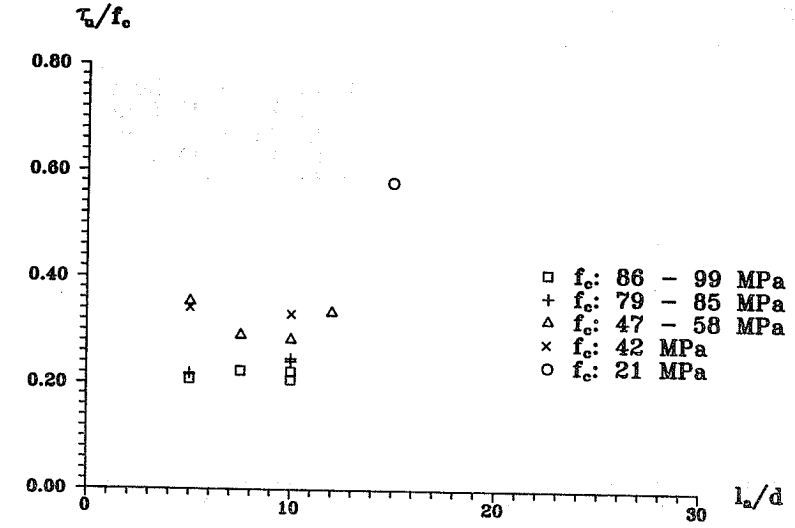

Fig. 4.22 τ_u/f_c-l_a/d illustration of the experimental results from the EF.-tests.

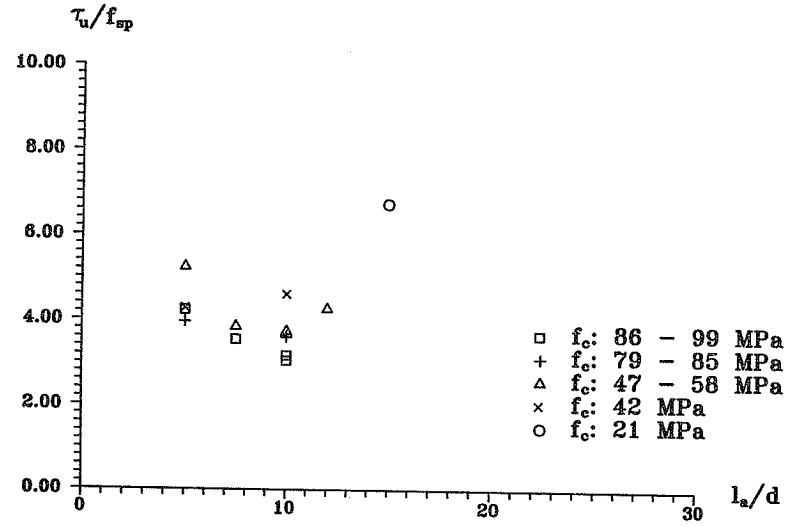

Fig. 4.23 τ_u/f_{sp}-l_a/d illustration of the experimental results from the EF.-tests.

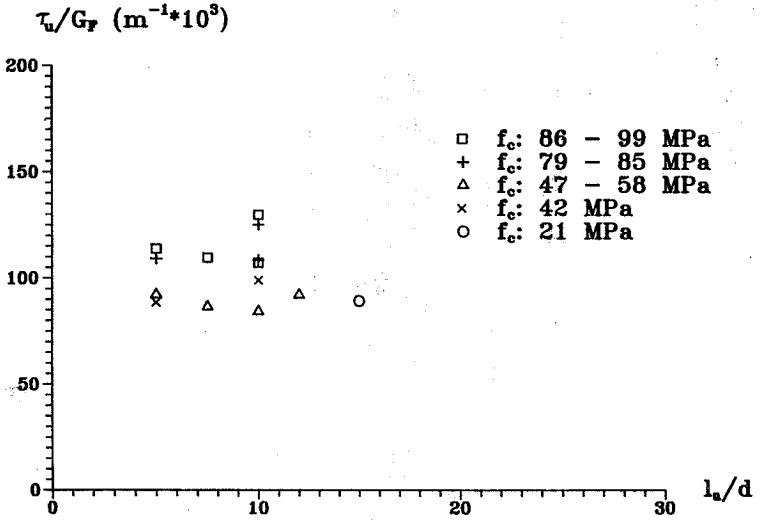

Fig. 4.24 τ_u/G_F-l_a/d illustration of the experimental results from the EF.-tests.

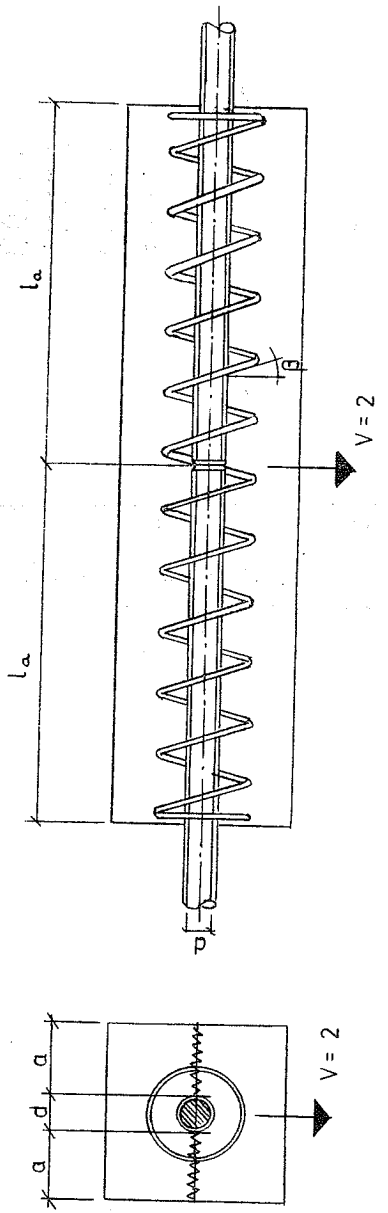

Fig. 4.25 Suggested failure mechanism of the EF.-test specimen.

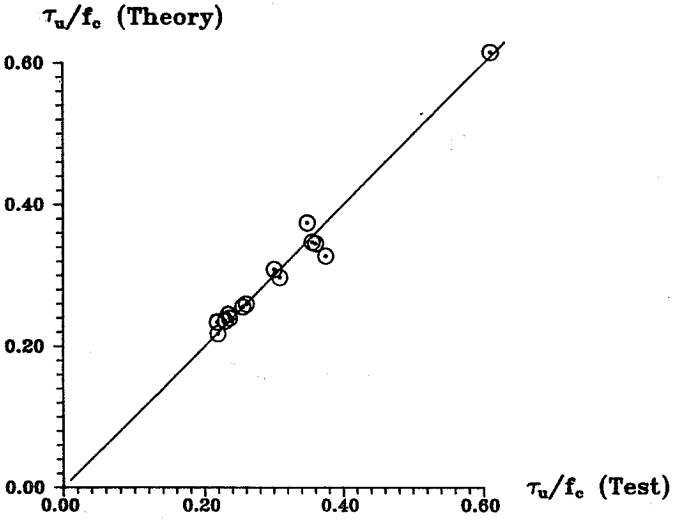

Fig. 4.26 Correspondence between the EF.-tests and the theory.

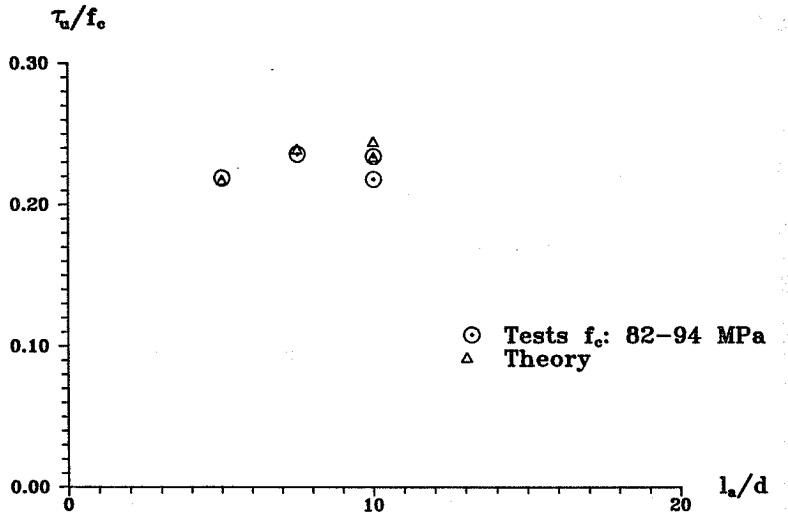

Fig. 4.27 Test results and estimated values of τ_u/f_c, for f_c: 82-94 MPa.

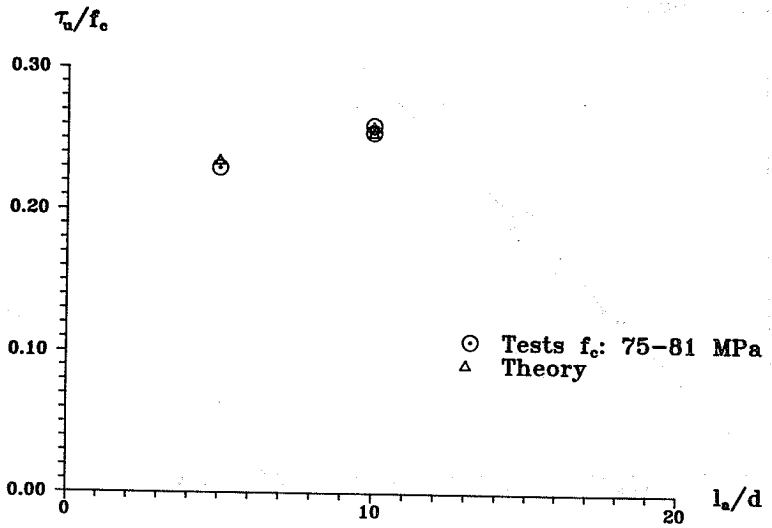

Fig. 4.28 Test results and estimated values of τ_u/f_c, for f_c: 75-81 MPa.

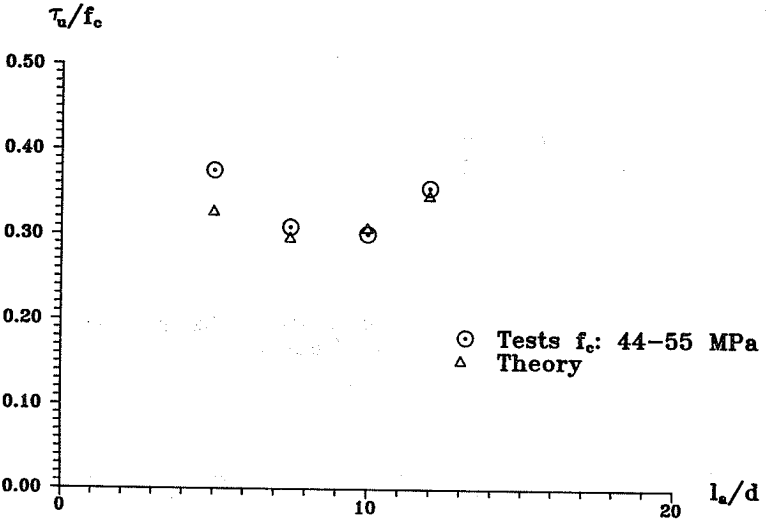

Fig. 4.29 Test results and estimated values of τ_u/f_c, for f_c: 44-55 MPa.

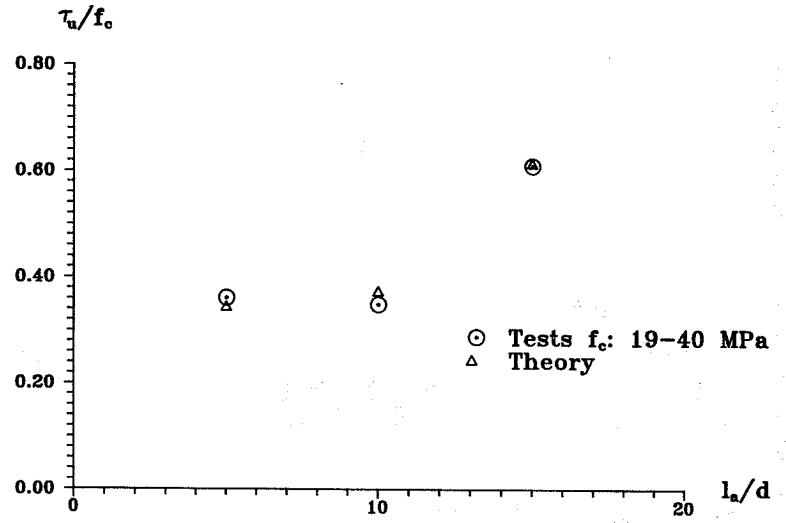

Fig. 4.30 Test results and estimated values of τ_u/f_c, for f_c: 19-40 MPa.

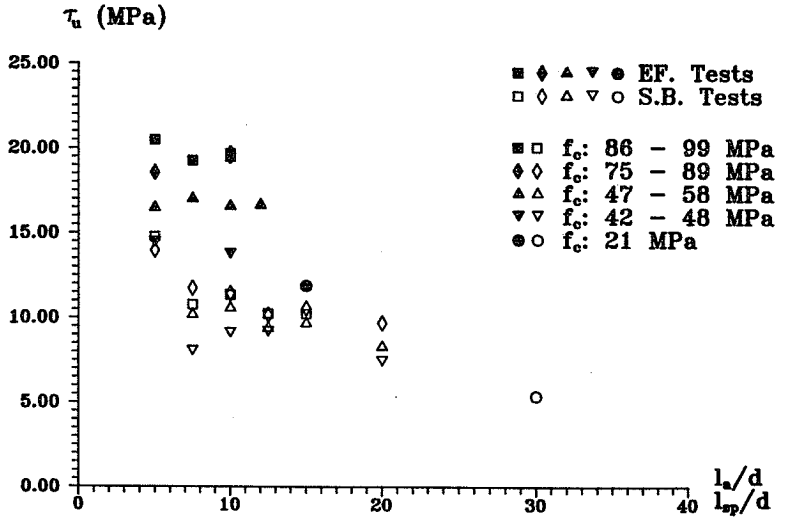

Fig. 4.31 τ_u-values from all EF.-tests and S.B.-tests.

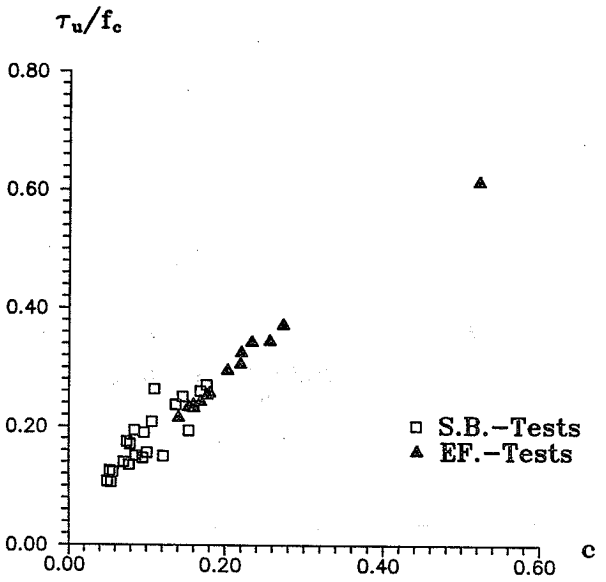

Fig. 4.32 Calculated τ_u/f_c-values of all EF.-tests and S.B.-tests and the corresponding values of C.

9. PHOTOS

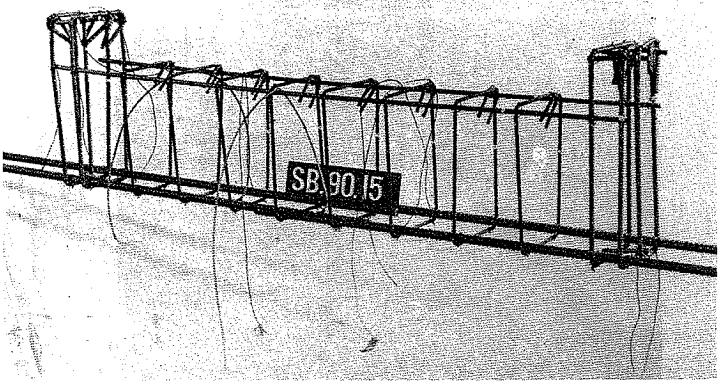

Photo 2.1 An example of S.B.-specimen reinforcement arrangement type I.

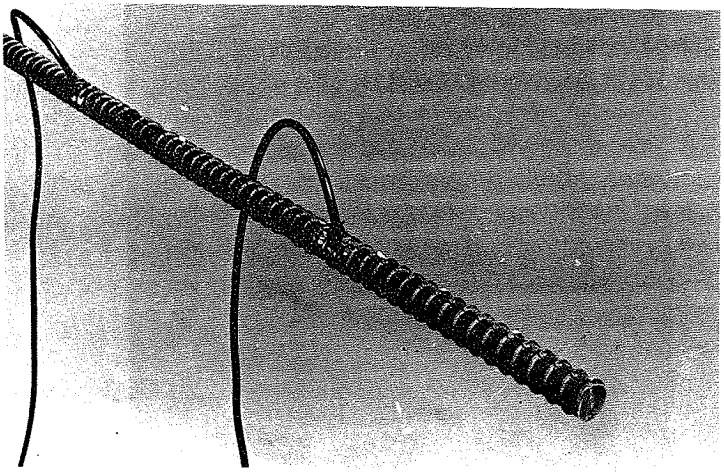

Photo 2.2 An example of a bar containing 9 strain gauges used in S.B.-specimens.

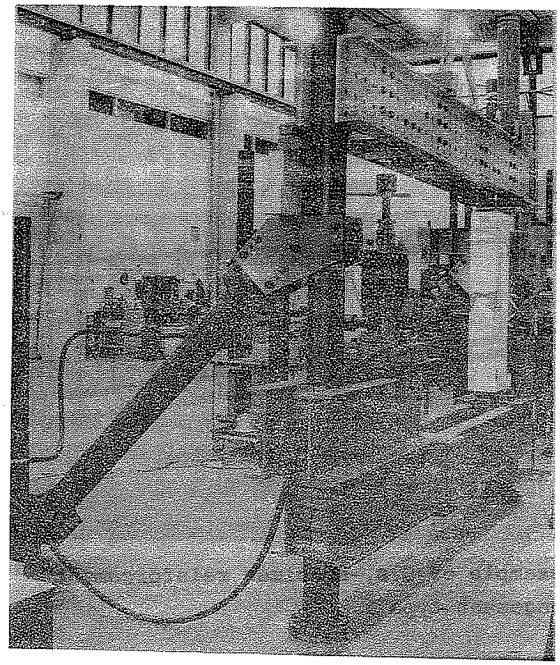

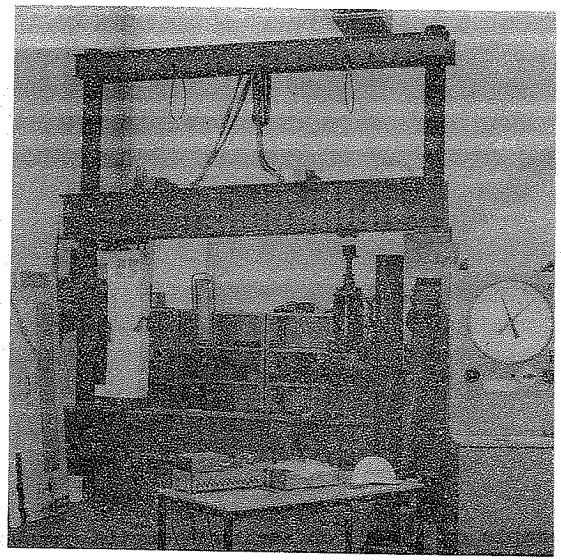

Photo 2.3 Test-rig used for the S.B.-specimens.

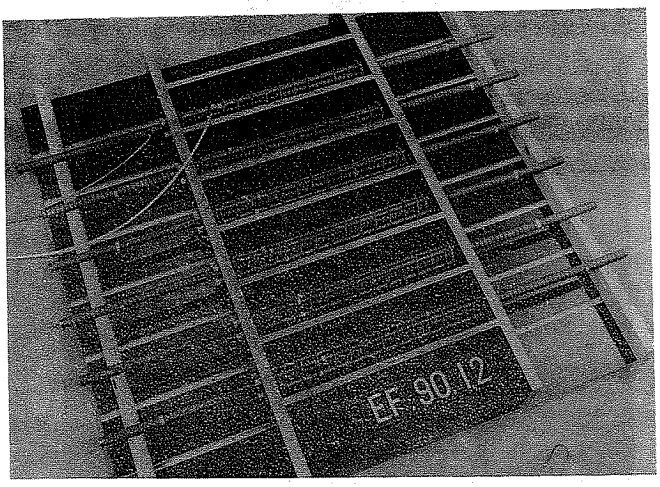

Photo 2.4 Form used when casting the EF.-specimens.

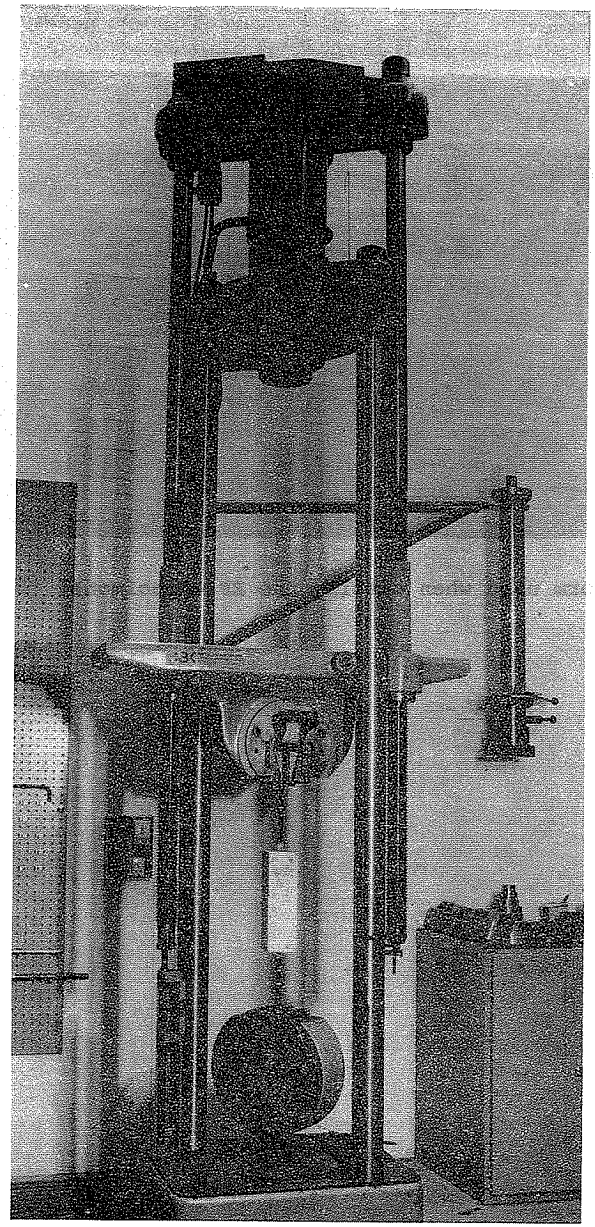

Photo 2.5 Test-rig used for the EF.-specimens.

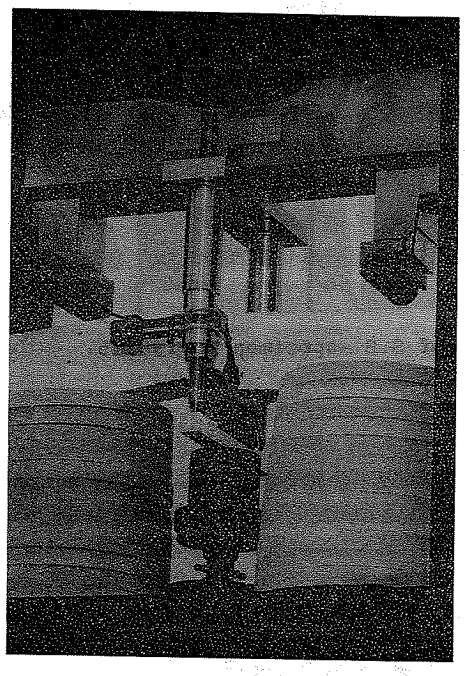

Photo 2.6 Test-rig used for the G_F-specimens.

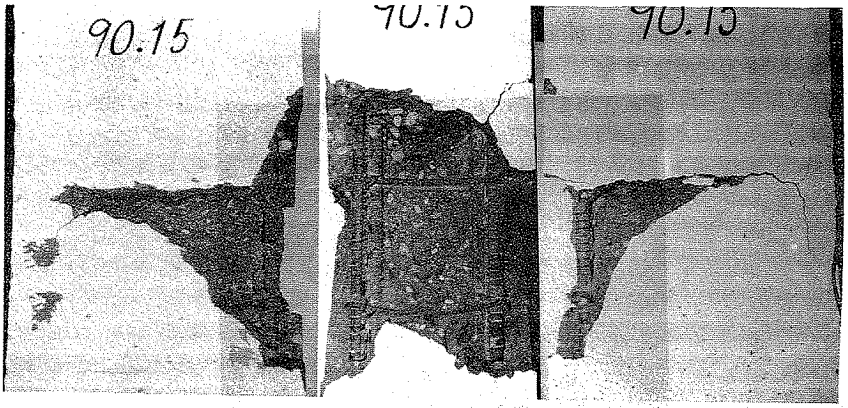

Photo 3.1 Failure of S.B.-specimen No. 90/15.

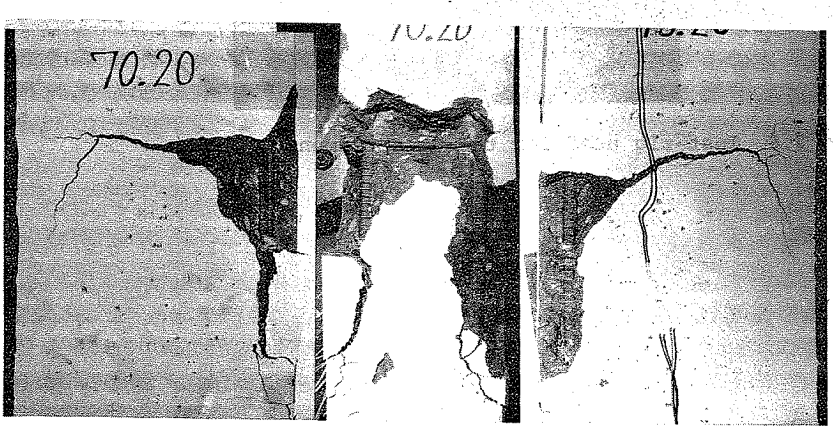

Photo 3.2 Failure of S.B.-specimen No. 70/20.

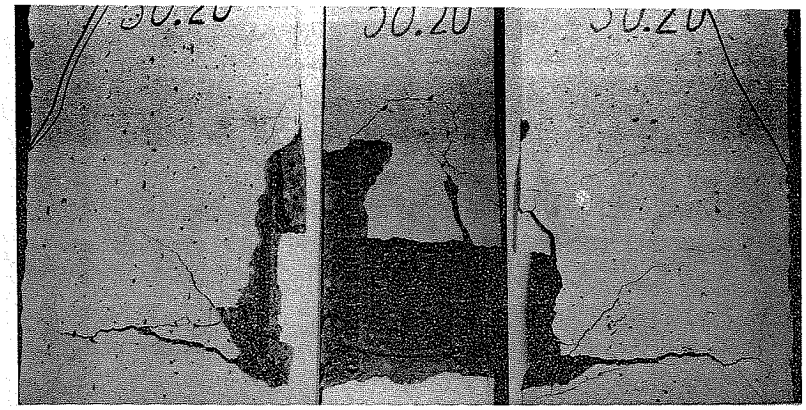

Photo 3.3 Failure of S.B.-specimen No. 50/20.

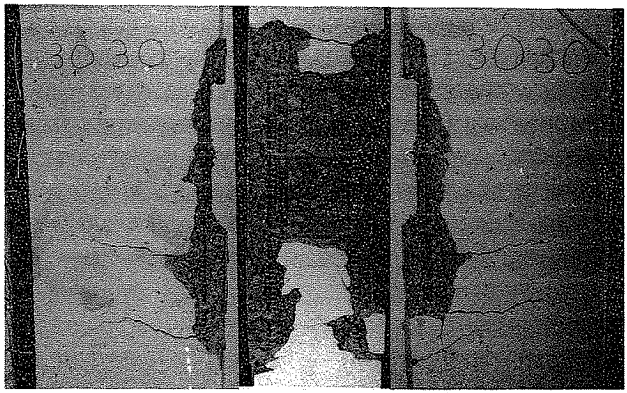

Photo 3.4 Failure of S.B.-specimen No. 30/30.

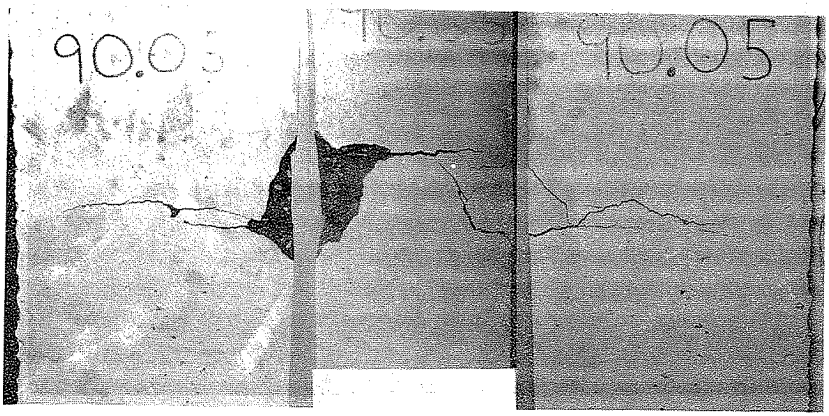

Photo 3.5 Failure of S.B.-specimen No. 90/05.

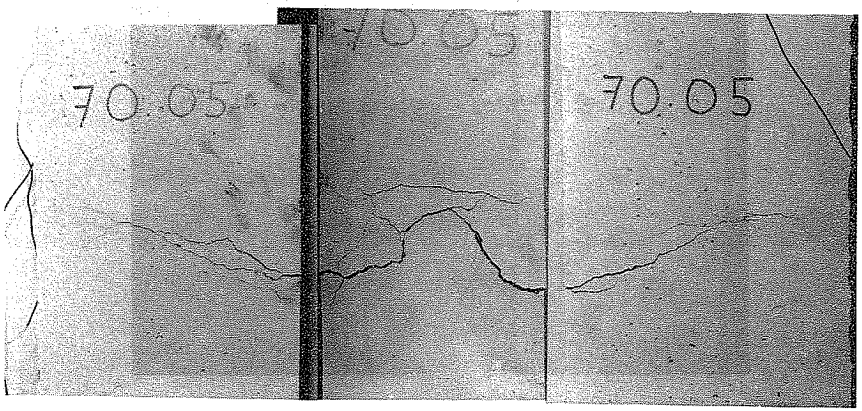

Photo 3.6 Failure of S.B.-specimen No. 70/05.

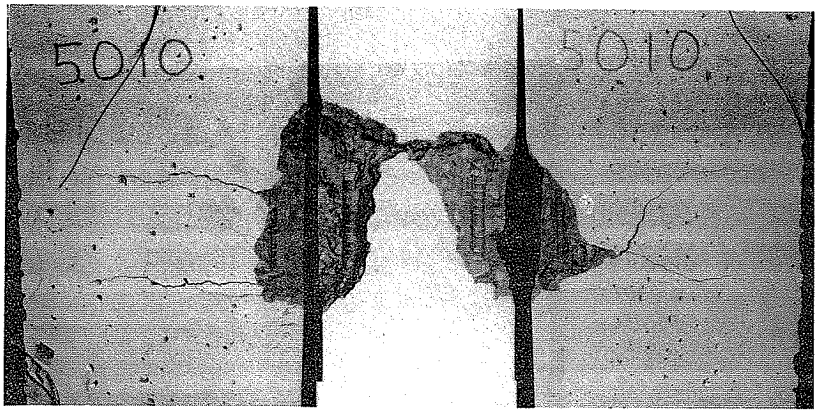

Photo 3.7 Failure of S.B.-specimen No. 50/10.

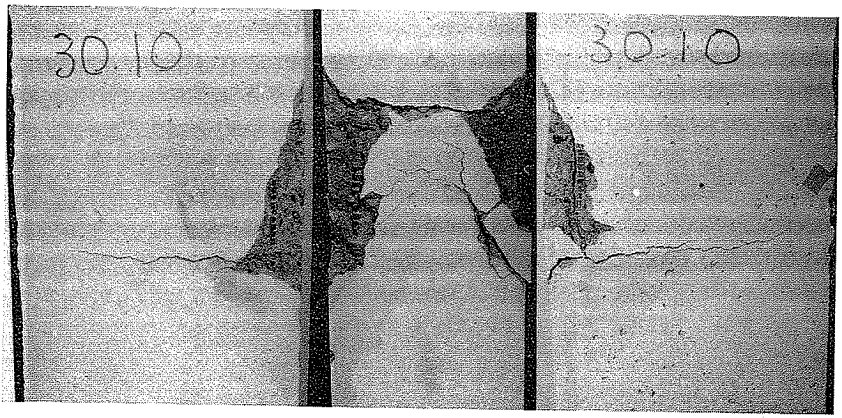

Photo 3.8 Failure of S.B.-specimen No. 30/10.

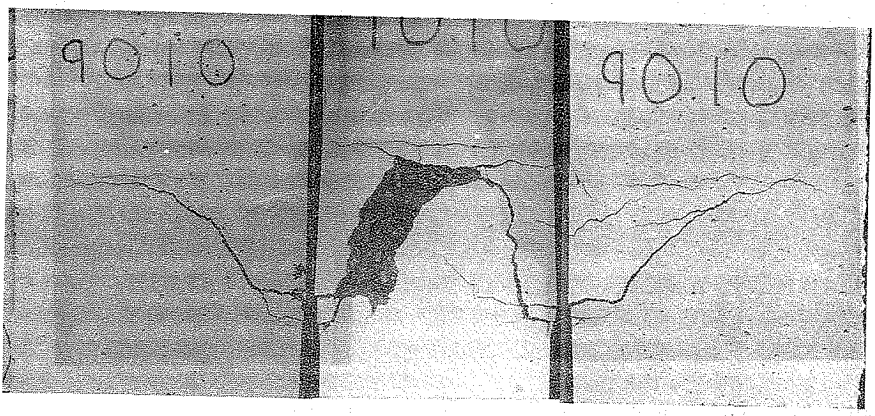

Photo 3.9 Failure of S.B.-specimen No. 90/10.

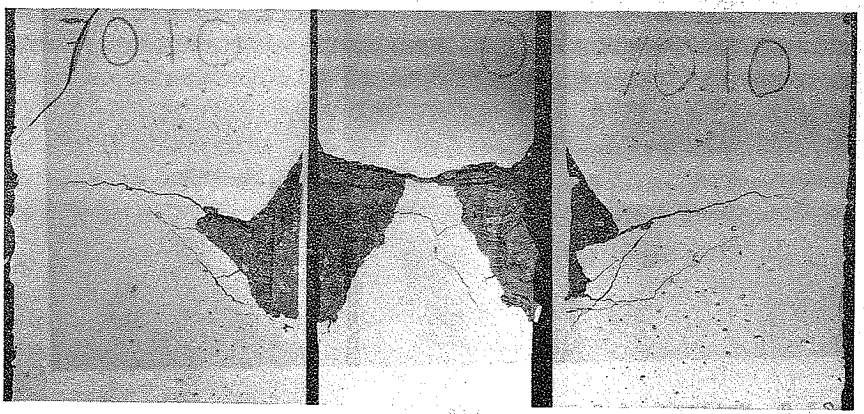

Photo 3.10 Failure of S.B.-specimen No. 70/10.

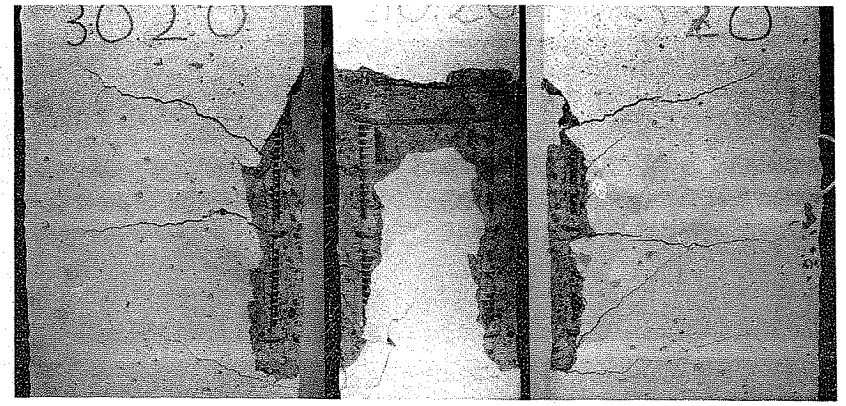

Photo 3.11 Failure of S.B.-specimen No. 30/20.

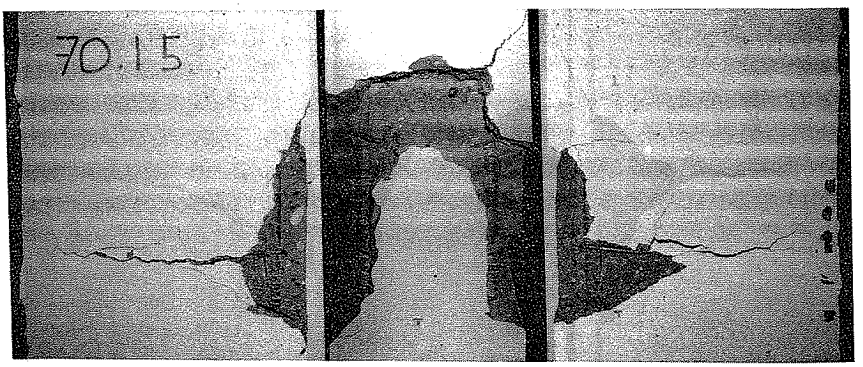

Photo 3.12 Failure of S.B.-specimen No. 70/15.

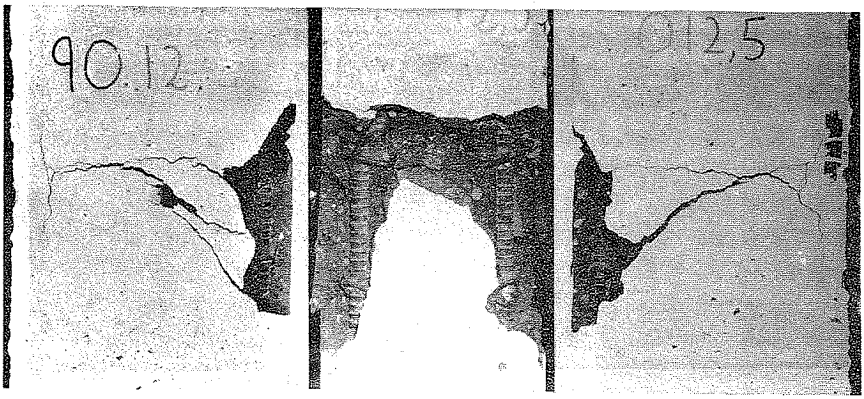

Photo 3.13 Failure of S.B.-specimen No. 90/12.5.

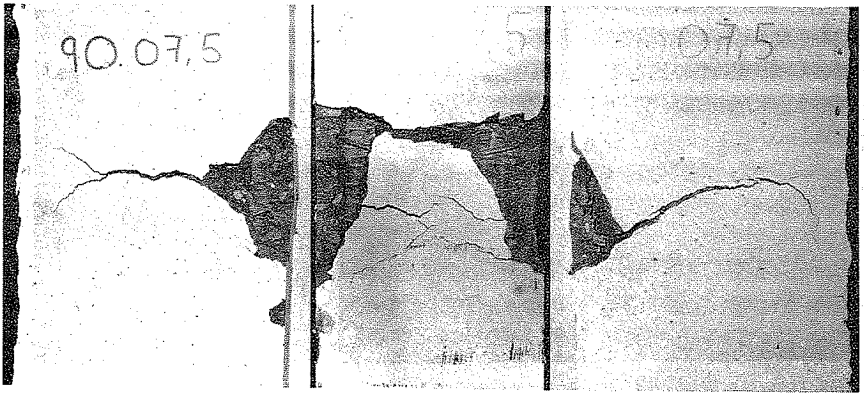

Photo 3.14 Failure of S.B.-specimen No. 90/07.5.

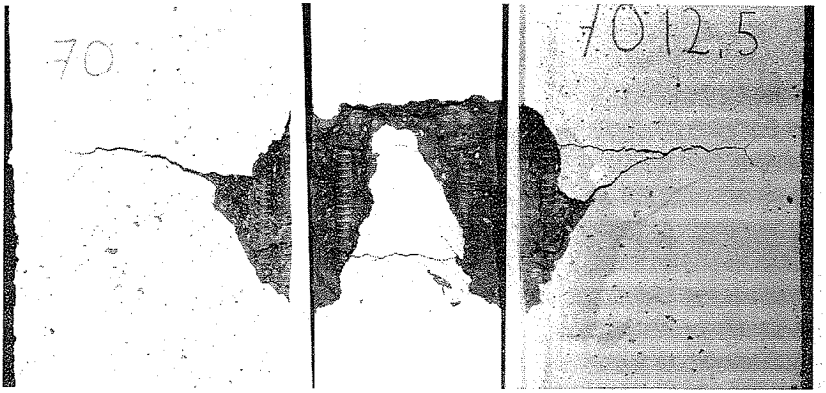

Photo 3.15 Failure of S.B.-specimen No. 70/12.5.

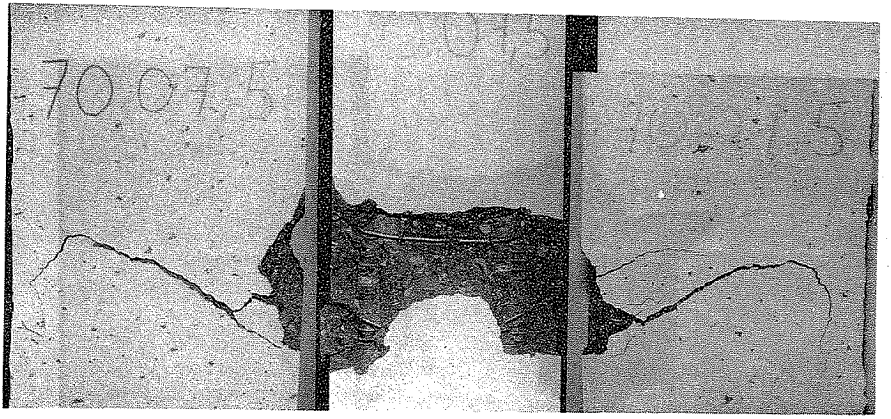

Photo 3.16 Failure of S.B.-specimen No. 70/07.5.

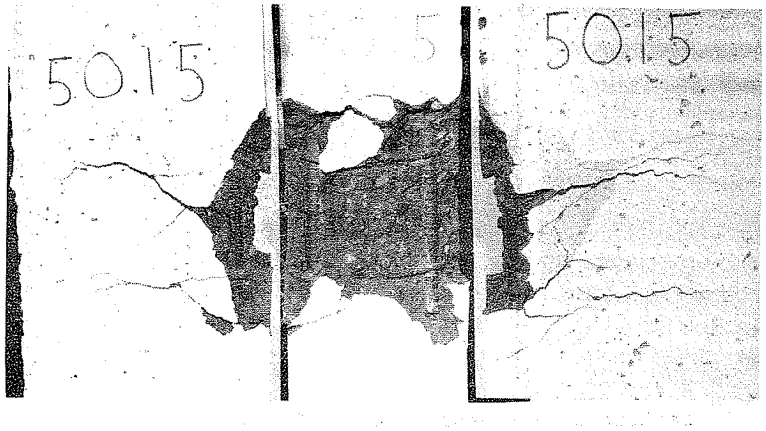

Photo 3.17 Failure of S.B.-specimen No. 50/15.

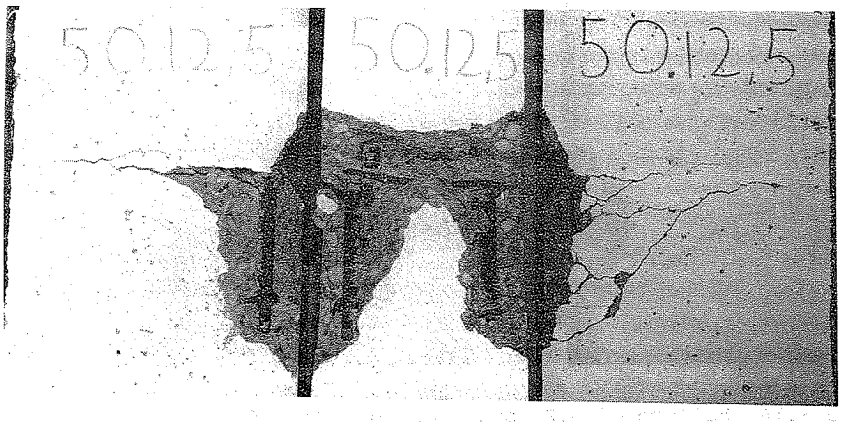

Photo 3.18 Failure of S.B.-specimen No. 50/12.5.

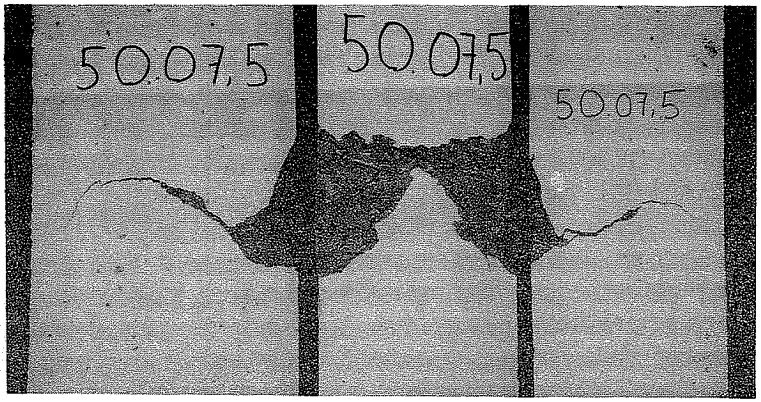

Photo 3.19 Failure of S.B.-specimen No. 50/07.5.

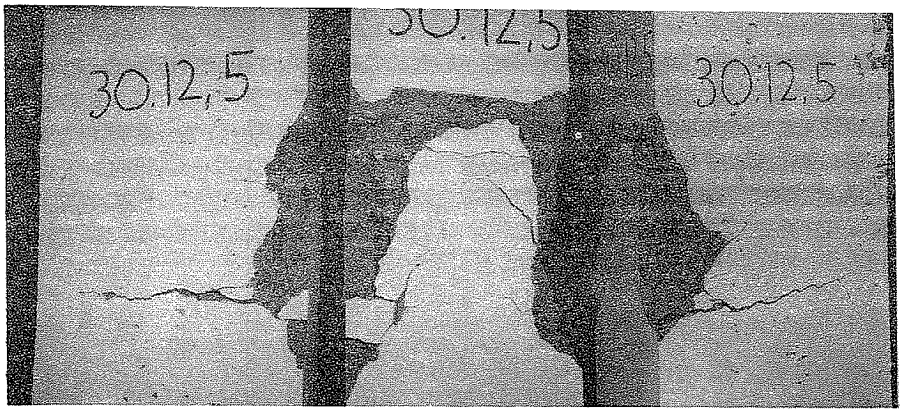

Photo 3.20 Failure of S.B.-specimen No. 30/12.5.

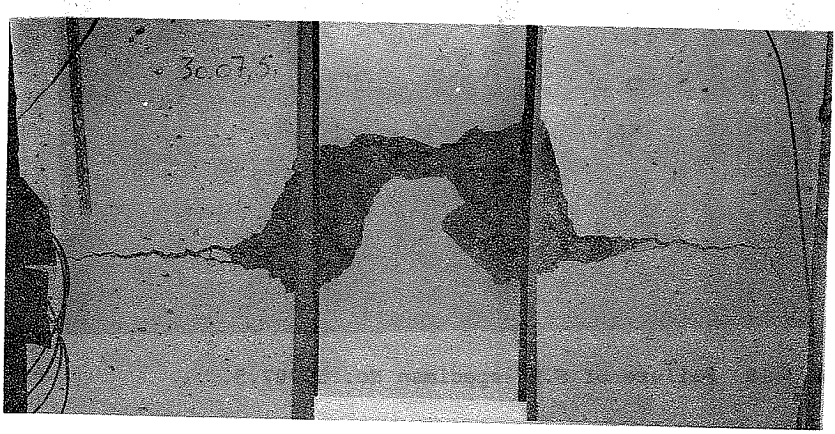

Photo 3.21 Failure of S.B.-specimen No. 30/07.5.

AFDELINGEN FOR BÆRENDE KONSTRUKTIONER
DANMARKS TEKNISKE HØJSKOLE

Department of Structural Engineering
Technical University of Denmark, DK–2800 Lyngby

SERIE R
(Tidligere: Rapporter)

R 230. RIBERHOLT, H.: Woodflanges under tension, 1988.
R 231. HOLKMANN OLSEN, N.: Implementation. 1988. (public. pending).
R 232. HOLKMANN OLSEN, N.: Uniaxial. 1988. (public pending)
R 233. HOLKMANN OLSEN, N.: Anchorage. 1988. (public pending)
R 234. HOLKMANN OLSEN, N.: Heat Induced. 1988. (public pending)
R 235. SCHEEL, HELLE: Rotationskapacitet. 1988. (public pending)
R 236. NIELSEN, MONA: Arbejdslinier. 1988. (public pending)
R 237. GANWEI, CHEN: Plastic Analysis of Shear in Beams. Deep Beams and Corbels. 1988.
R 238. ANDREASEN, BENT STEEN: Anchorage of Deformed Reinforcing bars. 1988.
R 239. ANDREASEN, BENT STEEN: Anchorage Tests with deformed Reinforcing Bars in more than one layer at a Beam Support. 1988.
R 240. GIMSING, N.J.: Cable–Stayed Bridges with Ultra Long Spans. 1988.
R 241. NIELSEN, LEIF OTTO: En Reissner–Mindlin Plade Element Familie. 1989.
R 242. KRENK, STEEN og THORUP, ERIK: Stochastic and Concrete Amplitude Fatigue Test of Plate Specimens with a Central Hole. 1989.
R 243. AARKROG, P., THORUP, E., KRENK, S., AGERSKOV, H. and BJØRNBAK–HANSEN, J.: Apparatur til Udmattelsesforsøg. 1989.
R 244. DITLEVSEN, OVE and KRENK, STEEN: Research Workshop on Stochastic Mechanics, September 13–14, 1988.
R 245. ROBERTS, J.B.: Averaging Methods in Random Vibration. 1989.
R 246. Resumeoversigt 1988 – Summaries of Papers 1988. 1989.
R 247. GIMSING, N.J., JAMES D. LOCKWOOD, JAEHO SONG: Analysis of Erection Procedures for Cable–Stayed Bridges. 1989.
R 248. DITLEVSEN, O. og MADSEN, H.O.: Proposal for a Code for the Direct Use of Reliability Methods in Structural Design. 1989.
R 249. NIELSEN, LEIF OTTO: Simplex Elementet. 1989.
R 250. THOMSEN, BENTE DAHL: Undersøgelse af "shear lag" i det elasto–plastiske stadium. 1990.
R 251. FEDDERSEN, BENT: Jernbetonbjælkers bæreevne. 1990.
R 252. FEDDERSEN, BENT: Jernbetonbjælkers bæreevne, Appendix. 1990.
R 253. AARKROG, PETER: A Computer Program for Servo Controlled Fatigue Testing Documentation and User Guide. 1990.
R 254. HOLKMANN OLSEN, DAVID & NIELSEN, M.P.: Ny Teori til Bestemmelse af Revneafstande og Revnevidder i Betonkonstruktioner. 1990.
R 255. YAMADA, KENTARO & AGERSKOV, HENNING: Fatigue Life Prediction of Welded Joints Using Fracture Mechanics. 1990.
R 256. Resumeoversigt 1989 – Summaries of Papers 1989. 1990.
R 257. HOLKMANN OLSEN, DAVID, GANWEI, CHEN, NIELSEN, M.P.: Plastic Shear Solutions of Prestressed Hollow Core Concrete Slabs. 1990.
R 258. GANWEI, CHEN & NIELSEN, M.P.: Shear Strength of Beams of High Strength Concrete. 1990.
R 259. GANWEI, CHEN, NIELSEN, M.P. NIELSEN, JANOS, K.: Ultimate Load Carrying Capacity of Unbonded Prestressed Reinforced Concrete Beams. 1990.
R 260. GANWEI, CHEN, NIELSEN, M.P.: A Short Note on Plastic Shear Solutions of Reinforced Concrete Columbs. 1990.
R 261. GLUVER, HENRIK: One Step Markov Model for Extremes of Gaussian Processes. 1990.

Abonnement 1.7.1990 – 30.6.1991 kr. 130,–
Subscription rate 1.7.1990 – 30.6.1991 D.Kr. 130.–.

Hvis De ikke allerede modtager Afdelingens resumeoversigt ved udgivelsen, kan Afdelingen tilbyde at tilsende næste års resumeoversigt, når den udgives, dersom De udfylder og returnerer nedenstående kupon.

Returneres til
Afdelingen for Bærende Konstruktioner
Danmarks tekniske Højskole
Bygning 118
2800 Lyngby

Fremtidig tilsendelse af resumeoversigter udbedes af
(bedes udfyldt med blokbogstaver):

Stilling og navn: .....

Adresse: .....

Postnr. og -distrikt: .....

The Department has pleasure in offering to send you a next year's list of summaries, free of charge. If you do not already receive it upon publication, kindly complete and return the coupon below.

To be returned to:
Department of Structural Engineering
Technical University of Denmark
Building 118
DK-2800 Lyngby, Denmark.

The undersigned wishes to receive the Department's
List of Summaries:
(Please complete in block letters)

Title and name .....

Address.....

Postal No. and district.....

Country.....